HISTONE DEACETYLASE 3 COORDINATES HEART DEVELOPMENT THROUGH STAGE-SPECIFIC ROLES IN CARDIAC PROGENITOR CELLS

A Dissertation Presented

By

SARA LYNN LEWANDOWSKI

Submitted to the Faculty of the
University of Massachusetts Graduate School of Biomedical Sciences, Worcester
in partial fulfillment of the requirements for the degree of

DOCTOR OF PHILOSOPHY

DECEMBER 21, 2016

TRANSLATIONAL SCIENCE PROGRAM

HISTONE DEACETYLASE 3 COORDINATES HEART DEVELOPMENT THROUGH STAGE-SPECIFIC ROLES IN CARDIAC PROGENITOR CELLS

A Dissertation Presented

By

SARA LYNN LEWANDOWSKI

Dissertation Defense Committee GSBS Members

Thomas Fazzio

Interdisciplinary Graduate Program

Nathan Lawson

Interdisciplinary Graduate Program

Jaime Rivera

Cell Biology Program

Chair of the Dissertation Committee

Roger Davis

Translational Science Program

External Dissertation Committee Member

Glenn Gaudette

Professor, WPI

Student Program

Translational Science Program

December 21, 2016

Acknowledgements

I would like to thank the many people who have provided support and guidance throughout this work. First, the past and present members of the Trivedi lab, including summer students, who have contributed to this work through experiments, discussions, and advice, and who have made the journey through graduate school an interesting one. I am grateful for everyone in cardiovascular medicine for being friendly and supportive and sharing their diverse expertise both to assist in my work and to broaden my understanding of topics in cardiovascular heath and disease. Members of my qualifying exam committee, TRAC committee, and dissertation exam committee, including Roger Davis, Tom Fazzio, Nathan Lawson, Jaime Rivera, Glenn Gaudette, Jane Freedman, Tony Imbalzano, have all generously shared their expertise to critically evaluate my work, offer input, and promote my development as a scientist. I am thankful for the support of the GSBS and their efforts to provide both a robust and successful graduate school experience. I appreciate everyone at UMass who has contributed to the success of my projects through their technical advice, insightful questions, sharing of ideas, equipment, and reagents, and general encouragement. Finally, I would like to thank my friends and family, as this work would not have been possible without their continuous encouragement and support.

Abstract

Disruptions in cardiac development cause congenital heart disease, the most prevalent and deadly congenital malformation. Genetic and environmental factors are thought to contribute to these defects, however molecular mechanisms remain largely undefined. Recent work highlighted potential roles of chromatin-modifying enzymes in congenital heart disease pathogenesis. Histone deacetylases, a class of chromatin-modifying enzymes, have developmental importance and recognized roles in the mature heart. This thesis aimed to characterize functions of Hdac3 in cardiac development. We found loss of Hdac3 in the primary heart field causes precocious progenitor cell differentiation, resulting in hypoplastic ventricular walls, ventricular septal defect, and mid-gestational lethality. In primary heart field progenitors, Hdac3 interacts with, deacetylates, and functionally suppresses transcription factor Tbx5. Furthermore, a disease-associated Tbx5 mutation disrupts this interaction, rendering Tbx5 hyperacetylated and hyperactive. By contrast, deletion of Hdac3 in second heart field progenitors bypasses these defects, instead causing malformations in the outflow tract and semilunar valves, with lethality prior to birth. Affected semilunar valves and outflow tract vessels exhibit extracellular matrix and EndMT defects and activation of the Tgfβ1 signaling pathway. In normal second heart field development, Hdac3 represses Tgfβ1 transcription, independent of its deacetylase activity, by recruiting the PRC2 methyltransferase complex to methylate the Tgfβ1 promoter. Importantly, knockouts of Hdac3 in differentiated

cardiac cells do not fully recapitulate the progenitor-specific knockout phenotypes. These results illustrate spatiotemporal roles of Hdac3, both deacetylase-dependent and deacetylase-independent, in cardiac development, suggesting that dysregulation of Hdac3 in cardiac progenitor cells could be a contributing factor in congenital heart disease pathogenesis.

TABLE OF CONTENTS

List of tables

List of figures

List of copyrighted Materials Produced by the Author

Chapter II is adapted from a published manuscript to include supplemental data and is included with permission:

Lewandowski SL, Janardhan HP, Smee KM, Bachman M, Sun Z, Lazar MA, and Trivedi CM. (2014). Histone deacetylase 3 modulates Tbx5 activity to regulate early cardiogenesis. *Human Molecular Genetics*, 23(14), 3801-3809.

Chapter III is a published manuscript and is included with permission not required:

Lewandowski SL, Janardhan HP, and Trivedi CM. (2015). Histone deacetylase 3 coordinates deacetylase-independent epigenetic silencing of transforming growth factor-β1 (TGF-β1) to orchestrate second heart field development. *Journal of Biological Chemistry*, 290(45), 27067-27089.

Chapter I: Introduction: The complex developmental basis of congenital heart disease – evidence for the role of chromatin-modifying enzymes as modifier genes

Congenital heart disease – importance and statistics

Congenital heart disease, the most prevalent and deadly class of congenital malformations, affects an estimated 1% of all live births, 10% of stillbirths, and 20% of spontaneous abortions [1-7]. Of the approximately 1.35 million infants born with heart defects each year, roughly a quarter of these cases will require medical intervention within the first year of life. Improvements in surgical interventions have prolonged survival such that millions of adults are now living with congenital heart disease [8,9]. However, despite our enhanced ability to manage this disease, the cause and molecular mechanisms which lead to cardiac malformations remain poorly understood [10]. As such, there are no preventative treatments or cures for heart defects and growing interest in the heritability and long-term consequences of congenital heart disease in adults. Advances in our understanding of normal and abnormal cardiogenesis help to shed light on potential pathogenic factors and mechanisms underlying the development of congenital cardiac malformations.

Cardiac development – morphogenesis and evolution of the mammalian heart

Much of our understanding of cardiac development comes from studies of model organisms. Although cardiac complexity varies, heart development, both morphologically and molecularly, is a highly conserved process across species [11-13]. Many land-dwelling organisms, such as mammals and birds, have four-chambered hearts featuring separate pulmonary and systemic circulations. Amphibians, which spend portions of their lifespans in water and on land, feature a three-chambered heart with two atria and a partially-septated ventricle, which pumps blood to both pulmonary and systemic circulations. This is similar to the arrangement observed in lungfish. Zebrafish, which do not have lungs, have a looped, two-chambered heart, which pumps blood to the gills for oxygenation and then on to nourish the rest of the body. Other small organisms, such as insects, have simple, vessel-like hearts with more open circulatory systems [12].

The basic heart tube in fish and higher organisms forms from two pools of pre-cardiac progenitor cells in the splanchnic mesoderm, which migrate to the embryonic midline, creating the cardiac crescent [14]. In mice, these progenitor pools arise around embryonic day (E) 6.5 and form the cardiac crescent a day later. In a process conserved across species, the two sides of the crescent converge and fuse in a caudal to cranial direction, generating a closed tube with an outer myocardial layer lined with endothelial cells [14]. Once closed, the linear

tube commences beating. The heart is the first functional organ in a mammalian embryo, first beating around E8.0 in mice and three weeks gestation in humans. A functional heart tube is required to supply sufficient circulation to support further development.

Once the primary heart tube has formed, it elongates and loops rightward, breaking the bilateral symmetry of the embryo. This rightward looping is observed in the two-chambered zebrafish heart, as well as the more complex amphibian, avian, and mammalian hearts [12,13]. Mammalian and avian hearts then proceed to undergo convergence of the inflow tract and outflow tract along the anterior-posterior axis of the embryo facilitating further looping of the tube. This convergence allows the outflow tract to nestle into the atrioventricular canal, aligning the septating vessels above the appropriate ventricles. With this arrangement, the pulmonary artery and aorta fuse with the right and left ventricles, respectively, establishing the distinct pulmonary and systemic circulations [15]. This elegant looping process transforms the linear heart tube into a mature, organized heart.

Progenitor cells in cardiac development – the primary heart field

Making a functional heart requires the development of cardiac lineages, including cardiomyocytes, smooth muscle cells, and endothelial cells to be coordinated in both time and space with the morphologic changes such as tube

formation, looping, and septation. This is achieved through dynamic regulation of multiple progenitor sources. The majority of the heart derives from the mesoderm, with the major exception of ectodermal-derived neural crest, which contributes to smooth muscle of the outflow tract [16-18].

The first of the two major mesodermal-derived heart fields, the primary heart field progenitor cells are initially specified in the cardiac crescent, identified by expression of the transcription factor Nkx2-5 [12,13]. These progenitors differentiate into cardiomyocytes, smooth muscle cells, and endothelial cells as they form the primary heart tube, which will later give rise to the left ventricle and contribute to both atria (Figure 1.1). Signals, including BMP and FGF, from the surrounding tissues promote this differentiation [16,19].

The key molecular regulators of heart development are highly conserved throughout evolution. In species down to insects, the progenitor cells that give rise to the primitive heart tube, or insect-equivalent dorsal vessel, express orthologs of Nkx2-5, which marks cardiac commitment [12]. The primitive heart tube, which initially expresses Nkx2-5, is later marked by expression of the transcription factor Tbx5 [20-22]. Tbx5-derived cells go on to contribute cardiomyocytes, smooth muscle, and endothelial cells of the left ventricle, atrioventricular canal, and parts of the atria [20-22]. Differences in expression patterns of Tbx5 in reptiles and mammals suggest that it may be evolutionarily important in the patterning of the four-chambered heart [11]. Loss of Tbx5 in mice causes failed septation while misexpression in a reptile-like pattern results in a

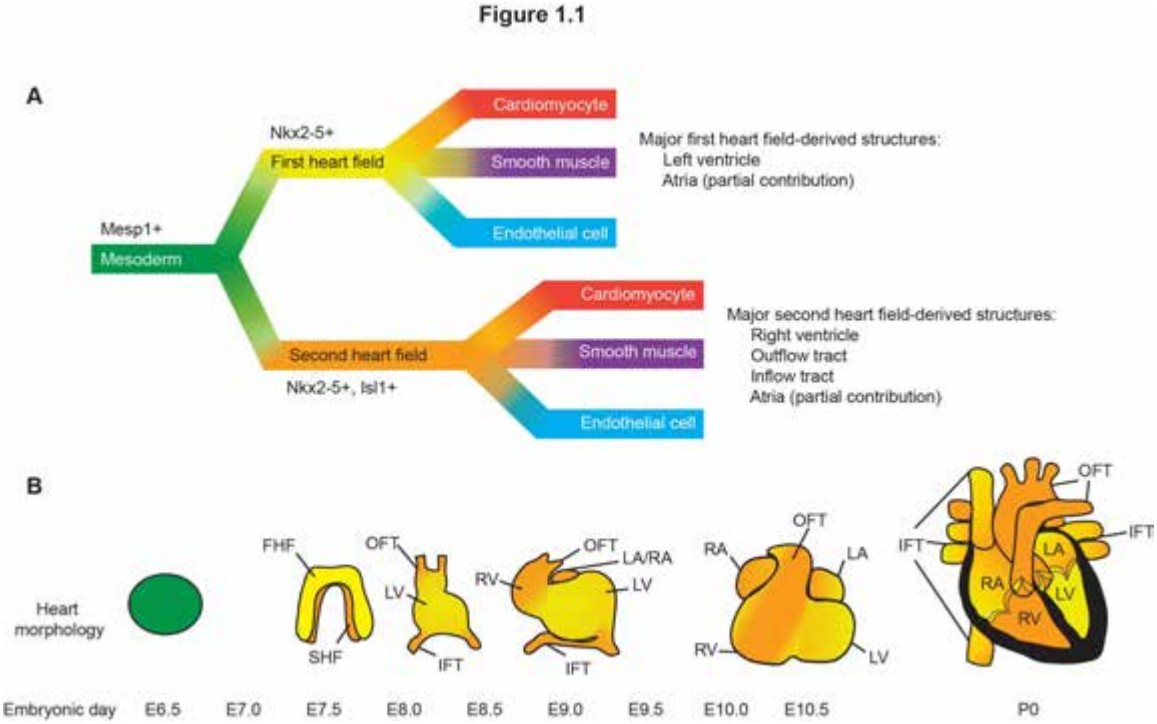

Figure 1.1: Diagram of mesodermal cardiac progenitor contribution to heart development. (A) Branching diagram illustrating progressive differentiation of mesoderm into primary heart field progenitors, second heart field progenitors, and subsequent end lineages. **(B)** Cartoon model of cardiac morphology from specification through birth. Yellow marks first heart field-derived regions while orange indicates regions of second heart field origin. FHF = first heart field, SHF = second heart field, OFT = outflow tract, IFT = inflow tract, LV = left ventricle, RV = right ventricle, LA = left atrium, RA = right atrium.

single ventricle similar to the reptilian heart [11]. Thus, Tbx5 is a critical factor in specifying the primary heart field structures.

Proper formation of the primary heart field and linear heart tube are essential to support further embryonic development. Failure of the primary heart field to form a closed tube results in cardia bifida, a severe and embryonic lethal malformation [23-25]. Due to the severity and early timing of this defect, it has not been documented in humans, though it has been described in model organisms [23-25]. This and other catastrophic failures in early primary heart field development may contribute to early miscarriage [5]. Less severe defects affecting the primary heart field include septal defects and malformations of the left ventricle, such as hypoplastic left heart syndrome and left ventricular noncompaction [26-29]. Mutations in key primary heart field transcription factors, including Nkx2-5 and Tbx5, have been causally implicated in congenital heart disease, as will be described below [26,29,30].

Progenitor cells in cardiac development – the second heart field

Lineage tracing experiments in chick embryos revealed that the outflow tract of the heart is not derived from the linear heart tube [31]. Instead, a population of splanchnic mesoderm in the pharyngeal region adjacent to the linear heart tube was found to express classic cardiac markers, including Nkx2-5 and Gata4, along with the differentiation marker Hnk1, suggesting an undifferentiated cardiac

progenitor population [32]. Explants of this pharyngeal mesoderm, termed the second heart field, were able to proliferate and differentiate *in vitro* into cardiac cells [31,32]. Similarly, *in vivo*, differentiation of this progenitor pool is suppressed by Wnt and β-catenin signaling from the neural tube, but upon migration into the ends of the linear heart tube, these progenitor cells lose Hnk1 expression and gain expression of the myocardial marker MF20 [32]. The second heart field cells differentiate to form the cardiomyocytes, smooth muscle cells, and endocardial cells of the outflow tract, inflow tact, and right ventricle (Figure 1.1) [31-33]. Consistent with that, ablation of the pharyngeal splanchnic mesoderm in chick embryos results in absence of outflow tract development [31,34].

While there is debate over whether the second heart field progenitor cells represent a completely separate progenitor population or merely a subpopulation of a singular progenitor source, the concept of a second heart field, in which cells from a specified region outside of the primitive heart tube differentiate to gradually add to and extend the heart tube, is observed in species from humans down to zebrafish [12,13,35]. Molecularly, the second heart field progenitors share many similar cardiac markers and modes of induction with the primary heart field, however they also express additional factors somewhat restricted to the second heart field, including the transcription factor Isl1 [32,33]. Cre-based lineage tracing studies in mice suggest that derivatives of Isl1-expressing cells comprise over 90% of cells in the right ventricle and outflow tract, 65-70% of cells in the atria, and less than 20% of cells in the left ventricle, the major derivative of the primary

heart field (Figure 1.1) [33]. Isl1 is conserved in humans, mice, *Xenopus*, zebrafish, lamprey, *Amphioxus*, *Ciona*, and *Drosophila*, though the invertebrate Isl1 is somewhat divergent from the vertebrate Isl1 [12]. In chick, the pattern of second heart field Isl1 expression is observed at later stages, though at early stages, Isl1 expression is observed throughout the heart. As development progresses, Isl1 expression becomes restricted to the second heart field region as it invades the ends of the heart tube [12]. This is similar in lower organisms.

Isl1 is important for second heart field development, as evidenced by deletion studies in mice. Isl1-null mice exhibit misshapen, un-looped hearts [33]. Staining analysis suggests a lack of outflow tract and right ventricle, with the entire heart expressing the left ventricular markers Tbx5 and EHand. These embryos show increased apoptosis and reduced proliferation and migration of second heart field cells into the heart tube, suggesting that Isl1 is necessary for survival and development of the second heart field [33]. Certain Isl1 haplotypes are associated with a 2-3 fold increased odds ratio of congenital heart disease in humans, further supporting its important role in heart development [36].

Nearly two-thirds of all congenital heart disease affects structures derived from the second heart field, outweighing the prevalence of defects in primary heart field or neural crest-derived structures [7]. These second heart field-associated defects include: double outlet right ventricle, Tetralogy of Fallot, right ventricular hypoplasia, pulmonary stenosis, and defects in the semilunar valves, including the most common congenital heart defect, bicuspid aortic valve [7,37].

Ablation of the second heart field in chick embryos causes conotruncal defects, including Tetralogy of Fallot and pulmonary atresia [34]. Furthermore, co-occurrence of conotruncal defects with malformations in the inflow tract in humans is consistent with their common second heart field origin [38]. Importantly, conotruncal defects, which arise from disruptions in the heart looping and septation process, have the highest risk of embryonic lethality [39,40]. Thus, second heart field development is critically relevant in addressing the etiology of congenital heart disease.

Genetic causes of congenital heart disease

The importance of cardiac progenitors and heart fields is reflected in our present knowledge of the molecular causes of congenital heart disease. Currently, mutations in over 60 genes have been causally linked to congenital heart disease in humans [10,28]. Many of the human disease-causing mutations are in key cardiac transcription factors involved in the specification and differentiation of cardiac progenitor cells, both in the primary and second heart fields.

Single gene mutations – TBX5 and the primary heart field

In 1997, two groups described mutations in the T-box transcription factor TBX5 in patients with Holt-Oram Syndrome, a disease that manifests as a

spectrum of cardiac and upper limb defects [29,30]. Through exon trapping experiments, these groups narrowed in on a previously described disease-associated region of chromosome 12 and identified several mutations in TBX5 that segregated with the disease in both familial and sporadic cases in an autosomal-dominant fashion.

In situ and antibody staining analysis in chick, mouse, and human embryonic hearts revealed expression of TBX5 in the cardiac crescent and subsequent strong staining for TBX5 in the posterior regions of the linear heart tube [41]. In chick and mouse, TBX5 expression becomes restricted to the atria and left ventricle in the looped heart, with little to no expression in the second heart field-derived right ventricle and outflow tract. Experiments in humans have suggested that TBX5 may be expressed in a broader domain including portions of the right ventricle in human embryos, however minimal expression was detected in the outflow tract segments [22,41]. The phenotypes associated with Holt-Oram Syndrome reflect the restricted expression pattern of TBX5, with atrial septal defects, ventricular septal defects, and hypoplastic left heart syndrome being the predominant defects presenting in patients [41].

Deletion studies in mice revealed critical roles of TBX5 in promoting growth and differentiation of the left ventricle and atria, classic derivatives of the primary heart field [20]. While TBX5 is not required for development of the cardiac crescent or linear heart tube, its expression is essential for growth and development of the left ventricle and atria from the posterior regions of the heart

tube. In TBX5 knockout mice, arrested development of the posterior regions of the linear heart tube disrupt looping and lead to embryonic lethality by E10.5 [20]. In these mice, the second heart field-derived right ventricle and outflow tract develop independently of TBX5. Importantly, mice heterozygous for deletion of TBX5 phenocopy human Holt-Oram Syndrome, supporting a role for TBX5 in this disease process [20].

Tbx5 synergistically interacts with Nkx2-5 to promote cardiomyocyte differentiation [42]. Tbx5 target genes include cardiomyocyte structural genes, such as myosin and troponin, and differentiation-inducing signaling molecules, including Bmp4 [43]. Consistent with this, overexpression of TBX5 in embryonic stem cells causes increased expression of cardiac markers and early onset of beating in embryoid bodies [44]. The TBX5-overexpressing embryoid bodies showed specific increased expression first heart field markers, including Nkx2-5 and troponin, but no changes in expression of second heart field markers, such as Isl1 and Tbx20 [44]. These findings suggest that TBX5 is important in promoting first heart field cardiomyocyte differentiation.

Since 1997, over 50 mutations in TBX5 have been reported in patients with Holt-Oram Syndrome [45]. The overwhelming majority of these mutations are predicted to be loss-of-function or null-alleles. This led to a theory that Holt-Oram Syndrome may arise due to haploinsufficency of TBX5 [29,45,46]. However, at least one gain-of-function mutation in TBX5 has been described in Holt-Oram Syndrome, indicating that strict regulation of TBX5 activity is required for proper

development [47]. Interestingly, while TBX5 mutations cause Holt-Oram Syndrome, individual mutations are not predictive of the disease presentation [29,46]. For example, two patients in the same family sharing the same mutation in TBX5 may exhibit differing types of cardiac and limb defects and variable severity of the disease. Mechanisms of how specific mutations manifest in variable phenotypes remain poorly understood.

Microdeletions – 22q11.2 deletion syndrome and the second heart field

While Holt-Oram syndrome cardiac defects primarily affect the septa and left side of the heart, other syndromes show arrays of defects focused on second heart field-derived structures. For example, 22q11.2 deletion syndrome is a disease characterized by cardiac, thymic, and craniofacial defects [48]. Patients with 22q11.2 deletion syndrome exhibit cardiac defects predominately affecting the outflow tract, including Tetralogy of Fallot, pulmonary atresia, interrupted aortic arch, double outlet right ventricle, and transposition of the great arteries [48].

This deletion syndrome, also known as DiGeorge Syndrome, is characterized by loss of a 1.5-3 Mb region of chromosome 22 [48-50]. Sequence analysis, mouse modeling, and gene rescue experiments suggest that loss of Tbx1 within this deleted region can account for many of the cardiac defects in DiGeorge Syndrome patients [50-54]. Tbx1, a T-box family member, shows a complimentary expression pattern to Tbx5. While Tbx5 expression is robust in

the primary heart field-derived left ventricle, cardiac expression of Tbx1 is restricted predominately to the second heart field, including the pharyngeal mesoderm and cardiac outflow tract [55]. Tbx1 is expressed in precursors of the right ventricle and outflow tract, structures commonly affected in DiGeorge Syndrome [55].

Importantly, deletion of Tbx1 in mice using different Cre drivers revealed that the Tbx1 has separate but complementary roles in various cell types during development [53]. They found that Tbx1 expression in the pharyngeal endoderm is required for septation of the outflow tract while expression in the second heart field is required for outflow tract alignment and truncal valve septation [53]. These findings illustrate that a single protein can have both timing- and cell-type specific roles during cardiac development.

Sequencing studies have identified several mutations in Tbx1 in patients with DiGeorge-like phenotypes but no accompanying deletion in chromosome 22 [51]. As with Tbx5, the majority of identified Tbx1 mutations are believed to be loss-of-function or null mutations [51,56]. This is consistent with the shared phenotypes between patients with Tbx1 mutations and those with deletion of the Tbx1 genomic region. However, several studies have also reported duplications or gain of function mutations in the Tbx1 locus in patients with DiGeorge-like phenotypes, suggesting that tight regulation of expression may be a critical factor in the disease process [57-59].

Signaling pathways – TGFβ1 and connective tissue disorders

Beyond transcription factors, signaling pathways are critical for coordinating cell processes during heart development. Consistent with this, mutations in key signaling pathways are associated with congenital heart diseases, with mechanisms highlighting the important connections between extracellular signals, intracellular responses, and interactions between cells and the extracellular matrix.

Loeys-Dietz Syndrome is classified as a connective tissue disorder, a type of condition affecting the formation or structure of the extracellular matrix [60]. This disease is caused by mutations in Tgfβ2, the Tgfβ receptors, TGFBRI and TGFBRII, and the downstream effector Smad3 [60-62]. Affected patients exhibit cardiac defects including septal defects, bicuspid aortic valve and, most severely, aneurysms in the ascending aorta [60].

In the heart, organized depositions of collagen, elastin, and other extracellular matrix components provide the vessels and valves with the structure, strength, and flexibility required for proper function [63-66]. The extracellular matrix composition is intricately tied to signal transduction, through its interaction with receptors and sequestration or activation of growth factors, including Tgfβ [67,68]. These growth factors, in turn, can regulate synthesis, deposition, and remodeling of the extracellular matrix [69]. Mutations in Tgfβ

pathway genes in patients with Loeys-Dietz Syndrome can disrupt this relationship, altering signal transduction and extracellular matrix homeostasis.

Related to this, mutations in genes encoding collagens and collagen-related enzymes result in Ehlers-Danlos Syndrome, another connective tissue disorder [70,71]. While this disease affects many organs, including the joints and skin, the most life-threatening complication is aortic dissection, resulting from weakened vessel walls. Similarly, mutations in fibrillin, a glycoprotein involved in elastin organization, cause Marfan Syndrome, a connective tissue disease associated with aortic aneurysm, among other defects [72,73]. In both of these diseases, patients have shown elevated levels of Tgfβ, further supporting a link between Tgfβ, extracellular matrix, and connective tissue disease [61,74,75]. This supports an established paradox in Tgfβ signaling, where functional analysis of TGFBRI and TGFBRII mutations found in patients with Marfan Syndrome or Loeys-Dietz Syndrome suggest that these mutations are functionally damaging, yet Tgfβ expression is elevated [76]. This paradox implies complex regulation and activation of the Tgfβ pathway, which is not yet completely understood.

Tgfβ receptor knockout mice have revealed important functions of Tgfβ signaling in regulating smooth muscle cell development and extracellular matrix organization [77]. Loss of TGFBRII in SM22-positive cells is embryonic lethal between E14.5 and E18.5 [77]. This model deletes TGFBRII in the myocardium at E9.5, dorsal aorta at E11.5, and epicardium at E12.5 [77]. Embryos lacking TGFBRII in these cells exhibit abnormal shape and thickness of the aorta, with

an incomplete or absent elastin network, and, in some instances, aortic aneurysms. These defects were partially attributed to deficiency in synthesis and deposition of tropoelastin, associated with impaired expression and synthesis of fibulin 5 [77].

In addition to extracellular matrix defects, the TGFBRII-deficient aortic smooth muscle cells appeared round and disorganized, suggesting defective differentiation [77]. This was most apparent in the descending thoracic aorta and less dramatic in the proximal aorta, suggesting regional differences in Tgfβ signaling requirements in aortic smooth muscle cells. Vascular smooth muscle cells arise from several lineages, including the neural crest, and second heart field in the proximal aortic arch, and the somites, and other stem cell sources in the descending aorta [78,79]. Treatment of neural crest stem cells with Tgfβ induces expression of vascular smooth muscle contractile proteins, suggestive of a role of Tgfβ signaling in smooth muscle differentiation [80]. Interestingly, vascular smooth muscle cells in culture responded to equal concentrations of Tgfβ in a lineage-specific manner [80]. Neural crest-derived vascular smooth muscle cells exhibited a 4-8-fold higher transcriptional response to Tgfβ than mesodermal-derived vascular smooth muscle cells despite equal expression of Tgfβ receptors [80]. This differential capacity to respond to Tgfβ may reflect lineage-specific differences in intracellular downstream effectors or chromatin states at the target promoters, which could either slow or amplify the response to receptor activation.

Beyond vessel integrity, Tgfβ signaling is implicated in valve development and disease. Bicuspid aortic valve is associated with connective tissue disorders, including Loeys-Dietz Syndrome and Marfan Syndrome [81,82]. There is also correlation between bicuspid aortic valve and aortic aneurysms, suggesting a shared molecular mechanism or a cause-effect relationship [68,81,83]. Patients with bicuspid aortic valve are at increased risk for developing aortic valve disease and calcification in adulthood [82]. These adult aortic valve pathologies are associated with valve interstitial cell activation, extracellular matrix changes, and, interestingly, show induction of Tgfβ [65,84,85]. The correlations between aortic aneurysm, bicuspid aortic valve, and calcific valve disease and the common involvement of Tgfβ dysregulation suggest a potential shared mechanism between congenital heart defects and acquired adult valve pathologies.

Beyond the single gene – disease penetrance and modifier genes in congenital heart disease

Despite identification of single genes and pathways as culprits for human congenital heart disease, the majority of cases appear to be multi-genic in origin. In humans, congenital heart disease is strongly associated with trisomy and monosomy disorders, including Down Syndrome (trisomy 21) and Turner Syndrome (females with a single X-chromosome) [86-88]. In these cases, loss or gain of an entire chromosome leads to copy number changes in hundreds to

thousands of genes. However, in both Down Syndrome and Turner Syndrome, the prevalence of congenital heart disease is between 25% and 60% [86,87]. This is well above the population-wide incidence of 1%, strongly suggesting that these syndromes predispose patients to congenital heart disease. However, the incomplete penetrance of cardiac phenotypes indicates that additional factors are required beyond the gain or loss of a single chromosome. In Down Syndrome, deletion of either Creld1 or Hey2, in conjunction with trisomy 21, increase the risk of congenital heart disease [89]. These genes are believed to be modifier genes.

Even among the “single gene” disorders discussed above, modifier genes may be important in influencing disease presentation. In both Holt-Oram and DiGeorge Syndromes, mutations in T-box transcription factors segregate with disease among families and occur in sporadic cases. However, there is a lack of concordance in type and severity of defects among patients sharing the same mutation [29,46,50,90]. Therefore, although a mutation in TBX1 or TBX5 is indicative of disease, they are not predictive of clinical presentation, suggesting that the mechanism of disease development involves interaction of other genetic or environmental factors beyond the single gene mutation.

Mouse models of congenital heart disease support the multi-genic etiology of congenital heart disease. For example, lethality of Tbx5 heterozygous mice is contingent upon genetic background, ranging from 40% to over 90% depending on mouse strain [20]. In a 22q11.2 deletion mouse model, modulation of sonic hedgehog or retinoic acid signaling pathways influences phenotypic expression

[91]. These findings reveal that the molecular etiology of congenital heart disease is complex and requires further understanding of interacting pathways and transcriptions factors during cardiac development.

Chromatin modifying enzymes in congenital heart disease

Considering the complex molecular pathogenesis of congenital heart disease, recent work has focused on understanding chromatin structure and the role of chromatin-modifying enzymes in cardiac development and disease. These enzymes control gene regulation through their modification or remodeling of chromatin, including DNA and histone methylation, histone acetylation, ubiquitination, and sumoylation, thereby modulating DNA accessibility [92,93]. However, many chromatin-modifying enzymes also have functions beyond the chromatin, covalently modifying transcription factors and other proteins or acting in multi-protein complexes or pathways to facilitate cellular processes [92,94]. In these capacities, epigenetic enzymes facilitate gene expression, relay and interpret signals, and mediate cellular responses and behaviors, including those essential for development.

One line of investigation into the involvement of chromatin-modifying enzymes in congenital heart disease is a search for mutations in histone-modifying genes in patients with congenital heart disease. Recently, whole exome sequencing was conducted on over 300 patients with various congenital

heart defects, searching for novel mutations [95]. Among the mutated genes identified in this study, the team found enrichment for histone-modification pathways, including H3K4 methylation and H3K27 acetylation, in the patient population. This suggests that disruption in histone-modifying pathways may be an important avenue of investigation into mechanisms of congenital heart disease.

Indeed, mutations in several histone-modifying genes have been causally linked to congenital heart disease. One prominent example is CHD7, an ATP-dependent chromatin-remodeling enzyme, which is mutated in patients with CHARGE syndrome [96-100]. The acronym CHARGE describes this complex, multi-organ disorder including: coloboma of the eye, heart defects, atresia choanae, retardation of growth and development, genital abnormalities, and ear abnormalities. Heart defects are present in 75% of CHARGE patients.

Mechanisms of CHD7 function have been dissected using mouse models. Knockout of CHD7 in Mesp1-positive mesoderm cells results in cardiac defects that correlate well with cardiac abnormalities in humans with CHARGE Syndrome [101]. Interestingly, CHD7 appears to facilitate key cardiac developmental processes through non cell-autonomous pathways. For example, embryos with mesodermal deletion of CHD7 exhibit coronary vein anomalies that are not recapitulated by deletion specifically in the endothelial cells, which give rise to these veins [101]. Likewise, the neural crest-derived neuronal axons are truncated in mesodermal CHD7 knockouts, despite retained expression of CHD7 in the

affected cells [101]. In the case of the neural crest, CHD7 acts by regulating expression of semaphorins, which function as signaling guides for neural crest migration. CHD7 is enriched at the enhancer of Sema3c, expression of which is reduced in mesodermal CHD7 knockouts, possibly explaining the neuronal axon defects [101]. CHD7 also interacts with other important cardiac enhancers, including the Nkx2-5 enhancer [102]. In this case, CHD7 is required for BMP-induced up-regulation of Nkx2-5. In response to active BMP signaling, CHD7 interacts with regulatory Smads and localizes to the Nkx2-5 enhancer, where its histone binding and nucleosome remodeling activities are required to promote Nkx2-5 expression [102]. In this ways, CHD7 demonstrates the importance of chromatin-modifying enzymes in facilitating a cell's competence to respond to extracellular signals.

In addition to their gene regulatory roles at enhancers, chromatin-modifying enzymes have critical chromatin-independent roles during cardiac development. Like CHARGE Syndrome, Cornelia de Lange Syndrome is a rare genetic disease that causes developmental delays and physical abnormalities affecting multiple organ systems, including the heart [103]. Congenital heart defects are present in 25-30% of patients with Cornelia de Lange Syndrome. Mutations in five genes involved in formation and function of the cohesin complex: NIPBL, SMC1A, SMC3, RAD21, and HDAC8, cause Cornelia de Lange Syndrome, with the presentation and severity of this disease correlating with the specific mutated gene [103]. HDAC8, one of the genes mutated in Cornelia de Lange Syndrome, is a

chromatin-modifying enzyme which functions in a chromatin-independent manner, deacetylating SMC3 to facilitate the renewal of the cohesin complex [103-106]. This complex regulates the interaction between sister chromatids during cell division. Mutations in HDAC8 lead to a severe form of Cornelia de Lange Syndrome, illustrating the importance of HDAC8's function in this context.

The complex relationship between transcription factors and chromatin – illuminating mechanisms and therapeutic potential

As seen in Cornelia de Lange Syndrome, mutations in any one of several genes can lead to overlapping phenotypes consistent with their participation in a shared biological process. Along the same lines, similar heart defects can be characteristic of seemingly unrelated disorders and investigation of these commonalities may reveal previously unknown connections between genes and pathways in cardiac development. For example, CHARGE Syndrome, caused by CHD7 mutations, shares clinical overlap with TBX1-associated DiGeorge Syndrome, which suggested a possible link between these two genes [107]. Indeed, further studies in mice uncovered a genetic interaction between CHD7 and Tbx1 that exists in mice [108].

Along with investigating overlapping phenotypes to identify molecular interactions, understanding the relationships between transcription factors, chromatin, and chromatin-modifying enzymes in the context of normal heart

development can help to identify potential affected interactions in disease conditions. Going further, a precise molecular understanding of how an identified gene mutation or pharmaceutical agent specifically alters a protein's activity or interactions can provide insight into how these disruptions result in disease and inform development of treatments to counter these detrimental effects. In pursuit of this understanding, model organisms and *in vitro* experiments are critical in probing molecular interactions and biological pathways.

Many basic science studies have focused on determining how a missense mutation affects a protein's stability and function. Such investigations into HDAC8 mutations associated with Cornelia de Lange Syndrome revealed predominately loss-of-function of mutant HDAC8 [104-106]. However, some of these mutants retained low levels of enzymatic activity [104]. These observations lead a team to ask whether a specific small molecule activator of HDAC8, known as TM251, could rescue the activity of mutant HDAC8 [104]. Through *in vitro* activity assays, the team found that the enzymatic activity of HDAC8 mutants could be rescued by drug treatment [104]. However, this rescue was only observed with mutants that had a measureable activity level at baseline. The activity of these catalytically inactive mutants could be enhanced; however catalytically-dead mutants were unresponsive to drug treatment [104]. This suggests that molecular rescue of a mutant protein's activity may be possible, with success dependent on the specific type of mutation involved.

Moving from a single-protein *in vitro* rescue to a disease-treatment model requires further understanding of both protein and drug interactions throughout a whole organism. It is well known that the state of chromatin can aid or hinder a transcription factor's access to regulatory regions of the genome. However, the transcription factors, themselves, can assist in shaping this chromatin structure. For example, ChIP-seq analysis of Tbx1 and histone modifications in differentiating mesoderm revealed an association between Tbx1 binding sites and regions of chromatin enriched for H3K4 monomethylation and poor in H3K4 acetylation [109]. Interestingly, deletion of Tbx1 altered the methylation states of some of these regions. The researchers found that Tbx1 co-localizes and co-immunoprecipitates with Kmt2 methyltransferases, possibly acting to recruit these methyltransferases to the chromatin [109]. This suggests that transcription factors may have roles in shaping the chromatin structure of their target sites.

Interaction between transcription factors and chromatin-modifying enzymes may have implications from a modifier gene perspective; chromatin-modifying genes may alter disease presentation in predisposed genetic backgrounds. In DiGeorge Syndrome patients, whole exome sequencing discovered single nucleotide variations in histone-modification related genes, including KDM2B, JMJD1C, and RREB1, associated with phenotypic disease presentation [95]. Further analysis revealed a disease association specifically with single nucleotide variations in genes related to active chromatin states and not with those in genes related to repressed chromatin [95].

Importantly, the interactions between Tbx1 and chromatin-modifiers open a potential therapeutic avenue to counteract mutations in transcription factors, such as Tbx1, by targeting chromatin-modification. Along this line, Fulcoli and colleagues treated pregnant mice with TCP, an inhibitor of Lsd1/2 histone demethylases, during the critical period for development of DiGeorge Syndrome phenotypes [109]. TCP treatment, alone, had no obvious adverse affects on embryonic development, thus establishing a proof of principle that prenatal treatment targeting histone-modifying enzymes could have beneficial results in counteracting the effects of transcription factor mutations in congenital heart disease development [109].

Chromatin-modifying enzymes as teratogenic drug targets

While prenatal exposure to pharmaceuticals may be a future therapeutic avenue to lessen the burden of congenital malformations, pharmaceuticals can also function as teratogens. Teratogens, or agents that cause embryonic malformations, have been identified to be associated with increased risk of congenital heart disease. These include environmental toxins, pharmaceuticals, and factors from the maternal environment, such as infections or maternal diabetes [8]. Importantly, many of these teratogens have been shown to modulate the epigenome.

One example of such a teratogen is sodium valproate, or valproic acid, which is a potent inhibitor of histone deacetylases. Valproic acid can induce hyper-acetylation in mouse embryos as quickly as one hour after treatment [110]. First used in clinical trials for treatment of epilepsy as early as 1964, valproic acid was approved by the US Food and Drug Administration in 1978 [111]. Four years later, the first reports were published by the Centers for Disease Control describing teratogenic effects of maternal valproic acid treatment on developing embryos [111]. Children exposed to valproic acid prenatally exhibit increased incidence of defects including neural tube defects, cleft palate and lip, and cardiac defects [112]. Supporting the teratogenic effects of valproic acid, treatment of pregnant mice with valproic acid resulted in a dose-dependent increase in embryonic cardiac defects including ventricular septal defects [113]. Administration of valproic acid at the time of cardiac crescent formation yielded the highest penetrance of cardiac defects, with 20% of all treated embryos affected [113]. Furthermore, exposure to either valproic acid or trichostatin A (TSA), another Hdac inhibitor, resulted in gross developmental defects and embryonic lethality in zebrafish and Xenopus [114]. Valproic acid analogs that do not inhibit Hdacs did not cause developmental defects [114]. These findings, together, illustrate the detrimental impact of prenatal exposure to agents that alter the activity of chromatin-modifying enzymes.

Histone deacetylases

The teratogenic effects of Hdac inhibitors suggest critical functions of Hdacs in cardiac development. In addition, as exemplified by the involvement of Hdac8 in Cornelia de Lange Syndrome, discussed above, Hdacs may also have mechanistic functions in genetic causes of congenital heart disease [106,115,116]. Determining the biological functions of Hdacs during development could identify links to known genetic pathways in congenital heart disease pathogenesis and illuminate the specific mechanisms of teratogenic pharmaceutical effects, informing further drug design to specifically target therapeutic actions and minimize harmful side effects.

Histone deacetylases are a class of enzymes that are responsible for removing acetyl groups from substrates, including histone tails. Unlike phosphorylation, which is regulated by over 500 kinases and more than 100 phosphatases, the acetylome is written and erased by a set of only 18 acetyltransferases and 18 deacetylases [117].

The traditional function of histone deacetylases, as their name suggests, is to remove acetyl groups from histone tails. Histone acetylation, catalyzed by histone acetyltransferases, is associated with chromatin relaxation and active gene expression [117]. Conversely, deacetylated histones are thought to condense chromatin and suppress gene expression. However, recent work examining the chromatin occupancy of histone deacetylases found enrichment for histone deacetylases at active promoters and a positive correlation between Hdac

occupancy and level gene expression [118]. The authors of this study propose that Hdacs function to regulate acetylation levels at active promoters and may participate in maintaining promoters in primed states to allow for rapid activation of these genes in response to a stimulus [118]. Additionally, Hdacs can regulate gene expression and cell behavior through mechanisms other than histone modification; Hdacs have been shown to deacetylate a variety of non-histone substrates, including transcription factors and cytoplasmic proteins, such as structural filaments [94,117]. Thus, the biologic functions of Hdacs extend well beyond the classical model of histone deacetylation.

Mammalian histone deacetylases are categorized into four classes based on their sequence homology [119]. The predominately nuclear class I Hdacs (Hdac 1, 2, 3, and 8) possess the major deacetylase activity within this gene family [119,120]. By contrast, class IIa Hdacs (Hdac 4, 5, 7, and 9) have up to 1000-fold less deacetylase activity than class I Hdacs due to the presence of a histidine residue rather than a tyrosine in the enzymatic active site [121]. These catalytically inactive Hdacs are known to complex with their more active class I counterparts [121]. Hdac6, a class IIb Hdac, is primarily cytoplasmic, restricting its ability to deacetylate nuclear proteins, such as histones.[120]

Consistent with their important roles as the major active deacetylase enzymes, global deletion of any of the class I Hdacs in mice leads to embryonic or perinatal lethality [119,122-126]. This lethality also suggests a lack of redundancy between class I Hdacs during development. Therefore, it is critical to consider the

functions of each Hdac individually to determine the roles of Hdacs in the context of cardiac development and congenital heart disease.

Hdac8 – a model for class I Hdac involvement in congenital heart disease

As discussed above, mutations in Hdac8, a class I Hdac, are causatively linked to Cornelia de Lange Syndrome [103-106,115]. This syndrome affects multiple organ systems, including the heart. In this context, Hdac8 participates in the cohesin complex, deacetylating SMC3, a non-histone protein, to facilitate recycling and renewal of complex components [103,104]. The established connection between Hdac8 and congenital heart disease substantiates the potential importance of Hdacs in disease pathogenesis.

Beyond its association with Cornelia de Lange Syndrome, very little is known about cardiac functions of Hdac8. First characterized in 2000, Hdac8 is expressed in several adult human tissues, including the heart [127]. Hdac8 exhibits nuclear localization and intrinsic deacetylase activity, allowing for a possible role in transcriptional regulation [127]. However, Hdac8 shares only 37% sequence homology with the other class I Hdacs and is believed to be the least closely related among this class [127]. Unlike the other class I Hdacs, Hdac8 has not been found to act in a co-repressor complex and does not require cofactors or post-translational modifications to facilitate its enzymatic activity [127]. These differences suggest distinct functional roles of class I Hdacs.

Hdac1 and Hdac2 – partial redundancy among Hdacs

The most closely related of all class I Hdacs, Hdac1 and Hdac2 are 83% identical and have been shown to have some functional redundancy [120,128,129]. Deletion of Hdac1 and Hdac2 simultaneously in T-cells or ES cells reduces total Hdac activity by 50%, suggesting that these are major active deacetylases [130,131]. Both of these Hdacs are found in the NuRD, CoREST, and Sin3a repressor complexes, which can associate with Hdac1 and Hdac2 heterodimers or homodimers. Disruption of any one of these complexes in mice leads to early embryonic lethality [132-134].

Despite their suspected redundancy, 40% of Hdac1 exists independent of Hdac2 [135]. For example, the Sin3a complex in T-cells contains predominately Hdac1 homodimers [130]. Interestingly, when Hdac1 is deleted in this T-cells, Hdac2 protein levels increase 2-fold and the mice exhibit only a mild increase in histone acetylation and no discernable T-cell phenotype [130]. In contrast, deletion of one copy of Hdac2 in these Hdac1-null T-cells returns Hdac2 protein expression to wild-type levels, leading to a significant increase in histone acetylation and defects in T-cell differentiation [130]. This demonstrates a retained compensatory relationship between Hdac1 and Hdac2, even in some cases when homodimers are dominant. However, this compensatory relationship is not absolute [130].

During embryonic development, Hdac1 is broadly expressed throughout the embryo, while Hdac2 shows a more restricted pattern, with strong expression in the heart and neural tube during mid-gestation [123,136]. Hdac1 is strongly expressed in pluripotent stem cells and expression levels of Hdac1 fluctuate over the course of ES cell differentiation [137]. Deletion of Hdac1, but not Hdac2, in ES cells affects expression of pluripotency genes and lineage commitment [138]. Consistent with its developmental importance in ES cells, global deletion of Hdac1 in mice results in lethality by E10.5, with widespread proliferation defects and developmental arrest [129,136].

Stem cell studies have revealed that non-redundant roles of Hdac1 impact cardiac differentiation. Hdac1-deficient embryonic stem cells develop into beating embryoid bodies with increased expression of cardiac and neuronal markers [138]. These Hdac1-deficient ES cells show a significant reduction in deacetylase activity of the NuRD, CoREST, and Sin3a complexes and an increase in H3K56 acetylation, indicative of an enzymatically-active role of Hdac1 in this context [138]. Consistent with these findings, administration of Hdac inhibitors to differentiating embryonic carcinoma stem cells increased histone acetylation at the Nkx2-5 locus and induced expression of Nkx2-5, a key transcription factor in cardiac lineage specification [139]. Further investigation revealed that Hdac1 occupies the Nkx2-5 promoter and its expression and occupancy of the Nkx2-5 promoter decrease as the stem cells differentiate into cardiomyocytes. Knockdown of Hdac1 promoted Nkx2-5 transcription and cardiomyocyte differentiation while

overexpression of Hdac1 suppressed both changes. What's more, Hdac1 was found to physically interact with and suppress the transcriptional activity of the Nkx2-5 protein [139]. In this way, Hdac1 regulates differentiation of stem cells into cardiomyocytes by modulating both the expression and activity of Nkx2-5.

As with Hdac1, Hdac2 has non-redundant functions relevant to cardiac development and disease. Global knockout of Hdac2 causes cardiac hypertrophy, with studies reporting either complete or partial neonatal lethality [123,129]. Interestingly, while Hdac2 knockout mice exhibit cardiac hypertrophy and decreased body size at birth compared to littermates, those knockouts that survive beyond the first month of life recover normal cardiac morphology and body size by the age of two months [123]. Furthermore, at this stage Hdac2 deficiency actually protects against hypertrophy and reactivation of the fetal gene program. Correspondingly, overexpression of Hdac2 in cardiomyocytes induced hypertrophy in the mature heart [123].

In embryonic cardiomyocytes, Hdac2 functions together with Hopx to regulate proliferation [140]. Combined deletion of Hdac2 and Hopx leads to complete perinatal lethality, with double knockout pups exhibiting ventricular septal defects, thickened ventricular walls, and a dramatic increase in cardiomyocyte proliferation [140]. In this context, Hopx facilitates the interaction of Hdac2 with Gata4, a key cardiac transcription factor, allowing Hdac2 to deacetylate Gata4 and suppress its transcriptional activity. In doing so, the Hdac2/Hopx complex inhibits expression of Gata4-dependent cell cycle

regulatory genes, thereby controlling cardiomyocyte proliferation [140]. These findings, together with the evidence for the role of Hdac2 in cardiac hypertrophy, suggest critical functions of Hdac2 in regulating the fetal and neonatal gene programs, both developmentally and in adult disease conditions.

In contrast to global deletion, cardiac hypertrophy was not observed upon loss of Hdac2 in any single cardiac cell population, including cardiomyocytes, second heart field, smooth muscle, endothelium, or neural crest [129]. This implies that multiple cell types are involved in the development of cardiac defects associated with Hdac2 deficiency. Similarly, mice lacking Hdac1 in cardiomyocytes, smooth muscle, endothelial cell, or neural crest are all viable [129]. While cardiomyocyte specific deletion of either Hdac1 or Hdac2 is tolerated, combined deletion of both Hdac1 and Hdac2 in cardiomyocytes leads to lethality by P14 [129]. These double knockout mice exhibited cardiomyopathy and conduction defects, with increased expression of cardiac stress markers, consistent with heart failure. Hdac1 and Hdac2 were found to jointly regulate skeletal muscle and calcium channel genes as part of a repressive complex [129]. In this context, Hdac1 and Hdac2 exhibit functional redundancy to regulate cardiac function.

Hdac3 – deacetylase dependent and independent functions in development and disease

While Hdac1 and Hdac2 are found in shared complexes and show both independent and redundant functions, Hdac3 acts in complexes separate from the other class I Hdacs, with non-redundant functions. Hdac3 is enzymatically active, exhibits nuclear localization, and is ubiquitously expressed throughout the developing embryo [141-143]. Global loss of Hdac3 in mice results in lethality by E9.5 due to defects in gastrulation, illustrating its developmental importance [124-126].

Although Hdac3 is known to be enzymatically active and most of its established roles involve deacetylation of substrates, including histones and transcription factors, recent evidence suggests that Hdac3 may have essential functions independent of its deacetylase capacity [144,145]. Hdac3 is found in multi-protein co-repressor complexes with N-CoR or SMRT [141,142,144,145]. Such complexes are necessary for Hdac3's recruitment to the chromatin, as Hdac3 lacks DNA binding ability. In addition to chromatin recruitment, N-CoR and SMRT contain deacetylase-activating domains (DADs), which have been shown to be essential for stimulating the enzymatic activity of Hdac3 [141,145]. However, although global loss of Hdac3 is embryonic lethal, mice with homozygous mutations in the deacetylase-activating domains of both N-CoR and SMRT are viable and live to adulthood [145]. In these mutants, chromatin recruitment of Hdac3 is reduced by nearly 90 percent and immunoprecipitated Hdac3 also shows significantly impaired deacetylase activity [145]. Viability of these mutant mice suggests that Hdac3's enzymatic activity may be developmentally dispensable.

Considering these findings, recent studies have begun to investigate both the deacetylase-dependent and deacetylase-independent functions of Hdac3 during development and disease. One group generated a series of point mutations in Hdac3 that abolish Hdac3's catalytic activity through a variety of mechanisms [144]. They then attempted *in vivo* rescue of liver-specific Hdac3 knockout phenotypes by viral introduction of wild type or deacetylase dead Hdac3. They found that interaction with N-CoR and SMRT was essential for rescuing liver phenotypes, but the catalytic activity of Hdac3 was dispensable [144]. The deacetylase-dead mutants that retained interaction with N-CoR and SMRT could rescue the cellular and molecular defects of liver-specific Hdac3 knockout mice, revealing a deacetylase-independent function of Hdac3 in liver metabolism [144].

Hdac3 has also been shown to be important in muscle and heart development and function, though the deacetylase-dependence of these mechanisms has yet to be explored. During muscle development, Hdac3, stimulated by SMRT, interacts with and deacetylates the transcription factor Mef2d, inhibiting its activity and repressing myogenesis [146]. In the context of heart development, Hdac3 is critical for promoting smooth muscle differentiation of neural crest cells within the cardiac outflow tract [147]. Mice lacking Hdac3 in the neural crest exhibit outflow tract defects, including interrupted aortic arch, and have a lack of smooth muscle cells within the outflow tract [147]. This smooth

muscle differentiation defect is attributed to a reduction in expression of the Notch ligand Jagged1 upon loss of Hdac3 in the neural crest [147].

Hdac3 has also been shown to play important roles in diseases processes affecting the postnatal heart. Mutations in Nkx2-5 are associated with congenital cardiac conduction defects in humans and haploinsufficiency of Nkx2-5 phenocopies these defects in mice [148]. Hdac3 was shown to be involved in regulating Nkx2-5 expression through its recruitment by Prox1 to the Nkx2-5 enhancer in the adult cardiac conduction system [148]. Disruption of Nkx2-5 activity leads to hypoplasia of Purkinje fibers and the atrioventricular node, the conduction components of the heart [148].

While Hdac3 is involved in regulating Nkx2-5 in the cardiac conduction system, deletion of Hdac3 in cardiomyocytes produces no observable arrhythmias or conduction defects [149]. Instead, Hdac3 has myocardial roles in regulating proliferation and cardiac metabolism. Mice with myocardial-specific deletion of Hdac3 are born in Mendelian ratios, but develop hypertrophy within four weeks which worsens until the mice succumb to heart failure and die by four months of age [149]. This phenotype was accompanied by up-regulation of genes involved in fatty acid metabolism, which is linked to increased activity of PPARα [149]. Upon fasting, lipids accumulate within myocardium of Hdac3 knockout hearts, consistent with disrupted cardiac metabolism [149]. Interestingly, postnatal deletion of Hdac3 in the cardiac and skeletal muscle does not recapitulate this lethal heart failure phenotype, suggesting a developmental importance for Hdac3 in

cardiomyocytes [150]. Mice with postnatal deletion of Hdac3 in cardiac and skeletal muscle survive normally on a chow diet, but are sensitive to high fat diet-induced hypertrophic cardiomyopathy and heart failure [150]. These mice die within weeks of switching to a high fat diet, exhibiting increased heart size, cardiac hypertrophy, and fibrosis, with down-regulation of genes associated with lipid metabolism [150]. In this way, Hdac3 is important in mediating the cardiac metabolic response to changes in diet.

Not only is loss of Hdac3 in damaging to cardiac health, but overexpression of Hdac3 in cardiomyocytes is also detrimental to cardiac development. Transgenic overexpression of Hdac3 in cardiomyocytes results in severe hyperplasia that nearly obliterates the ventricular lumens of murine hearts at birth [151]. The thickened cardiac walls exhibit increased myocyte proliferation without altering myocyte cell size. Hdac3 acts within cardiomyocytes to regulate proliferation through suppression of the Cdkn1a, a cyclin-dependent kinase inhibitor [151]. Interestingly, as is observed in the case of Hdac2 and cardiac hypertrophy, the cardiomyocyte proliferation and hyperplasia of Hdac3 transgenic hearts resolves by two months of age [151]. Furthermore, trisomy 5q31.1q35.1, which involves duplication of the genomic region surrounding and including Hdac3, has been reported in a patient with complex congenital heart disease, including interrupted aortic arch and septal defects, suggesting a possible involvement of Hdac3 copy number in human congenital heart disease [152]. Together, the current knowledge of Hdac3 in the heart suggests multiple cell

type, stage-specific, and dose-dependent requirements for Hdac3 in cardiac development and function.

Aims of this work

While its roles in the neural crest, conduction system, and myocardium have been investigated, developmental functions of Hdac3 within the mesodermal cardiac progenitor cells have not previously been explored. This thesis aims to fill in this gap in understanding by examining the roles of Hdac3 in the first heart field and second heart field progenitor cells. Distinct developmental and postnatal requirements for Hdac3 in cardiomyocytes argue that Hdac3 has evolving functions as an organism develops and matures. The work presented in this thesis expands on this theme, describing separate roles of Hdac3 in the primary heart field and second heart field. Furthermore, these findings reveal novel mechanisms for Hdac3 relevant to congenital heart disease etiology, including both deacetylase-dependent and deacetylase-independent functions of Hdac3.

Chapter II: Histone deacetylase 3 modulates Tbx5 activity to regulate early cardiogenesis

Chapter II is adapted from a published manuscript to include supplemental data and is included with permission:

Lewandowski SL, Janardhan HP, Smee KM, Bachman M, Sun Z, Lazar MA, and Trivedi CM. (2014). Histone deacetylase 3 modulates Tbx5 activity to regulate early cardiogenesis. *Human Molecular Genetics*, 23(14), 3801-3809.

Author contributions:

I provided all data shown in figure 2.1 A, D, E, and G-K, figure 2.2 A-D, figure 2.3 A-C, figure 2.4 J, and figure 2.5 A, B, E, K, and N. In addition, I provided the model in figure 2.4 B, promoter analysis and primer design relevant to figure 2.2 E-F, generated the TBX5 mutants used in figure 2.4 H-F, figure 2.5 C-D, G-H, and L-M, prepared lentiviruses relevant to figure 2.2 F-I, figure 2.3 D-F, and figure 2.4 K. I conducted the mouse breeding relevant to figure 2.2 E-I, figure 2.3 D-F, and figure 2.4 K and provided the data in table 2.1 and table 2.2. Harish P. Janardhan developed the immunoprecipitation protocol used in figure 2.4 A, and C-I, and figure 2.5 C-D, F-H, and L-M. Kevin M. Smee performed the sequence analysis in figure 2.5 I and purified the HDAC3 protein used in figure 2.4 E. Marcos Bachman assisted in generating the HDAC3 terminal deletion constructs

used in figure 2.4 B-F. Zheng Sun and Mitchell A. Lazar provided the Hdac3 ChIP-seq dataset seen in figure 2.2 A-E. Chinmay M. Trivedi performed the experiments in figure 2.1 B, C, and F, figure 2.2 E-I, figure 2.3 D-H, figure 2.4 A, C-I, and K, figure 2.5 C-D, F-H, and L-M, constructed the cartoon model in figure 2.6, and supplied the data in tables 2.3 and 2.4.

Abstract

Congenital heart defects often result from improper differentiation of cardiac progenitor cells. Although transcription factors involved in cardiac progenitor cell differentiation have been described, the associated chromatin modifiers in this process remain largely unknown. Here we show that mouse embryos lacking the chromatin modifying enzyme histone deacetylase 3 (Hdac3) in cardiac progenitor cells exhibit precocious cardiomyocyte differentiation, severe cardiac developmental defects, up-regulation of Tbx5 target genes, and embryonic lethality. Hdac3 physically interacts with Tbx5 and modulates its acetylation to repress Tbx5-dependent activation of cardiomyocyte lineage-specific genes. These findings reveal that Hdac3 plays a critical role in cardiac progenitor cells to regulate early cardiogenesis.

Introduction

Multipotent cardiac progenitor cells are specified during the early stages of gastrulation from lateral plate mesoderm in the murine embryo [153]. Around embryonic day 7.0 (E7.0), these cells migrate to form the cardiac crescent, which contains two populations of cardiac progenitors, the first and second heart fields [24]. The cells of the cardiac crescent migrate medially to form a single linear heart tube, which subsequently gives rise to a four-chambered heart [25]. During this process, multipotent cardiac progenitor cells differentiate into various endpoint lineages including cardiomyocytes, smooth muscle cells, endothelial cells, and specialized conduction cells [154-156]. For instance, Nkx2-5-positive bipotent cardiac progenitor cells give rise to cardiomyocytes and smooth muscle cells [157].

Despite recent progress in identifying cardiac progenitor cells, the epigenetic and chromatin modifiers regulating progenitor cell fate specification are poorly defined [158]. Site-specific histone modifications, like acetylation and methylation, regulate chromatin structure and provide a signal to recruit lineage-defining transcription factors [159]. For instance, histone acetyltransferase (HAT)-mediated acetylation of core-histones leads to relaxation of the chromatin structure and subsequent recruitment of transcription factors for gene activation. Conversely, histone deacetylase (Hdac)-dependent deacetylation leads to chromatin condensation and gene repression [119].

The mammalian Hdacs are classified into four sub-families based on their conserved sequences and structure [160]. Class I Hdacs (Hdac1, 2, 3, and 8) are ubiquitously expressed and play critical roles during development [119]. For

example, we demonstrated that global loss of Hdac2 in mice causes severe cardiac developmental defects including cardiomyocyte hyperplasia [161]. Global deletion of Hdac3 results in embryonic lethality around E9.5 [124,125]. In a tissue-specific context, Hdac3 regulates lipid metabolism and mitochondrial functions in the adult heart [124,150].

Hdacs lack intrinsic DNA binding ability and are recruited to target genes via their incorporation into large multi-protein transcriptional complexes as well as direct association with transcriptional activators or repressors [160]. For instance, our recent findings show that Hdac2 interacts with Gata4 and inhibits its acetylation and transcriptional activity to regulate embryonic cardiomyocyte proliferation [140]. Several evolutionarily conserved transcription factors from the T-box, GATA, b-HLH, MADS box, and homeodomain families are expressed in cardiac progenitor cells and regulate various stages of cardiogenesis [162]. With regards to the T-box family, Tbx5 gain or loss-of-function mutations can result in Holt-Oram syndrome, characterized by the presence of atrial and ventricular septal defects [20,30]. Recent reports demonstrate that gain-of Tbx5 function in progenitor cells induces precocious differentiation into spontaneously beating cardiomyocytes, suggesting a lineage-defining role for Tbx5 during early cardiogenesis [44,163]. However, how Tbx5 activity is regulated during cardiomyocyte lineage specification remains largely unknown.

Here we show that cardiac progenitor cell-specific loss of Hdac3 in mice leads to complete embryonic lethality, precocious cardiomyocyte differentiation,

and severe cardiac developmental defects. Hdac3 regulates Tbx5 acetylation and activation of Tbx5-dependent cardiomyocyte lineage-specific genes. Our results suggest a novel cardiac progenitor cell-specific function of ubiquitously expressed Hdac3 during early developmental stages of cardiogenesis.

Material and methods

Mice - Transgenic *Nkx2-5* Cre and *Hdac3*^{Flox} mice have been previously described [164,165]. *Myh6*-Cre (αMHC-Cre) mice were obtained from The Jackson Laboratory. The University of Massachusetts Medical School Institutional Animal Care and Use Committee approved all animal protocols.

Cell culture, transient transfection and luciferase assays - HEK293T cells were maintained in DMEM with 10% FBS, 100 μg/ml penicillin, and 100 μm/ml streptomycin in a 37C incubator with 5% CO_2. Hearts from E8.5 mouse embryos were collected in DMEM with 10% FBS and plated on gelatin-coated dishes. Sub-confluent HEK-293T cells were transfected in 100-mm plates with 12.5μg of DNA and 25μl of Polyethylenamine, linear, in 10 ml of 10% FBS medium. Luciferase assays were conducted by transfecting sub-confluent HEK-293T cells in 6-well plates with 1μg of DNA and 2μl of Polyethylenamine, linear, in 2ml of 10% FBS media. DNA amount was maintained constant using pcDNA3.1$^{(-)}$ or pLJM1-EGFP DNA. Cells were lysed with passive lysis buffer 16 hours after

transfection and lysates were analyzed using a dual luciferase reporter assay kit according to manufacturers guidelines. Luciferase activity was measured using an Omega microplate reader according to manufacturer's guidelines.

GST protein purification - Cultures of transformant *E. coli* were grown to an optical density at 600 nm (OD_{600}) between 0.6 and 0.8. Transformants were induced upon reaching appropriate OD_{600} with 0.1 mM isopropyl-β-D-thiogalactopyranoside (IPTG) for 2 hours at 37°C. Fusion proteins were bound to GST bead slurry and eluted by Thrombin cleavage for 16 hours at 22°C with 10 units of Thrombin enzyme.

In vitro acetylation assay - TBX5 protein, purified from *E. coli*, was incubated with 600ng P300-HAT domain, 1mM Acetyl-CoA, 50μM TSA, and 50mM Nicotinamide in HAT Buffer (50nM Tris-HCl, pH8, 0.1mM DTT, 10% glycerol) for one hour at 30°C. Acetylated protein was resolved by SDS-PAGE and analyzed by Western blot.

Plasmids and site-directed mutagenesis - To generate luciferase reporters, tandem repeats of Tbx5 (CTGAGGTGTGAG) or Nkx2-5 (CCACTTAA) consensus binding sites were subcloned from pIDT-SMART to pLuc-MCS using BglII and HindIII. HDAC3-Flag has been previously described [166]. The TBX5 lentiviral vector was generated by PCR-amplifying TBX5 cDNA from TBX5

PCMV-SPORT6 (Open Biosystems), subcloning into pCRII-TOPO (Life Technologies), and finally into pLJM1 (Addgene plasmid 19319) [167] using NheI and EcoRI. To construct GST-HA-TBX5 bacterial expression vector, HA- TBX5 was PCR amplified from TBX5 PCMV SPORT6, cloned into pCRII-TOPO (Life Technologies), and subcloned to pGEX4T1 (GE Life Sciences) using EcoRI. The HDAC3 lentiviral vector was generated by subcloning Flag-HDAC3 cDNA to CSCGW2 using NheI and XhoI. Tbx5 and scrambled shRNA lentiviral vectors were obtained from the University of Massachusetts shRNA core facility. GFP lentiviral vector was obtained from Addgene (Addgene plasmid 15949) [168]. Lentiviral packaging plasmids were obtained from Addgene: pCMV-dR8.2 (Addgene plasmid 8455) and pCMV-VSVG (Addgene plasmid 8454) [169]. EP300 was obtained from Addgene (Addgene plasmids: 30489 and 10717). Nkx2-5 was obtained from Open Biosystems. Hdac1-Flag was obtained from Addgene (Addgene plasmid 13820) [143]. KAT5 has been previously described [170]. KAT2B was obtained from Addgene (Addgene plasmid 8941) [171]. C-terminal deletions of TBX5 were generated by PCR amplification from HA-TBX5 pLJM1. An internal deletion of TBX5 was generated from HA-TBX5 pLJM1 by nested PCR. Deletion constructs were cloned into pCR2.1 TOPO and subcloned to pcDNA3.1(-) (Life Technologies). $TBX5^{G125R}$ and $TBX5^{K157A, K159A}$ were generated by site-directed mutagenesis as per manufacturers protocol, using TBX5 pCRII-TOPO as a template. $TBX5^{G125R}$ was used as a template to generate $TBX5^{G125R,}$

$^{K157A, K159A}$ by site-directed mutagenesis. All plasmids were verified by restriction analysis, sequencing, and Western blot analysis.

Antibodies and reagents - The following antibodies were used in this study: Hdac3 (Abcam, Santa Cruz), Tbx5 (Santa Cruz), Myh7 (Santa Cruz), phospho-histone H3 (Cell Signaling), cleaved caspase-3 (Cell Signaling), acetylated lysine (Cell Signaling, Millipore), HA (Santa Cruz), Troponin (Hybridoma bank, Iowa), Nkx2-5 (Abcam), Gapdh (Millipore), HRP-conjugated secondary antibodies (Santa Cruz), IRDye-conjugated secondary antibodies (Licor), and Alexa Fluor® 488/546-conjugated secondary antibodies (Life Technologies). Paraformaldehyde, paraffin, Harris Modified Hematoxylin, and Eosin-Y were purchased from Fisher Scientific. Vectastain Elite ABC Kit, DAB Peroxidase Substrate Kit, and VectaShield Mounting Medium were purchased from Vector Laboratories. Donkey serum, fetal bovine serum, gelatin, nicotinamide, acetyl-CoA, and magnetic anti-flag beads were purchased from Sigma. Horse serum, Trizol, Superscript First Strand Synthesis Kit, CellsDirect^{TM} One-Step qRT-PCR Kit, Power SYBR Green PCR Master Mix, DMEM high glucose with Na pyruvate, and Pen/Strep were purchased from Life Technologies. QuikChange II XL Site-Directed Mutagenesis Kit was purchased from Stratagene. Passive lysis buffer and dual-luciferase reporter assay kit were purchased from Promega. Agarose IgG and IgA bead slurry were purchased from Santa Cruz and Life Technologies. P300-HAT domain was purchased from Millipore. EZ-ChIP assay kit and

Trichostatin A (TSA) were purchased from Millipore. GST bead slurry was purchased from Qiagen. Polyethylenamine, linear was purchased from Polysciences.

Histology, Immunohistochemistry, and Immunofluorescent staining

Embryos were fixed overnight in 2% paraformaldehyde at 4°C, ethanol dehydrated, embedded in paraffin, and sectioned at 6 μm thickness using a microtome. Hematoxylin and eosin staining was conducted by deparaffinizing and rehydrating sections, two minute incubation in Harris Modified Hematoxylin and 30 second Eosin-Y stain. Slides were rinsed and dehydrated with ethanol and mounted using Vectashield mounting medium. For immunohistochemistry and immunofluorescent staining, sections were deparaffinized and pre-treated using heat antigen retrieval with 10mM sodium citrate, 0.05% Tween 20. Immunohistochemistry was performed using Vectastain Elite ABC Kit and DAB Peroxidase Substrate Kit according to manufacturers guidelines. Sections were incubated with primary antibodies against Hdac3 (1:500) or cleaved caspase-3 (1:100) for one hour at room temperature. Slides were counter-stained with hematoxylin for two minutes and mounted with Vectashield mounting medium. For immunofluorescent staining, samples were blocked with 10% donkey serum and 0.3% Triton X- 100 in 1X PBS for one hour at room temperature. After washing with PBS, samples were incubated with Myh7 (1:50) and phospho-histone H3 (1:100) antibodies for one hour at room temperature or Troponin

(1:25) and Nkx2-5 (1:50) antibodies for overnight at 4°C. The samples were washed with PBS and incubated for one hour with secondary antibodies: 1:500 donkey anti-mouse, 1:500 donkey anti-rabbit, 1µg/mL Hoechst in 10% donkey serum. Slides were then washed with PBS and mounted with Vectashield mounting medium.

Proliferation assay - Sections from three *Hdac3*$^{Nkx2\text{-}5KO}$ and three control E8.5 embryos were immunostained with Myh7 and phospho-histone H3 antibodies and Hoechst nuclear stain. Images were taken of each heart section at 40X magnification and images were compiled using ImageJ. The total number of nuclei and phospho-histone H3-positive nuclei in Myh7-positive cells were counted using ImageJ; the percentage of Myh7-positive nuclei that were phospho-histone H3 positive was used as a proliferation index.

Apoptosis assay - Five sections from three *Hdac3*$^{Nkx2\text{-}5KO}$ and three control E8.5 embryos were immunostained with cleaved caspase-3 antibody and counterstained with hematoxylin. Images of the hearts were taken at 20X magnification. The total number of nuclei and the number of cleaved caspase-3 nuclei were counted in the heart wall. The number of cleaved caspase-3 positive nuclei per 1000 nuclei was used as an index of apoptosis.

Differentiation assay - Sections from three *Hdac3*$^{Nkx2\text{-}5KO}$ and three control E8.5 embryos were immunostained with Myh7 or Troponin and Nkx2-5 antibodies. Hoechst was used to stain the nuclei. Images were taken of each heart section at 40X magnification. Images were compiled using ImageJ. The number of Myh7-positive cells relative to the total number of nuclei in the cardiac wall was used as a differentiation index. The number of Nkx2-5^{+}, Troponin-negative cells relative to the total Nkx2-5^{+} cells in the cardiac wall was used as a differentiation index.

Real Time quantitative PCR - Total RNA was isolated from cardiac cells using the CellsDirect^{TM} One-Step qRT-PCR Kit according to manufacturers guidelines. Total RNA was isolated from dissected mouse heart using Trizol. RNA was reverse transcribed using random hexamers and the Superscript First Strand Synthesis Kit. Gene expression was measured by qRT-PCR using SYBR Green PCR Master Mix. Signals were normalized to their corresponding Gapdh controls, and ratios were expressed as relative expression compared to wild-type controls. PCR conditions and primer set sequences are available upon request.

Western blotting - Tissue and cell lysates were prepared in lysis buffer consisting of 20mM Tris HCl (pH 7.5), 15mM NaCl, 1mM Na_2EDTA, 1mM EGTA, 1% Triton X-100, 1 µg/mL leupeptin, 2.5mM sodium pyrophosphate, 1mM

Na_3VO_4, and 1mM β-glycerophosphate; 1mM phenylmethylsulfonyl fluoride was added before use. Protein samples were resolved by 4-12% SDS-PAGE acrylamide gel and transferred to PVDF (poly-vinylidene difluoride) membranes. We used primary antibodies to Hdac3 (1:1000), Tbx5 (1:500), acetylated lysine (1:1000), and HA (1:1000). Primary antibodies were visualized by chemiluminescence with HRP-conjugated secondary antibodies or by infrared using IRDye®-conjugated secondary antibodies. Blots were stripped and reprobed with Gapdh (1:1000) as a loading control.

Immunoprecipitation - Embryonic heart samples or 293T cells were homogenized in immunoprecipitation buffer (50mM Tris-HCl [pH 8.0], 150mM NaCl, 0.5% Nonidet P-40, 1mM EDTA, and 1mM DTT) containing 1mM PMSF, phosphatase inhibitors (Sigma), and protease inhibitors mixture (Sigma). The samples were sonicated using Branson 250 Digital Sonifier with 1s ON and 1s OFF pulses at 40% power amplitude for 15s. The lysates were collected by centrifugation at 16,000g for 10min at 4°C. Precleared lysates with beads were incubated with primary antibodies for 16hrs at 4°C. After incubation for 1hr at 4°C with beads, immune-complexes were collected, washed four times with immunoprecipitation buffer, and applied to 4-12% SDS-polyacrylamide gels for western blot analysis. Efficacy of immunoprecipitation was determined by western blot for the immunoprecipitated protein. To measure acetylation of TBX5, total cell lysates were prepared from isolated cardiac tissue or transfected 293T

cells (48hrs post-transfection) using acetylation assay buffer (20mM Tris-HCl [pH 7.5], 150mM NaCl, 1mM Na_2EDTA, 1mM EGTA, 1% Triton X- 100, 2.5mM sodium pyrophosphate, 1mM β-glycerophosphate, 1mM Na_3VO_4, 1µg/ml leupeptin, 1mM PMSF, and 20mM Na-butyrate).

Lentiviral infection - Subconfluent 293T cells were transfected in 100mm plates with 5µg of lentiviral cDNA, 5µg of pCMV-dR8.2, and 2.5µg of pCMV-VSVG, in 10ml of 2% FBS media. Viral media was collected 48 hours after transfection and filtered through a 40 µm cell strainer. Isolated mouse embryonic hearts were infected with filtered viral media with 10µg/ml polybrene reagent. The volume of viral media was maintained constant using GFP viral media. Infected cells were harvested 24- hours post-infection.

Binding site overlap of Hdac3 and cardiac transcription factors - We identified consensus Hdac3 binding motif within 10kb upstream of the transcriptional start site of four cardiomyocyte-specific genes: *Tnnt1, Tnnt2, Tnni2, and Myh7*. Real-time PCR primers were designed for each of these Hdac3 sites and binding of Hdac3 to these regions was evaluated by ChIP-qPCR from E8.5 mouse hearts. Regions of Hdac3 enrichment were mapped to the mm9 mouse genome. We obtained ChIP-seq datasets for Tbx5, Nkx2-5, Gata4, Srf, and Mef2a from the NCBI Gene Expression Omnibus (GEO) website (accession: GSE21529) and aligned on the mm9 mouse genome and converted to the mm8

assembly using UCSC genome browser with liftOver tool to map along with regions of Hdac3 enrichment. To measure the degree of overlap between Hdac3 and each transcription factor, we determined the percentage of Hdac3 enrichment sites that overlapped with the transcription factor ChIP-seq peaks.

Chromatin immunoprecipitation (ChIP) analysis - ChIP experiments were carried out as previously described [172-174]. Briefly, isolated cardiac tissue or cells from E8.5 mouse embryos were cross-linked in cross-linking solution (1% formaldehyde, 1.5mM EGS, 20mM Na-butyrate, 10% FBS) for 15 min, followed by quenching with 125mM glycine solution for 5 min and two washes with 1X PBS. Chromatin fragmentation was performed by sonication in ChIP SDS lysis buffer (50mM Tris-HCl pH 8.0, 10mM EDTA, 1% SDS, 1X Protease Inhibitors), using the Branson Sonifier 250 (40% power amplitude, 110s). Proteins were immunoprecipitated in ChIP dilution buffer (0.01% SDS, 1.1% Triton X-100, 1.2mM EDTA, 16.7mM Tris-HCl pH 8.0, 167mM NaCl, 20mM Na-butyrate, 1X protease inhibitor) using IgG, Hdac3 or Tbx5 antibodies. IgG antibody was used to determine specificity of Hdac3 or Tbx5 antibodies at the relevant locus. Antibody-chromatin complexes were washed two times with low salt wash buffer (20 mM Tris-HCl pH 8.0, 150mM NaCl, 2mM EDTA, 0.1% SDS, and 1% Triton X-100) followed by two washes with lithium chloride wash buffer (10mM Tris-HCl pH 8.0, 250mM LiCl, 1mM EDTA, 1% deoxycholate, and 1% Nonidet P-40) and TE buffer (10mM Tris-HCl pH 8.0, and 1mM EDTA). After removing wash buffer,

cross-linking was reversed overnight at 65°C using Proteinase K buffer (20mM Tris-HCl pH7.5, 5mM EDTA, 50mM NaCl, 1% SDS, 20mM Na-butyrate, 50µg/ml Proteinase K). The next day, DNA was purified using phenol/chloroform/isoamyl alcohol. Precipitated DNA was analyzed by real-time quantitative PCR as previously described [165,174,175]. Enrichment of target sequences was measured by RT-PCR using primers designed against predicted Hdac3 binding motifs in the 10 kb upstream of the transcription start site of four cardiomyocyte-specific genes: *Myh7, Tnni2, Tnnt1,* and *Tnnt2*. Relevant locus of Traf or Supth was used as a negative control for Tbx5 binding. Relevant locus of Supth was used as a negative control for Hdac3 binding. PCR conditions and primer set sequences are available upon request.

Hdac3 ChIP-seq analysis - ChIP-seq of HDAC3 in adult mouse heart was conducted as described previously [176]. Briefly, hearts were grounded in liquid N2 and cross-linked in 1% Formaldehyde for 20 min. Whole cell extracts were sonicated followed by immunoprecipitation with HDAC3 antibodies (Abcam). The precipitated DNA from independent ChIP of 4 difference mice were then pooled and amplified according to the guideline of Illumina, followed by deep sequencing on Illumina Genome Analyzer IIx. ChIP-seq results were mapped to mouse genome (mm8) using Bowtie v0.12.8. Peak calling was carried out by HOMER v4.2 (FDR 0.1%) using uniquely mapped reads.

Acetylation site prediction - The TBX5 cDNA sequence was retrieved from PubMed (accession: BC027942). A predicted protein product was generated using the MacVector translation tool. Acetylation site predictions were made using three software programs: PAIL, under medium stringency, Premod, and Phosida. For analysis using Premod, the sequence was split in two parts (residues 1-224 and 225-518). To assess conservation of predicted acetylation sites, cDNA sequences were retrieved from PubMed, translated using MacVector translation tool, and aligned using ClustalW in MacVector software.

Statistical analysis - Statistical significance between groups was assessed using two-tailed Student's *t* test or χ^2 test. A *P* value of < 0.05 was considered significant.

Results

Loss of Hdac3 in cardiac progenitor cells results in embryonic lethality and severe cardiac developmental defects

Hdac3 is ubiquitously expressed in the developing heart (Fig. 2.1A). Germline deletion of Hdac3 results in embryonic lethality at E9.5 [125,177]. To determine the function of Hdac3 during early cardiogenesis, we used Nkx2.5-driven Cre recombinase to delete Hdac3 in cardiac progenitor cells (*Hdac3*$^{Nkx2\text{-}5KO}$). *Hdac3*$^{Nkx2\text{-}5KO}$ mice were not identified at birth (P0), indicating complete

Figure 2.1

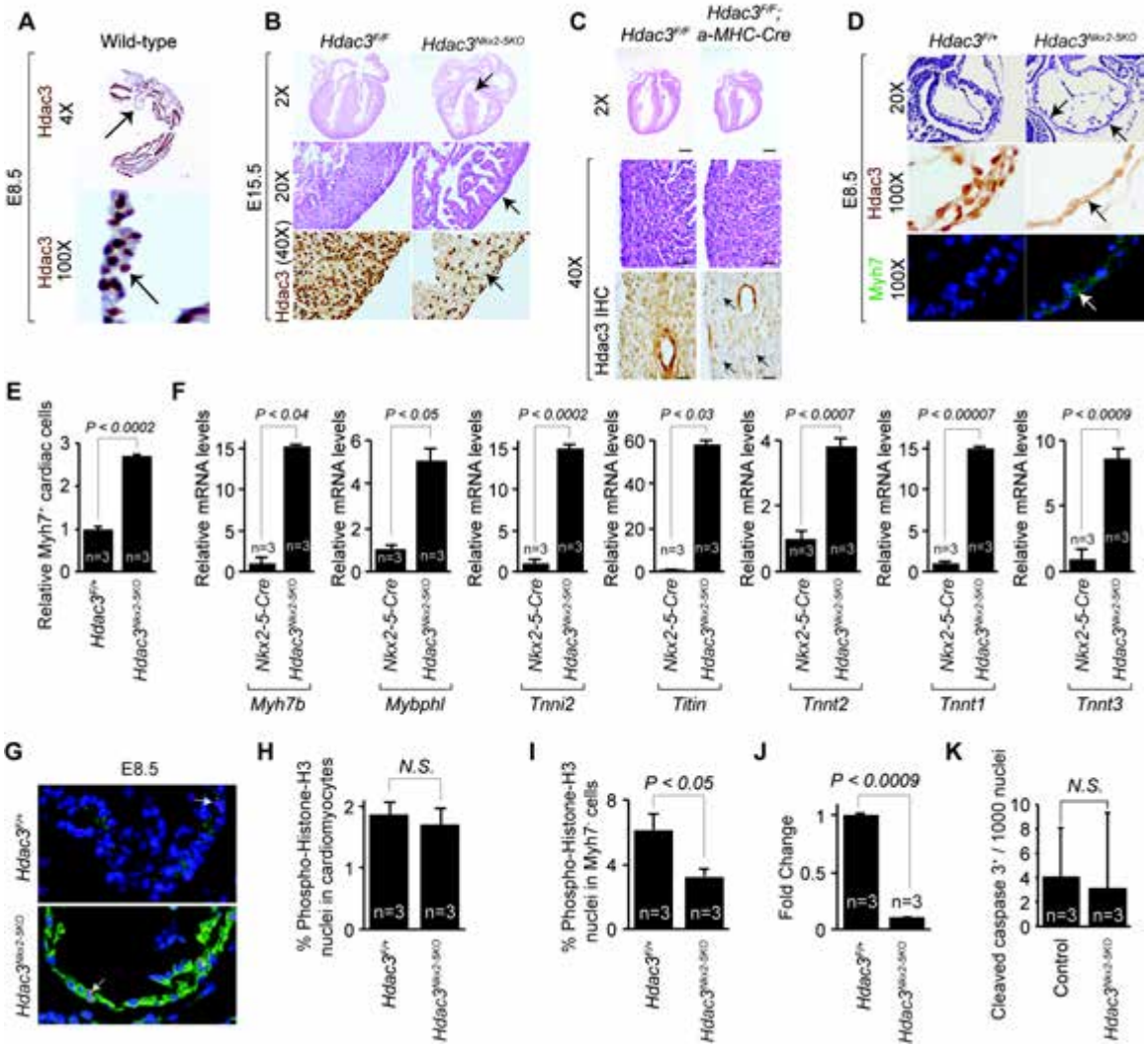
A
Wild-type
E8.5
Hdac3 4X
Hdac3 100X
B
Hdac3F/F
Hdac3Nkx2-5KO
E15.5
2X
20X
Hdac3 (40X)
C
Hdac3F/F
Hdac3F/F; a-MHC-Cre
2X
40X
Hdac3 IHC
D
Hdac3F/+
Hdac3Nkx2-5KO
20X
E8.5
Hdac3
100X
Myh7
100X
E
Relative Myh7+ cardiac cells
P < 0.0002
n=3
Hdac3F/+
Hdac3Nkx2-5KO
F
Relative mRNA levels
P < 0.04
P < 0.05
P < 0.0002
P < 0.03
P < 0.0007
P < 0.00007
P < 0.0009
Nkx2-5-Cre
Hdac3Nkx2-5KO
Myh7b
Mybphl
Tnni2
Titin
Tnnt2
Tnnt1
Tnnt3
G
E8.5
Hdac3F/+
Hdac3Nkx2-5KO
H
% Phospho-Histone-H3 nuclei in cardiomyocytes
N.S.
I
% Phospho-Histone-H3 nuclei in Myh7+ cells
P < 0.05
J
Fold Change
P < 0.0009
K
Cleaved caspase 3+ / 1000 nuclei
N.S.
Control

Figure 2.1: Developmental myocardial defects due to loss of Hdac3 in Nkx2-5^{+} cardiac progenitor cells. (A) Hdac3 expression was determined in E8.5 murine embryo (top) and heart (bottom) by immunohistochemistry. Arrow indicates expression of ubiquitous Hdac3. **(B)** Hematoxylin and eosin-stained sections demonstrate membranous ventricular septal defect (top, arrow) and hypoplastic ventricular myocardium (middle, arrow) in *Hdac3$^{Nkx2\text{-}5KO}$* E15.5 hearts. Immunohistochemistry staining of Hdac3 shows loss of Hdac3 in cardiac cells derived from Nkx2-5^{+} progenitor cells (bottom, arrow). **(C)** Hematoxylin and eosin-staining section of the P0 hearts from *Hdac3$^{F/F}$* and *Hdac3$^{F/F}$;αMHC-Cre* mice demonstrate normal ventricular septum and myocardium (top, middle). Immunohistochemistry staining of Hdac3 shows loss of expression in differentiated cardiomyocytes (bottom, arrows). **(D)** Hematoxylin and eosin-stained sections demonstrate abnormally hypoplastic ventricular myocardium in *Hdac3$^{Nkx2\text{-}5KO}$* E8.5 hearts (top, arrow). Hdac3 immunohistochemistry shows loss of expression in *Hdac3$^{Nkx2\text{-}5KO}$* E8.5 hearts (middle, arrow) compared to control. Precocious cardiomyocyte differentiation was assessed by Myh7 immunofluorescent staining (green, bottom, arrow) in *Hdac3$^{F/F}$* and *Hdac3$^{Nkx2\text{-}5KO}$* E8.5 hearts. **(E)** Quantification of Myh7^{+} cells in Hdac3$^{F/+}$ and *Hdac3$^{Nkx2\text{-}5KO}$* E8.5 hearts (mean ± SEM, n=3). **(F)** Transcripts for *Myh7*, *Mybphl, Tnni2, Titin, Tnnt2, Tnnt1,* and *Tnnt3* were detected by real-time qPCR in *Nkx2-5*-Cre and *Hdac3$^{Nkx2\text{-}5KO}$* hearts derived from E8.5 embryos (mean ± SEM, n=3). **(G)** Cardiomyocyte (green, stained by Myh7) proliferation was assessed by phospho-histone H3 co-staining (red, arrows) in *Hdac3$^{F/+}$* and *Hdac3$^{Nkx2\text{-}5KO}$* E8.5 hearts. **(H)** Quantification of phospho-histone H3 positive, Myh7+ in *Hdac3$^{F/+}$* and *Hdac3$^{Nkx2\text{-}5KO}$* E8.5 hearts (mean $\pm$ SEM, n=3). *N.S.*, not significant. **(I)** Quantification of phospho-histone H3 positive, Myh7- cells in *Hdac3$^{F/+}$* and *Hdac3$^{Nkx2\text{-}5KO}$* E8.5 hearts (mean $\pm$ SEM, n=3). **(J)** The population of undifferentiated cardiac progenitor cells (Nkx2-5+, Troponin-negative) was assessed by Troponin and Nkx2-5 co-immunostaining in *Hdac3$^{F/+}$* and *Hdac3$^{Nkx2\text{-}5KO}$* E8.5 hearts. The number of Nkx2-5+, Troponin-negative cells relative to the total Nkx2-5+ cells in the cardiac wall was used as a differentiation index.

embryonic lethality (Table 2.1). *Hdac3*$^{Nkx2\text{-}5KO}$ embryos displayed significant lethality as early as E11.5 (Table 2.2, 2.3). However, some *Hdac3*$^{Nkx2\text{-}5KO}$ embryos were identified until mid-gestation (Fig. 2.1B, Table 2.3). *Hdac3*$^{Nkx2\text{-}5KO}$ embryos were characterized by cardiac defects such as hypoplastic ventricular walls and membranous ventricular septal defects (Fig. 2.1B-C). Interestingly, genetic deletion of *Hdac3* using α*MHC-Cre,* which is expressed in differentiated cardiomyocytes at E9.5 [178]*,* did not reveal any embryonic lethality or developmental cardiac defects (Fig. 2.1D, Table 2.4) [124]. Together, these data suggest a primary role of Hdac3 in cardiac progenitor cells during early cardiogenesis.

Cardiomyocyte marker immunostaining revealed a significant increase in precociously differentiated cardiomyocytes (Fig. 2.1C, 2.1E). Consistent with these findings, we observed robust precocious expression of cardiomyocyte lineage-specific genes, including *Myh7*, *Tnni2*, *Tnnt1*, and *Tnnt2*, in E8.5 *Hdac3*$^{Nkx2\text{-}5KO}$ hearts compared to control (Fig. 2.1F). We did not observe proliferation or apoptosis defects in differentiated *Hdac3*$^{Nkx2\text{-}5KO}$ cardiomyocytes at E8.5 (Fig. 2.1G-K). These results suggest that Hdac3 represses differentiation of cardiac progenitor cells and expression of cardiomyocyte lineage-specific genes during early cardiogenesis.

Table 2.1

Genotyping of *Nkx2-5-Cre; Hdac3$^{F/+}$* x *Hdac3$^{F/+}$*

Age: P0

	Observed	Expected	
Hdac3$^{+/+}$	9	9	
Hdac3$^{F/+}$	24	18	
Hdac3$^{F/F}$	10	9	
Nkx2-5-Cre; Hdac3$^{+/+}$	11	9	
Nkx2-5-Cre; Hdac3$^{F/+}$	18	18	
Nkx2-5-Cre; Hdac3$^{F/F}$	**0**	9	$P < 0.04$
Total	72	72	

Table 2.2

Genotyping of *Nkx2-5-Cre; Hdac3$^{F/+}$* x *Hdac3$^{F/F}$*

Age: E9.5

	Observed	Expected	
Hdac3$^{F/+}$	42	28	
Hdac3$^{F/F}$	25	28	
Nkx2-5-Cre; Hdac3$^{F/+}$	23	28	
Nkx2-5-Cre; Hdac3$^{F/F}$	22	28	$P < 0.03$
Total	112	112	

Table 2.3

Genotyping of *Nkx2-5-Cre; Hdac3$^{F/+}$* x *Hdac3$^{F/+}$*

Age: E11.5-E12.5

	Observed	Expected	
Hdac3$^{+/+}$	20	16	
Hdac3$^{F/+}$	37	32	
Hdac3$^{F/F}$	18	16	
Nkx2-5-Cre; Hdac3$^{+/+}$	19	16	
Nkx2-5-Cre; Hdac3$^{F/+}$	31	32	
Nkx2-5-Cre; Hdac3$^{F/F}$	3	16	$P < 0.02$
Total	128	128	

Table 2.4

Genotyping of a*MHC-Cre; Hdac3$^{F/+}$* x *Hdac3$^{F/+}$*

Age: P0

	Observed	Expected	
Hdac3$^{+/+}$	5	5	
Hdac3$^{F/+}$	10	11	
Hdac3$^{F/F}$	5	5	
a*MHC-Cre; Hdac3$^{+/+}$*	5	5	
a*MHC-Cre; Hdac3$^{F/+}$*	11	11	
a*MHC-Cre; Hdac3$^{F/F}$*	6	5	$P < 0.9$
Total	42	42	

Hdac3 represses Tbx5-dependent transactivation during early cardiogenesis

We next explored the mechanism of cardiomyocyte lineage-specific gene regulation by Hdac3 during early cardiogenesis. We identified chromatin occupancy of Hdac3 in the conserved noncoding regions within 10 kb upstream of *Myh7*, *Tnni2*, *Tnnt1*, and *Tnnt2*, using an Hdac3 ChIP-seq dataset (Fig. 2.2A-D, unpublished). ChIP-qPCR analysis confirmed 13 sites occupied by Hdac3 in E8.5 wild-type hearts (Fig. 2.2A-D). Comparison with a recent ChIP-seq dataset of core cardiac transcription factors revealed significant overlap (>61%) between Tbx5 enriched regions and Hdac3 occupied sites [179]. ChIP-qPCR analysis showed that 11 sites are occupied by both Hdac3 and Tbx5 (Fig. 2.2A-E). To determine whether Tbx5 recruits Hdac3 to chromatin in the developing heart, we expressed Tbx5-shRNA in E8.5 cultured cardiac cells. Hdac3 ChIP-qPCR analysis revealed a significant decrease in Hdac3 enrichment in Tbx5-shRNA expressing compared to control cardiac cells at all overlapping regions (Fig. 2.2F). Tbx5 is known to activate expression of cardiomyocyte-specific genes [43,44,163]. Hence, we examined the requirement of Tbx5 for aberrant expression of cardiomyocyte-specific genes in $Hdac3^{Nkx2\text{-}5KO}$ hearts. Loss of Hdac3 resulted in significant activation of *Myh7*, *Tnni2*, and *Tnnt2*, and this activation was largely abolished by Tbx5 knockdown (Fig. 2.2G-I).

Figure 2.2

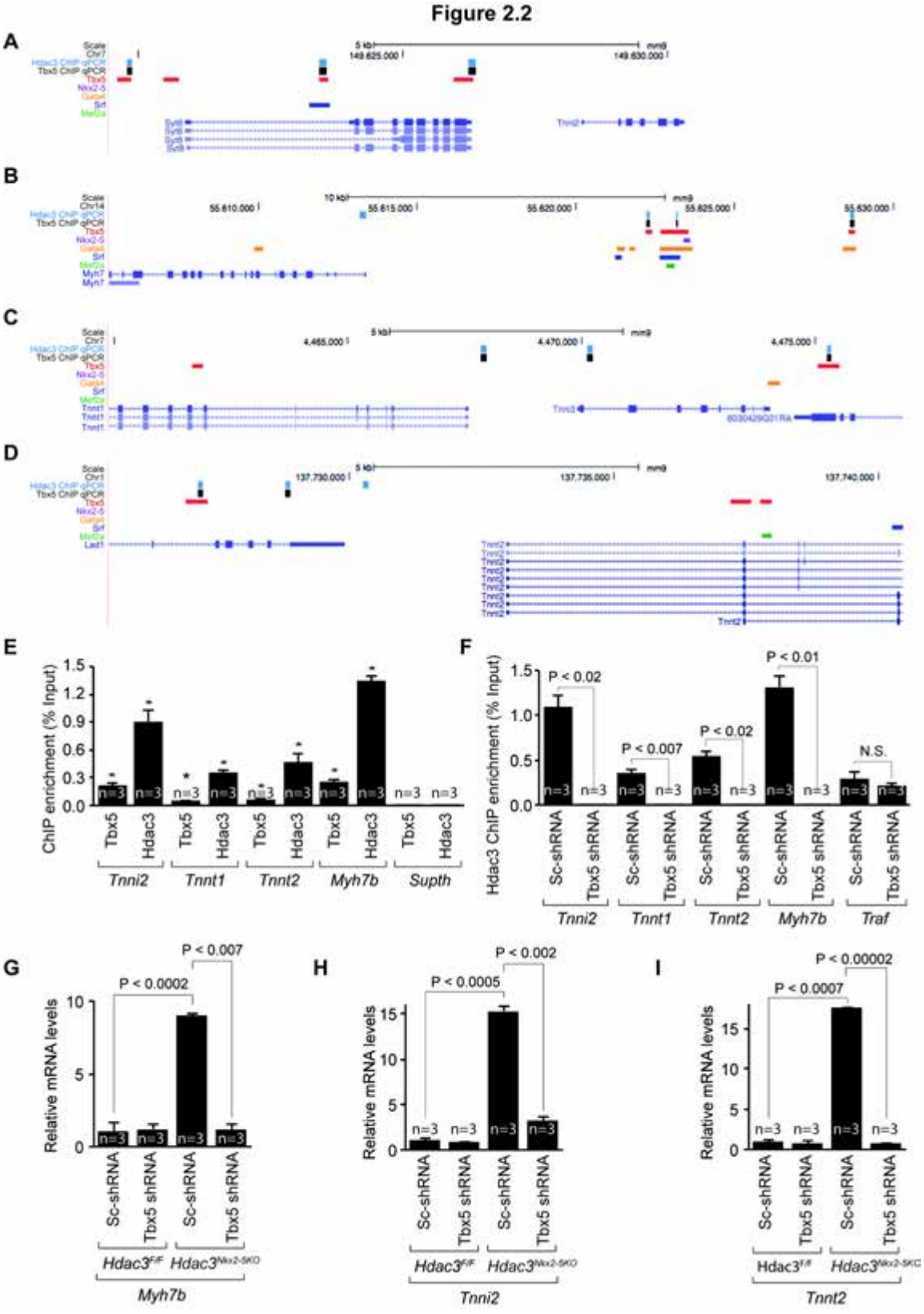
A
B
C
D
E
F
G
H
I
ChIP enrichment (% Input)
Tbx5
Hdac3
Tnni2
Tnnt1
Tnnt2
Myh7b
Supth
Hdac3 ChIP enrichment (% Input)
P < 0.02
P < 0.007
P < 0.01
N.S.
Sc-shRNA
Tbx5 shRNA
Traf
Relative mRNA levels
P < 0.0002
P < 0.0005
P < 0.0007
P < 0.00002
Hdac3F/F
Hdac3Nkx2-5KO

Figure 2.2: Hdac3 localizes to a subset of Tbx5-bound cardiomyocyte-specific enhancers. Tbx5 recruits Hdac3 to enhancer regions of dysregulated cardiomyocyte-specific genes. Aberrant expression of cardiomyocyte-specific genes in Hdac3-null hearts requires Tbx5 transcriptional activity. (A-D) Genome browser images showing sites of Hdac3 enrichment and Tbx5 enrichment in E8.5 mouse hearts along with ChIP-seq datasets of core cardiac transcription factors (He et al. 2011) and Hdac3 upstream of cardiomyocyte-specific genes: **(A)** Tnnt1, **(B)** Tnni2, **(C)** Myh7, and **(D)** Tnnt2. **(E) Hdac3 localizes to a subset of Tbx5-bound cardiomyocyte-specific enhancers.** ChIP qPCR analysis of Hdac3 and Tbx5 recruitment to promoter-proximal regions of dysregulated cardiomyocyte-specific genes performed in wild-type E8.5 hearts (mean ± SEM, n=3). *Supth* promoter-proximal region served as a control. **P* < 0.05 by Student's two-tailed *t* test. **(F) Tbx5 recruits Hdac3 to enhancer regions of dysregulated cardiomyocyte-specific genes.** ChIP-qPCR analysis of Hdac3 recruitment to Tbx5-bound sites interrogated in scramble (Sc) shRNA or Tbx5 shRNA expressing cultured cardiac cells derived from wild-type E8.5 hearts (mean ± SEM, n=3). Traf promoter-proximal region served as a control. *N.S.,* not significant. **(G-I) Aberrant expression of cardiomyocyte-specific genes in Hdac3-null hearts requires Tbx5 transcriptional activity.** Transcripts for *Myh7* **(G)**, *Tnni2* **(H)***, and Tnnt2* **(I)** were detected by real-time qPCR in $Hdac3^{F/F}$ and $Hdac3^{Nkx2\text{-}5KO}$ cultured cardiac cells, derived from E8.5 embryos, expressing scramble (Sc) shRNA or Tbx5 shRNA (mean ± SEM, n=3).

To determine the effect of Hdac3 gain-of-function on Tbx5-dependent transactivation, we generated a *Tbx5*-luciferase reporter construct containing five consensus Tbx5-binding sites. Transfection of Tbx5 resulted in an approximate 15-fold activation of the *Tbx5*-luciferase reporter and this activation was significantly inhibited by co-transfection of Hdac3, but not by Hdac1 (Fig. 2.3A-C). Likewise, Hdac3 gain-of-function repressed Tbx5-mediated activation of *Myh7*, *Tnni2*, and *Tnnt2* in developing cardiac cells (Fig. 2.3D-F). Importantly, Tbx5 mRNA and protein levels were unaltered in $Hdac3^{Nkx2\text{-}5KO}$ hearts (Fig. 2.3G-H).

Hdac3 and Tbx5 physically interact

Immunoprecipitation of endogenous Hdac3 protein from E8.5 heart lysates, followed by immunoblotting for Tbx5, indicates that Hdac3 and Tbx5 proteins interact *in vivo* (Fig. 2.4A). Hdac3 and Tbx5 also interact in transfected HEK-293T cells (Fig. 2.4B). Deletion analysis indicates that the interaction between Hdac3 and Tbx5 requires the partial T-box domain of Tbx5 and is specific (Fig. 2.4B-G). Approximately 40 different genetic mutations of Tbx5 have been identified in human patients with Holt-Oram syndrome [45,180]. Interestingly, the human $TBX5^{G125R}$ gain-of-function mutation [47] coincides with the T-box domain required for interaction with Hdac3 (Fig. 2.4B-G). We found that the $TBX5^{G125R}$ mutation affects its interaction with Hdac3 (Fig. 2.4H-I). This finding had functional implications, as Hdac3 failed to repress $TBX5^{G125R}$-mediated

Figure 2.3

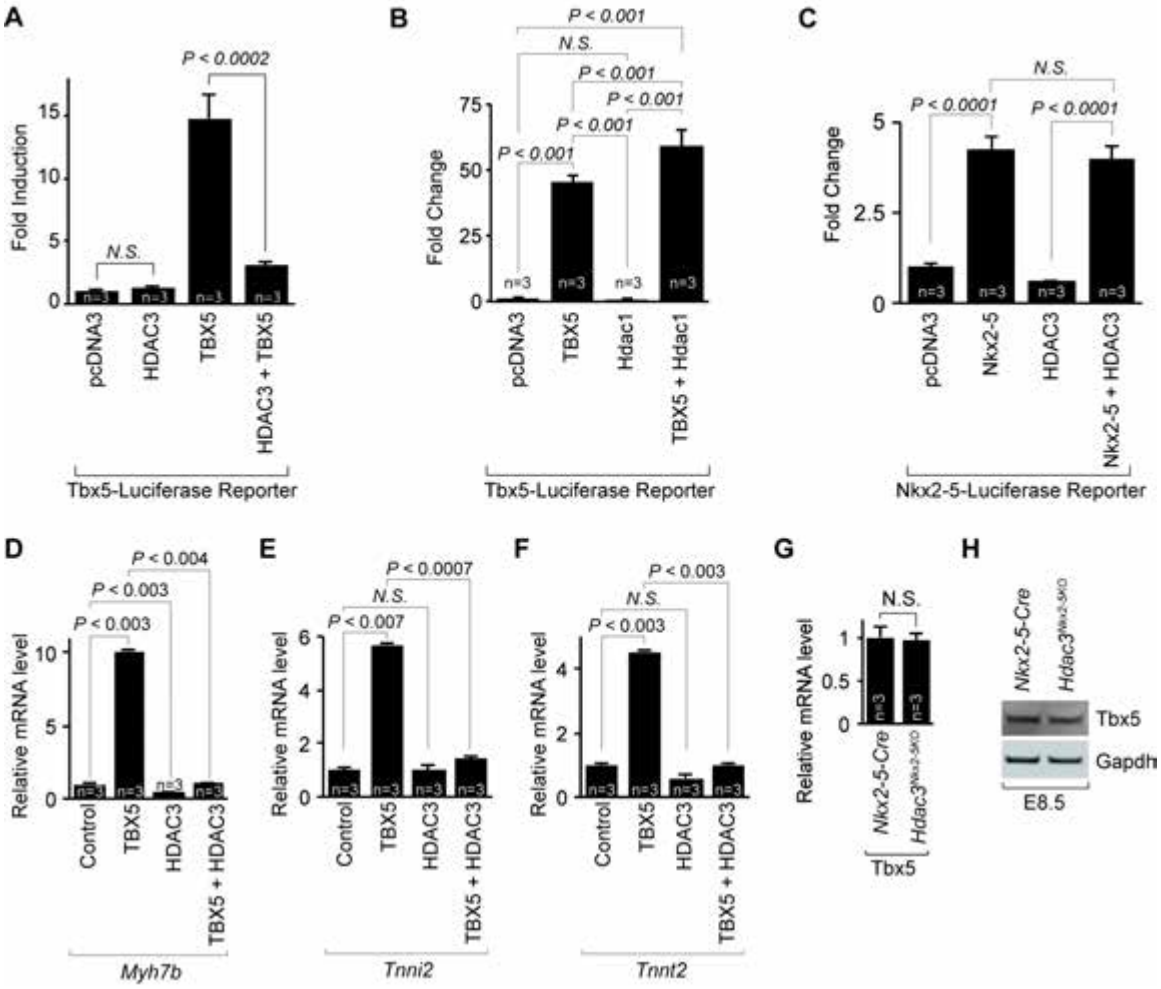
A
Fold Induction
P < 0.0002
N.S.
pcDNA3
HDAC3
TBX5
HDAC3 + TBX5
Tbx5-Luciferase Reporter
B
Fold Change
P < 0.001
N.S.
P < 0.001
P < 0.001
P < 0.001
P < 0.001
pcDNA3
TBX5
Hdac1
TBX5 + Hdac1
Tbx5-Luciferase Reporter
C
Fold Change
N.S.
P < 0.0001
P < 0.0001
pcDNA3
Nkx2-5
HDAC3
Nkx2-5 + HDAC3
Nkx2-5-Luciferase Reporter
D
Relative mRNA level
P < 0.004
P < 0.003
P < 0.003
Control
TBX5
HDAC3
TBX5 + HDAC3
Myh7b
E
Relative mRNA level
P < 0.0007
N.S.
P < 0.007
Control
TBX5
HDAC3
TBX5 + HDAC3
Tnni2
F
Relative mRNA level
P < 0.003
N.S.
P < 0.003
Control
TBX5
HDAC3
TBX5 + HDAC3
Tnnt2
G
Relative mRNA level
N.S.
Nkx2-5-Cre
Hdac3Nkx2-5KO
Tbx5
H
Nkx2-5-Cre
Hdac3Nkx2-5KO
Tbx5
Gapdh
E8.5

Figure 2.3: Hdac3 represses Tbx5-dependent transcriptional activity during early cardiogenesis. (A) *Tbx5*-Luciferase reporter construct was transfected in 293T cells with or without TBX5 and HDAC3 expression constructs. The induction is represented as fold-induction over the normalized luciferase activity in the control-transfected cells (mean ± SEM, n=3). **(B)** Hdac1 does not inhibit Tbx5-dependent transactivation. Tbx5-Luciferase reporter construct was transfected in 293T cells with or without Tbx5 and Hdac1 expression constructs. (mean ± SEM, n=3). N.S. – not significant. **(C)** Hdac3 does not inhibit Nkx2-5-dependent transactivation. Nkx2-5-Luciferase reporter construct was transfected in 293T cells with or without Nkx2-5 and Hdac3 expression constructs. The induction is represented as fold-induction over the normalized luciferase activity in the control transfected cells (mean ± SEM, n=3). **(D-F)** Transcripts for *Myh7* **(D)**, *Tnni2* **(E)***, and Tnnt2* **(F)** were detected by real-time qPCR in TBX5 and/or HDAC3 cDNA expressing cultured cardiac cells derived from E8.5 embryos (mean ± SEM, n=3). *N.S.,* not significant. **(G)** *Tbx5* transcripts were detected by real-time qPCR from E8.5 *Nkx2-5*-Cre and $Hdac3^{Nkx2\text{-}5KO}$ hearts (mean ± SEM, n=3). **(H)** Western blot analysis was performed on total lysates from E8.5 *Nkx2-5*-Cre and $Hdac3^{Nkx2\text{-}5KO}$ hearts. Gapdh is shown as a loading control.

activation of the *Tbx5*-luciferase reporter construct and transcription of *Myh7*, *Tnni2*, and *Tnnt2* in developing cardiac cells (Fig. 2.4J-K). These results suggest that Hdac3 interacts with Tbx5 to repress its transcriptional activity during early cardiogenesis.

Hdac3 and EP300 regulate Tbx5 acetylation

Post-translational modifications such as acetylation and deacetylation regulate the activity of cardiac transcription factors [140,181]. We examined the ability of various Tbx5-associated HATs to modify Tbx5-dependent activation of the *Tbx5*-luciferase reporter construct [182,183]. TBX5 activity was significantly augmented by co-transfection of EP300 but not by KAT5 or KAT2B (Fig. 2.5A-B). Transfection experiments in 293T cells followed by TBX5 immunoprecipitation and acetyl lysine immunoblotting revealed that acetylated TBX5 levels are markedly enhanced by co-transfection of EP300 (Fig. 2.5C-D). Transfection of mutant $TBX5^{G125R}$ alone results in a significant increase of the acetylated signal compared to wild-type TBX5 (Fig. 2.5C-D). However, co-transfection of mutant $TBX5^{G125R}$ with EP300 does not augment the acetylation signal (Fig. 2.5C-D). An *in vitro* acetylation assay confirmed that EP300 acetylates TBX5 (Fig. 2.5E). Immunoprecipitation experiment revealed that Tbx5 is significantly acetylated in E9.5 wild-type hearts (Fig. 2.5F). Co-transfection with HDAC3 significantly diminished acetylated-TBX5 but not acetylated-$TBX5^{G125R}$ (Fig. 2.5G-H).

Figure 2.4

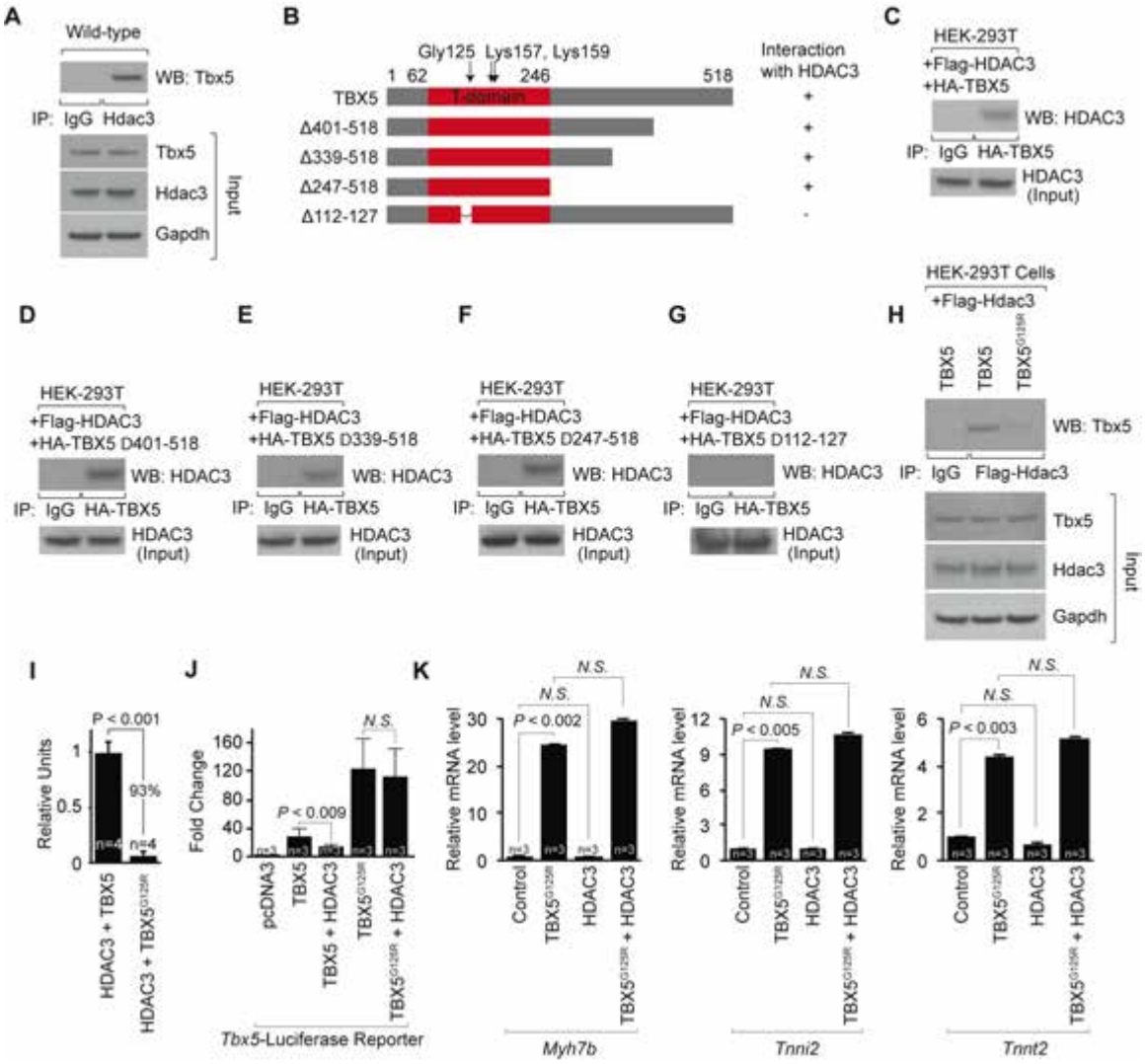
A
Wild-type
WB: Tbx5
IP: IgG Hdac3
Tbx5
Hdac3
Gapdh
Input
B
Gly125 Lys157, Lys159
1 62 246 518
TBX5
T-domain
Δ401-518
Δ339-518
Δ247-518
Δ112-127
Interaction with HDAC3
+
+
+
+
-
C
HEK-293T
+Flag-HDAC3
+HA-TBX5
WB: HDAC3
IP: IgG HA-TBX5
HDAC3 (Input)
D
HEK-293T
+Flag-HDAC3
+HA-TBX5 D401-518
WB: HDAC3
IP: IgG HA-TBX5
HDAC3 (Input)
E
HEK-293T
+Flag-HDAC3
+HA-TBX5 D339-518
WB: HDAC3
IP: IgG HA-TBX5
HDAC3 (Input)
F
HEK-293T
+Flag-HDAC3
+HA-TBX5 D247-518
WB: HDAC3
IP: IgG HA-TBX5
HDAC3 (Input)
G
HEK-293T
+Flag-HDAC3
+HA-TBX5 D112-127
WB: HDAC3
IP: IgG HA-TBX5
HDAC3 (Input)
H
HEK-293T Cells
+Flag-Hdac3
TBX5
TBX5
TBX5G125R
WB: Tbx5
IP: IgG Flag-Hdac3
Tbx5
Hdac3
Gapdh
Input
I
Relative Units
P < 0.001
93%
n=4
n=4
HDAC3 + TBX5
HDAC3 + TBX5G125R
J
Fold Change
P < 0.009
N.S.
pcDNA3
TBX5
TBX5 + HDAC3
TBX5G125R
TBX5G125R + HDAC3
Tbx5-Luciferase Reporter
K
Relative mRNA level
N.S.
P < 0.002
Control
TBX5G125R
HDAC3
TBX5G125R + HDAC3
Myh7b
P < 0.005
Tnni2
P < 0.003
Tnnt2

Figure 2.4: Hdac3 interacts with Tbx5. (A) Total lysates from E8.5 wild-type hearts were immunoprecipitated by Hdac3 antibody, and western blot was performed using Tbx5 antibody. Tbx5, Hdac3 and Gapdh are shown as an input control. **(B)** Schematic representation of TBX5 showing posttranslational modification sites and deletion constructs. Tbx5 acetylation sites Lys157 and Lys159 throughout human T-box family proteins and between various different vertebrate species. A gain-of-function TBX5 mutation, Gly125Arg, is associated with Holt-Oram syndrome. **(C-G)** Total lysates from TBX5 or various TBX5 deletion constructs transfected 293T cells were immunoprecipitated with anti-HA antibody, and western blot analysis was performed with anti-Hdac3 antibody to detect Hdac3. **(H)** Total lysates from Flag-HDAC3 and TBX5 or $TBX5^{G125R}$ cDNA expressing 293T cells were immunoprecipitated by Flag antibody to immunoprecipitate HDAC3, and western blot was performed with Tbx5 antibody to detect TBX5. **(I)** TBX5 was quantified and normalized to total input Gapdh using ImageJ software (mean ± SEM, n=4). **(J)** *Tbx5*-Luciferase reporter construct was transfected in 293T cells with or without TBX5, $TBX5^{G125R}$ and HDAC3 expression constructs. The induction is represented as fold-induction over the normalized luciferase activity in the control-transfected cells (mean ± SEM, n=3). **(K)** Transcripts for *Myh7*, *Tnni2, and Tnnt2* were detected by real-time qPCR in $TBX5^{G125R}$ and/or HDAC3 cDNA expressing cultured cardiac cells derived from E8.5 embryos (mean ± SEM, n=3). *N.S.,* not significant.

We identified Lys157 and Lys159 as conserved acetylation sites of TBX5 using three independent acetylation site prediction software programs (Fig 2.5I-K). Replacement of lysines with alanine to mimic deacetylation resulted in a mutant form of TBX5, $TBX5^{K157A-K159A}$, that could only weakly transactivate the *Tbx5*-luciferase reporter (Fig. 2.5K). EP300 failed to enhance $TBX5^{K157A-K159A}$ activity (Fig. 2.5K). Furthermore, co-transfection of $TBX5^{K157A-K159A}$ with EP300 showed significantly reduced acetylation signal compared to wild-type TBX5 (Fig. 2.5L-M). We sought to determine whether loss of hyperacetylation of human mutant $TBX5^{G125R}$ modulates its activity. We generated a mutant form of TBX5, $TBX5^{G125R-K157A-K159A}$, in which lysine residues 157 and 159 are mutated to alanine. This mutant form of TBX5 could not be robustly acetylated by EP300 and failed to transactivate the *Tbx5*-luciferase reporter (Fig. 2.5L-N). Taken together, these results suggest that Hdac3 functions to deacetylate Tbx5 and thus regulate transcriptional activity and differentiation of cardiac progenitor cells during early cardiogenesis (Fig. 2.6).

Discussion

Recent studies identified a population of multipotent cardiac progenitor cells that progressively become lineage restricted and differentiate into various cardiac cell types in a developmental stage-specific manner [184]. However, epigenetic and chromatin modifiers regulating fate specification of cardiac

Figure 2.5

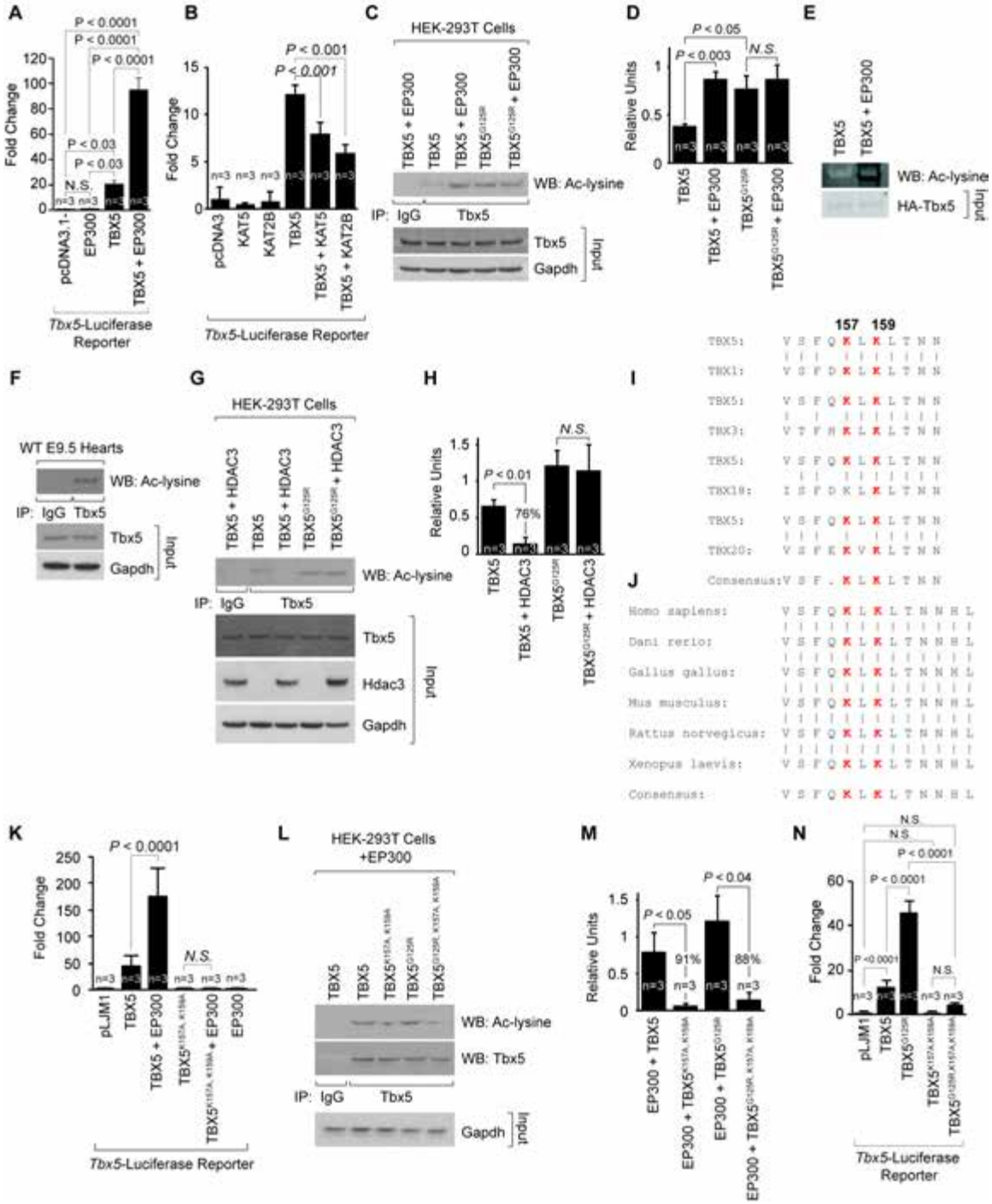
A
B
C
D
E
F
G
H
I
J
K
L
M
N
HEK-293T Cells
WT E9.5 Hearts
Fold Change
Relative Units
WB: Ac-lysine
WB: Tbx5
WB: Hdac3
HA-Tbx5
IP: IgG Tbx5
Input
Gapdh
Tbx5-Luciferase Reporter
N.S.
157 159
Homo sapiens:
Dani rerio:
Gallus gallus:
Mus musculus:
Rattus norvegicus:
Xenopus laevis:
Consensus:

Figure 2.5: Hdac3 regulates Tbx5 acetylation. (A) EP300 induces TBX5-dependent transactivation. *Tbx5*-Luciferase reporter construct was transfected in 293T cells with or without TBX5 and EP300 expression constructs. Induction is represented as fold-induction over the normalized luciferase activity in the control-transfected cells (mean ± SEM, n=3). **(B)** KAT5 and KAT2B do not induce TBX5-dependent transactivation. Tbx5-Luciferase reporter construct was transfected in 293T cells with or without TBX5 and KAT5 or KAT2B expression constructs. The induction is represented as fold-induction over the normalized luciferase activity in the control transfected cells (mean ± SEM, n=3). **(C)** EP300 acetylates TBX5 *in vivo*. Total lysates from TBX5, $TBX5^{G125R}$ and/or EP300 cDNA expressing 293T cells were immunoprecipitated by TBX5 antibody. Acetylated TBX5 was detected by western blot analysis using acetyl lysine antibody. **(D)** Acetylated TBX5 was quantified and normalized to total TBX5 using ImageJ software (mean ± SEM, n=3). N.S. – not significant. **(E)** EP300 acetylates TBX5 *in vitro*. Purified GST/HA-tagged TBX5 was subjected to *in vitro* acetylation using purified EP300. Western blot analysis was performed to determine acetylated TBX5 using acetyl lysine antibody. HA-TBX5 is shown as a loading control. **(F)** Tbx5 is acetylated in developing myocardium. Total lysates from E9.5 wild-type hearts were immunoprecipitated by Tbx5 antibody, and western blot was performed using acetyl lysine antibody to detect acetylated Tbx5. Western blot for Tbx5 and Gapdh is shown as an input control. **(G)** HDAC3 deacetylates TBX5. Total lysates from TBX5, $TBX5^{G125R}$ and/or HDAC3 cDNA expressing 293T cells were immunoprecipitated by TBX5 antibody and acetylated TBX5 was detected by western blot analysis using acetyl lysine antibody. **(H)** Acetylated TBX5 was quantified and normalized to total TBX5 using ImageJ software (mean ± SEM, n=3). **(I)** Conservation of Tbx5 acetylation sites Lys157 and Lys159 throughout human cardiac T-box family proteins. **(J)** Conservation of Tbx5 acetlyation sites 157 and 159 across vertebrate species. **(K)** Lys157 and Lys159 are required for EP300-dependent transactivation of Tbx5. Tbx5-Luciferase reporter construct was transfected in 293T cells with or without EP300 and TBX5 or TBX5K157A, K159A expression constructs. The induction is represented as fold-induction over the normalized luciferase activity in the control transfected cells (mean ± SEM, n=3) **(L)** EP300 acetylates TBX5 at Lys157 and Lys159. Total lysates from TBX5, $TBX5^{G125R}$, $TBX5^{K157A,\ K159A}$, $TBX5^{G125R,\ K157A,\ K159A}$ and/or EP300 cDNA expressing 293T cells were immunoprecipitated by TBX5 antibody, and acetylated TBX5 was detected by western blot analysis using acetyl lysine antibody. **(M)** Acetylated TBX5 was quantified and normalized to total TBX5 using ImageJ software (mean ± SEM, n=3). **(N)** Lys157 and Lys159 acetylation modulate TBX5-dependent transactivation. *Tbx5*-Luciferase reporter construct was transfected in 293T cells with or without TBX5, $TBX5^{G125R}$, $TBX5^{K157A,\ K159A}$, and $TBX5^{G125R,\ K157A,\ K159A}$ expression constructs. The induction is represented as fold-induction over the normalized luciferase activity in the control-transfected cells (mean ± SEM, n=3).

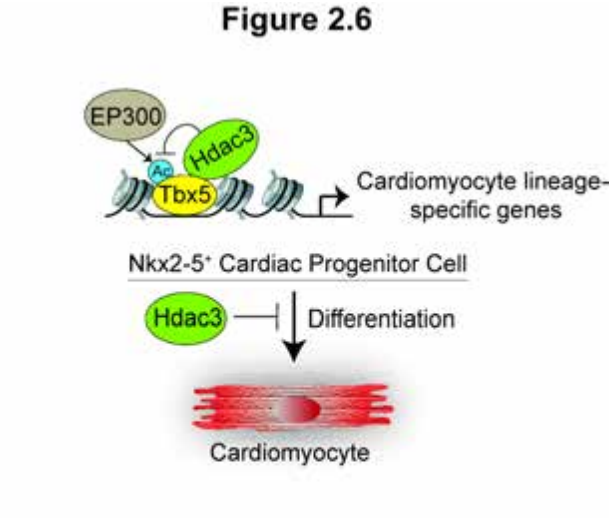

Figure 2.6: Proposed model depicting Hdac3 interacting with Tbx5 to repress cardiomyocyte lineage-specific genes in Nkx2-5+ cardiac progenitor cells during early cardiogenesis.

progenitor cells remain elusive. Our present work suggests that ubiquitously expressed Hdac3 plays a critical role in cardiac progenitor cells during early stages of cardiogenesis. Mice lacking Hdac3 in cardiac progenitor cells exhibit complete embryonic lethality and precocious differentiation into the cardiomyocyte lineage. The resulting hearts show hypoplastic ventricular walls and membranous ventricular septal defects. Cardiomyocyte lineage-specific genes are upregulated. Our data suggest that this is due, at least in part, to enhanced Tbx5 transcriptional activity, which in turn is due to Tbx5 hyper-acetylation.

We observed that Hdac3 binds at a subset of Tbx5-bound sites within regulatory regions of cardiomyocyte lineage-specific genes. Moreover, Tbx5 is able to recruit Hdac3 to chromatin. The available data suggest that several transcription factors synergistically interact with Tbx5 to promote early cardiogenesis [185]. For example, Tbx5 associates with Nkx2-5 to promote cardiomyocyte differentiation [42]. In contrast, our findings support a model in which Hdac3 interacts with Tbx5 to block the Tbx5-dependent activation of cardiomyocyte lineage-specific genes in cardiac progenitor cells. Consistent with our findings, recent work demonstrates that Tbx5 gain-of-function is sufficient to induce cardiomyocyte lineage specification from cardiac mesoderm [163]. Conversely, loss of Tbx5 function results in early embryonic lethality due to impaired cardiac differentiation [20]. Of note, Hdac3 gain-of-function failed to inhibit

Nkx2-5-dependent transactivation, suggesting that the functional relationship between Hdac3 and Tbx5 is specific (Fig. 2.3C).

TBX5, the causative gene in Holt-Oram Syndrome, was the first identified single-gene mutation giving rise to congenital heart defects (CHDs) [29,30]. Several pathogenic mutations of *TBX5*, located within the highly conserved T-box domain, have been reported in patients with or without Holt-Oram Syndrome [45]. Further studies demonstrated that several of these mutations cause, at least in part, defective interactions between TBX5 and NKX2-5 or GATA4 to affect cardiac gene expression and lead to CHDs [20,186]. Our studies revealed that the human $TBX5^{G125R}$ mutation, located within the T-box domain, disrupts interaction between TBX5 and HDAC3. Furthermore, HDAC3 fails to repress the transcriptional activity of $TBX5^{G125R}$, resulting in activation of cardiomyocyte lineage-specific genes in cardiac progenitor cells. Consistent with our findings, $TBX5^{G125R}$ mutation results in gain-of-function in human patients with Holt-Oram-Syndrome [47].

Recent reports demonstrate that acetylation of cardiac transcription factors modulate their activity [181]. Acetylation of Tbx5 has not been reported, however, there are reports suggesting cooperation between Tbx5 and histone acetyltransferases [182,183]. We show that EP300 directly acetylates TBX5 to enhance its transcriptional activity. Further, we identified conserved acetylation sites of TBX5, Lys157 and Lys159, that are important for EP300-mediated acetylation and transcriptional activation. Although Lys157 and Lys159 are

conserved among various TBX genes, functional acetylation targets could be different within TBX family. Indeed, we observed that Lys234, conserved among TBX family, was not required for TBX5 acetylation or activity (not shown). Future mass spectrometry analysis will be needed to identify all the acetylated lysine residues within TBX5.

HDACs regulate gene expression by deacetylating histone and non-histone proteins [119]. Our data suggest that Tbx5 is a novel non-histone catalytic target of Hdac3 in the embryonic heart. Overall, our findings support a model in which Hdac3 deacetylates Tbx5 and represses Tbx5-dependent transcriptional activity to maintain the multipotent state of cardiac progenitor cells. Loss of Hdac3 removes this brake to precociously activate cardiomyocyte lineage-specific genes in progenitor cells, likely explaining precocious differentiation of cardiomyocytes in *Hdac3*$^{Nkx2\text{-}5KO}$ embryos. This is consistent with the model where transient binding of HDACs maintain a low level of acetylation and prevent activation of primed genes in pluripotent cells [118]. However, alternate functions of Hdac3, related to proliferation, histone deacetylation, or chromatin remodeling, remain as plausible causes of precocious differentiation observed in *Hdac3*$^{Nkx2\text{-}5KO}$ heart. Indeed, transient proliferation arrest of undifferentiated cardiac cells could explain, in part, precocious differentiation and hypoplastic ventricular walls in E8.5 *Hdac3*$^{Nkx2\text{-}5KO}$ hearts (Fig. 2.2G-J). Recent studies have suggested that functions unrelated to catalytic activity of Hdac3 may also exist and may require nuclear compressor corepressor NCoR [144,187]. Thus, it will be critical in future

experiments to determine whether the catalytic activity of Hdac3 and NCoR is required for its normal function during early cardiogenesis.

Acknowledgements:

We gratefully acknowledge Dr. Eric Olson (UT Southwestern) for providing Nkx2-5 Cre mice. We thank Dr. John F. Keaney Jr. (UMass Medical School) and Dr. Jonathan Epstein (U. Pennsylvania) for critical reading of the manuscript. We thank Dan Feng (U. Pennsylvania) for ChIP of HDAC3 in adult mouse heart.

Chapter III: Histone deacetylase 3 coordinates deacetylase-independent epigenetic silencing of TGFβ1 to orchestrate second heart field development

Chapter III is a published manuscript and is included with permission not required:

Lewandowski SL, Janardhan HP, and Trivedi CM. (2015). Histone deacetylase 3 coordinates deacetylase-independent epigenetic silencing of transforming growth factor-β1 (TGF-β1) to orchestrate second heart field development. *Journal of Biological Chemistry*, 290(45), 27067-27089.

Author contributions:

I contributed the data shown in figures 3.1, 3.2, and 3.3, in their entirety, along with microarray data and analysis in figure 3.4 A, B, C, D, and E, and 3.5 A, immunohistochemistry in figures 3.4 M and 3.5 G, Hdac3 mutant generation and characterization in figure 3.9 A and B, and contributed all data related to Isl1-Cre and Mef2c-Cre crosses in all tables. I also prepared the cartoon models in figure 3.10. In addition, I designed and generated the Tgfβ wild-type and mutant luciferase constructs used in figure 3.9 G and performed all mouse breeding, primer design, promoter analysis, plasmid generation, and lentivirus preparation relevant to figure 3.4 F-L, figure 3.5 B-F and H-M, figure 3.8, in its entirety, and

figure 3.9 C-L. Harish P. Janardhan provided the data in figure 3.6, in its entirety, the phenotypic data in figure 3.7 A-L, data regarding $Hdac3^{TaglnKO}$ mice in table 3.2, and mouse breeding relevant to figure 7 M-Q. Chinmay M. Trivedi conducted the experiments shown in figure 3.4 F-L, figure 3.5 B-F, and H-M, figure 3.7 M-Q, figure 3.8, and figure 9 C-L.

Abstract

About two-thirds of human congenital heart disease (CHD) involves second heart field (SHF) derived structures. Histone-modifying enzymes, histone deacetylases (HDACs), regulate the epigenome; however, their functions within the second heart field remain elusive. Here we demonstrate that histone deacetylase 3 (Hdac3) orchestrates epigenetic silencing of Tgfβ1, a causative factor in CHD pathogenesis, in a deacetylase-independent manner to regulate development of SHF-derived structures. In murine embryos lacking Hdac3 in the SHF, increased Tgfβ1 bioavailability is associated with ascending aortic dilatation, outflow tract malrotation, overriding aorta, double outlet right ventricle, aberrant semilunar valve development, bicuspid aortic valve, ventricular septal defects, and embryonic lethality. Activation of Tgfβ signaling causes aberrant endothelial-to-mesenchymal transition (EndMT) and altered extracellular matrix homeostasis in Hdac3-null outflow tracts and semilunar valves and pharmacological inhibition of Tgfβ rescues these defects. Hdac3 physically recruits methyltransferase Ezh2 to

the Ncor complex to enrich trimethylation of lys27 on histone H3 at the Tgfβ1 regulatory region and thereby maintains epigenetic silencing of Tgfβ1 specifically within the SHF-derived mesenchyme. Wild-type Hdac3 or catalytically-inactive Hdac3 expression rescue aberrant EndMT and epigenetic silencing of Tgfβ1 in Hdac3-null outflow tracts and semilunar valves. These findings reveal that epigenetic dysregulation within the SHF is a predisposing factor for CHD.

Introduction

Congenital heart disease is the most common of all birth defects, the leading cause of infant mortality [188]. Cardiac morphogenesis in the mouse begins at around embryonic day 7.0 (E7.0), when subset of cells derived from antero-lateral mesoderm forms the cardiac crescent [153]. This crescent contains first and second heart field cardiac progenitor cells [24]. The first heart field progenitor cells are the principal contributor to the primary heart tube, the left ventricle, AV canal and atria [189]. The second heart field progenitor cells extensively contribute to the outflow tract, semilunar valves, atria, right ventricle, primary atrial septum, and ventricular septum [31-33,190,191]. Indeed, ablation or genetic manipulation of second heart field progenitor cells and their derivatives leads to outflow tract malrotation, overriding aorta, double outlet right ventricle, aberrant semilunar valve development, and ventricular septal defects [34,192,193]. In humans, about two-thirds

of congenital cardiac defects involve the outflow tract, semilunar valves or ventricular septum [7].

Patterning of the second heart field requires several signaling pathways and their interaction with transcriptional regulators [194]. Transforming growth factor-β (Tgf-β) family members are among the pioneer signaling molecules that induce endothelial-to-mesenchymal transition (EndMT) to form semilunar valve cushions in the developing outflow tract [195-197]. Subsequent elongation, expansion and extracellular matrix remodeling transform these cushions into the mature semilunar valves [66,85,198]. During these valvular remodeling processes, regulation of TGF-β bioavailability appears to be crucial. For instance, patients with semilunar valve pathologies, such as semilunar valve stenosis, regurgitation, and aberrant deposition of myofibroblasts and extracellular matrix, display elevated TGF-β levels [84,199,200]. Indeed, exogenous Tgf-β transforms cultured valvular interstitial cells into myofibroblasts and promotes excessive secretion of extracellular matrix [201-203]. Elevated Tgf-β level is also implicated in the pathogenesis of connective tissue disorders such as Marfan syndrome, Ehlers-Danlos syndrome and Loeys-Dietz syndrome [61,74,75]. Interestingly, patients with these syndromes frequently display congenital cardiovascular anomalies, such as aortic dilatation, outflow tract defects, bicuspid aortic valve, semilunar valve stenosis, and ventricular septal defects [60,204,205]. How the second heart field progenitor cells interpret elevated TGF-β at the chromatin level in these connective tissue disorders remains to be elucidated.

Extracellular matrix tightly regulates the bioavailability of active TGF-β [206]. For instance, extracellular matrix proteoglycans, such as decorin (Dcn), biglycan (Bgn), and fibromodulin (Fmod), sequester Tgf-β to limit its activity [207]. Mice lacking Dcn, Bgn or Fmod display elevated Tgf-β activity and phenotypes observed in Marfan syndrome or Ehlers-Danlos syndrome [208-210]. Indeed, proteoglycan deficiencies have been demonstrated in patients with these syndromes [211]. Proteoglycans expressed in the developing outflow tract and semilunar valves also play a key role in the assembly of collagen fibers in the extracellular matrix [210,212]. Patients with collagen deficiency, such as COL3A1 mutations in Ehlers-Danlos syndrome, show elevated TGF-β levels [75]. How extracellular matrix homeostasis is regulated remains an area of intense research.

The active form of TGF-β binds to TGFBR2 and TGFBR1, which in turn phosphorylate Smad2/3 (R-Smads) to promote assembly of heteromeric complex with Smad4. Activated SMAD complex accumulates in the nucleus, where it recruits transcription co-factors and chromatin modifiers to regulate the expression of target genes [206]. Several factors, in addition to TGF-β, play critical roles to trigger activation and amplification of intracellular TGF-β signaling pathway at multiple levels [206]. For instance, transcription factor Snai1 interacts with Smad3/4 to repress endothelial gene expression and thereby augments TGF-β mediated mesenchymal transition [213]. EndMT, a specialized form of EMT, is the complex biological process in which endothelial cells trans-differentiate into

mesenchymal cell types, including smooth muscle-like and fibroblast-like cells. EndMT has been implicated in several pathological processes including fibrotic disorders and cardiac valvular diseases. A complex orchestration of several signaling pathways, including TGF-β signaling, initiates and promotes EndMT. However, the molecular and epigenetic mechanisms regulating termination of EndMT remain elusive.

Histone deacetylases (HDACs) are chromatin-modifying enzymes that regulate the epigenome [160]. The mammalian HDACs are classified into five subfamilies based on their phylogenetic analysis and sequence homology. Class I HDACs (Hdac1, Hdac2, Hdac3, and Hdac8) play critical roles at various stages of development [119]. For instance, global loss of Hdac1 or Hdac3 results in early embryonic lethality around E9.5 [119]. Similarly, mice lacking Hdac2 or Hdac8 display lethality at birth [123,214,215]. Our group and others, using gene inactivation studies in mice, have demonstrated vital functions for Class I Hdacs in cardiomyocyte proliferation, differentiation and hypertrophy [123,140,151,216]. However, functions of Hdacs in second heart field development remain undefined.

Hdacs lack intrinsic DNA-binding domains but are recruited to the chromatin via their interaction with transcription factors, co-factors, and large multiprotein transcriptional complexes [160]. For instance, Hdac3 is an integral part of nuclear receptor corepressor (Ncor) or its homologue silencing mediator of retinoic and thyroid receptors (SMRT). Interaction of Hdac3 with the deacetylase

activating domain of Ncor/SMRT is required for its enzyme activity. Interestingly, recent evidences suggest that enzymatic activity of Hdac3 is dispensable, but its interaction with Ncor/SMRT is essential for transcriptional repression. However, molecular mechanisms that mediate the deacetylase-independent function of Hdac3 remain to be defined. Recent study shows that Hdac4 controls histone methylation in response to elevated cardiac overload, suggesting Hdacs may recruit histone methyltransferases to the chromatin.

In this study, we demonstrate a deacetylase-independent role for Hdac3 as an epigenetic-silencer of Tgf-β1 within the second heart field with direct implications for human Tgf-β pathway-associated cardiovascular anomalies. As a part of the Ncor complex, Hdac3 recruits enhancer of zeste homologue 2 (Ezh2), the major histone methyltrasferase of the polycomb repressor complex 2 (PRC2), to mediate epigenetic silencing of TGF-β1 specifically within the second heart field-derived mesenchymal cells and thereby promotes termination of EndMT. Genetic deletion of Hdac3 in the murine second heart field results in increased Tgf-β bioavailability within mesenchymal cells, perpetual activation of mesenchymal cells, aberrant EndMT, and altered extracellular matrix homeostasis, observed in patients with semilunar valve pathologies. Together, these results uncover that epigenetic silencing mediated by Hdac3 in a deacetylase-independent manner orchestrates second heart field development, which may be a molecular target in human cardiovascular anomalies.

Materials and Methods

Mice - Transgenic *Mef2C*-AHF-Cre, *Cdh5*-Cre, *Hdac3*^{flox} and knock-in *Isl1*-Cre mice were previously described [165,190,217,218]. *Tagln*-Cre (Sm22α-Cre), *Myh6*-Cre (αMhc-Cre), and *R26R-LacZ* mice were obtained from The Jackson Laboratories. The University of Massachusetts Medical School Institutional Animal Care and Use Committee approved all animal protocols.

Histology - Tissue samples were fixed in 2% paraformaldehyde at 4°C overnight, ethanol dehydrated, embedded in paraffin and sectioned at 6-8 micron thickness using a microtome.

Antibodies and reagents - The following antibodies were used in this study: Hdac3 (Abcam and Santa Cruz), phospho-Hdac3 (S424) (Cell Signaling), Tgf-β pan specific polyclonal antibody (R&D Systems), Smad2/3 (Santa Cruz), phospho-Smad2/3 (Ser 423/425) (Santa Cruz), Vimentin (Santa Cruz), PECAM1 (BD Pharmingen), Troponin T (Hybridoma Bank, Iowa), MF-20 (Hybridoma Bank, Iowa), cleaved caspase-3 (Cell Signaling), RNA polymerase II (Abcam), Ezh2 (Abcam), Ncor1 (Abcam), H3K27ac (Abcam), H3K27me3 (Abcam), IgG (R&D Systems), Gapdh (R&D Systems), Flag (Sigma), α-tubulin (Sigma), IRDye-conjugated secondary antibodies (Licor), Alexa Fluor® 546-conjugated secondary antibody (Life Technologies), and biotinylated universal pan-specific

antibody (Horse anti-mouse/rabbit/goat IgG) (Vector Laboratories). Recombinant Tgf-β was purchased from R&D Systems. Alcian blue, alkaline alcohol, Orcein, alcoholic hematoxylin, ferric chloride, Lugol's Iodine, Woodstain Scarlet-Acid Fuchsin, phosphotungstic acid, Saffron, Bouin's fixative, Weigert's Iron Hematoxylin A, Weigert's Iron Hematoxylin B, phosphomolybdic acid-phosphotungstic acid, Aniline blue, and Van Gieson's solution were purchased from Electron Microscopy Sciences. Harris Modified Hematoxylin, Eosin-Y, ethanol, Xylenes, glacial acetic acid, paraformaldehyde, paraffin, potassium ferricyanide, potassium ferrocyanide, and deoxycholic acid were purchased from Fisher Scientific. Polyethylenamine, linear, was purchased from Polysciences. X-gal was purchased from 5 Prime. VectaShield Mounting Medium, Vectastain Elite ABC Kit, and DAB Peroxidase Substrate Kit were purchased from Vector Laboratories. RNeasy Mini Kit and GST bead slurry were purchased from Qiagen. Power SYBR Green PCR Master Mix, Superscript First Strand Synthesis Kit, TOPO-TA Cloning Kit, DMEM high glucose with NA pyruvate, Pen/Strep, and horse serum were purchased from Invitrogen. CellsDirect™ One-Step qRT-PCR Kit, insulin-transferrin-selenium (ITS), Epoxy M-450 dynabeads, and Trizol were purchased from Life Technologies. Rat tail collagen type I was purchased from BD Biosciences. iScript reverse transcription supermix was purchased from BioRad. Sandwich ELISA assay kit for Tgfβ1 was purchased from R&D Systems. Sandwich ELISA assay kit for phospho-Smad2/3 was purchased from Cell Signaling. QuikChange II XL Site-Directed Mutagenesis Kit was purchased from

Stratagene. Passive lysis buffer and dual-luciferase reporter assay kit were purchased from Promega. Fetal bovine serum, donkey serum, gelatin, and magnetic anti-flag beads were purchased from Sigma. Agarose IgG and IgA bead slurry were purchased from Santa Cruz and Life Technologies. EZ-ChIP assay kit was purchased from Millipore. TaKaRa DNA ligation kit was purchased from Clontech.

Hematoxylin and eosin staining - Hematoxylin and eosin staining was performed by deparaffinizing sections in Xylenes, rehydrating through an ethanol gradient, 30 second or 2 minute stain with 30% or 100% Harris Modified Hematoxylin, and a 30 second counter-stain with Eosin-Y. Slides were rinsed and dehydrated with ethanol, cleared with Xylenes, and mounted with Vectashield mounting medium.

Movat's pentachrome staining - Movat's pentachrome staining was conducted by deparaffinizing and rehydrating slides, followed by a 20 minute stain in Alcian blue, 1 hour differentiation in alkaline alcohol, 20 minute stain in Orcein-Verhoeff solution (Orcein, alcoholic hematoxylin, ferric chloride, and Lugol's Iodine), 2 minute stain with Woodstain Scarlet-Acid Fuchsin, rinse in acetic acid, and 10 minute differentiation in 5% phosphotungstic acid, followed by a 15 minute stain in Saffron. Sections were dehydrated in ethanol, cleared in Xylenes, and mounted with Vectashield mounting medium.

Masson's trichrome staining - Masson's trichrome staining was performed by deparaffinizing and rehydrating sections through an ethanol gradient followed by a 1 hour mordant in Bouin's fixative at 56C. Samples were then washed and stained for 5 minutes in a solution of Weigert's Iron Hematoxylin A and Weigert's Iron Hematoxylin B. Following washing, samples were differentiated in phosphomolybdic acid-phosphotungstic acid for 15 minutes, stained in Aniline blue solution for 20 minutes, and differentiated in 1% acetic acid for 3 minutes. Samples were then dehydrated in ethanol, cleared in Xylenes, and mounted with Vectashield mounting media.

Modified Verhoeff Elastic-Van Gieson stain - Modified Verhoeff Elastic-Van Gieson stain was conducted by deparaffinizing and rehydrating sections, staining for 7 minutes in Verhoeff working solution (1.8% alcoholic hematoxylin, 0.8% ferric chloride, 20% Lugol's iodine), washing in running water, differentiating for 1 minute in 0.4% ferric chloride, and counterstaining for 3 minutes in Van Gieson's solution. Samples were then ethanol dehydrated, cleared with Xylenes, and mounted with Vectashield mounting media.

LacZ staining - Tissue samples were dissected in PBS, and then fixed in 2% paraformaldehyde for 30 minutes at 4C. After washing in PBS at room temperature, samples were stained overnight in LacZ staining solution (5 mM

potassium ferricyanide, 5 mM potassium ferrocyanide, 2 mM MgCl2, 0.01% deoxycholic acid, 0.04% NP-40, 0.1% X-gal, in 1X PBS) at 37C in the dark. Samples were then washed in PBS and fixed overnight in 4% paraformaldehyde.

Plasmids and site-directed mutagenesis - Flag-HDAC3 pcDNA3.1(-) and the Flag-HDAC3 lentiviral vector were previously described [216]. GFP lentiviral vector and lentiviral packaging plasmids were obtained from Addgene: pLOVE-GFP (Addgene plasmid 15949), pCMV-dR8.2 (Addgene plasmid 8455) and pCMV-VSVG (Addgene plasmid 8454). Lentiviral plasmids expressing Hdac3-shRNA, Ezh2-shRNA, Ncor1-shRNA, and scrambled-shRNA control were obtained from the University of Massachusetts shRNA Core Facility. Flag-HDAC3$^{H134A/H135A}$ was generated by site-directed mutagenesis as per manufacturer's protocol, using Flag-HDAC3 pcDNA3.1(-) as a template and subcloned to CSCGW2. To generate the Tgf-β1 luciferase construct, a 1309bp promoter-proximal region immediately upstream of the translational start site of Tgf-β1 was PCR amplified from mouse genomic DNA, gel-purified, and cloned into pCR2.1 TOPO (Life Technologies) following the manufacturer's protocol. The promoter was subcloned from pCR2.1 TOPO to pGL3-basic (Promega). An Hdac3 binding site, identified using published ChIP-seq data and confirmed by ChIP-qPCR from murine valve tissue, was deleted from the 3' end of the Tgf-β1 promoter-proximal region by PCR amplification using the Tgf-β1 luciferase vector as a template. The Tgf-β1 deletion promoter was gel-purified, cloned into pCR2.1 TOPO, and

subcloned into pGL3-basic. All generated plasmids were verified by restriction analysis and sequencing.

Immunohistochemistry - For immunohistochemistry, sections were deparaffinized in Xylenes and pre-treated using heat antigen retrieval in sodium citrate buffer (10mM sodium citrate, 0.05% Tween 20, pH 6). Immunohistochemistry was conducted using Vectastain Elite ABC Kit and DAB Peroxidase Substrate Kit according to manufacturers guidelines. Sections were incubated with cleaved caspase-3 antibody (1:100) for one hour at room temperature or Hdac3 antibody (1:250) or phospho-Smad2/3 antibody (1:50) overnight at 4^{o}C. Biotinylated universal pan-specific antibody (horse anti-mouse/rabbit/goat IgG) was used for phospho-Smad2/3 immunostaining in place of the Vectastain Elite ABC Kit secondary antibody according to manufacturer's guidelines. For counter-staining, slides were rinsed and then incubated with 30% hematoxylin for 30 seconds after DAB developing. All slides were ethanol dehydrated, cleared with Xylenes, and mounted with Vectashield mounting medium. For immunofluorescent staining, sections were deparaffinized and rehydrated through xylenes and an ethanol gradient. Slides were rinsed in PBS and antigen retrieval was performed in sodium citrate buffer (10mM sodium citrate, 0.05% Tween 20, pH 6.0) for 10 minutes at 95C. After rinsing, sections were blocked in 10% donkey serum, 0.3% Triton X-100 in PBS for one hour at room temperature. Sections were then washed in PBS and incubated with

smooth muscle actin antibody (1:100) in 10% donkey serum and PBS for one hour at room temperature or MF-20 (1:50) or Troponin (1:25) antibodies in 10% donkey serum in PBS overnight at 4C. Finally, slides were washed in PBS, incubated in secondary antibody (donkey anti-mouse 546, 1:500, with Hoechst, 1:1000, in 10% donkey serum, PBS) for one hour at room temperature, rinsed in PBS, and mounted with Vectashield mounting media.

Biometric analysis - Aortic diameter was measured from 2X images of dissected hearts at three levels (tubular aortic trunk, proximal aortic arch, and intermediate aortic arch) using NIS-Elements analysis software (Nikon). Ventricular wall thickness and valve area measurements were made from 2X and 10X images, respectively, of position-matched hematoxylin and eosin-stained sections using NIS-Elements analysis software (Nikon). Nuclei numbers per section in the valves were counted manually in 10X hematoxylin and eosin-stained sections using ImageJ counting tools. Differences between groups were compared using Student's *t* tests.

Real Time quantitative PCR - Total RNA was extracted and reverse transcribed using iScript reverse transcription supermix (BioRad) or CellAmp whole trascriptome amplification kit (Takara) according to the manufacturer's guidelines. Transcript expression was measured by qRT-PCR using SYBR Green PCR Master Mix. Signals were normalized to corresponding Gapdh

controls, and represented as relative expression ratios of experimental samples relative to *Hdac3*$^{F/F}$ controls. Primer sequences are available upon request.

Apoptosis assay - Sections of aortic and pulmonic valves from five *Hdac3*^{Isl1KO} and five control E13.5 hearts were immunostained with cleaved caspase-3 antibody and counter-stained with hematoxylin. Images of the aortic and pulmonic valves were taken at 20X magnification. The total number of nuclei and the number of cleaved caspase-3 positive nuclei within the valve cusp were manually counted for each sample. The aortic and pulmonic valves were compared separately. The number of cleaved caspase-3 positive nuclei per 1000 nuclei served as an apoptosis index.

Microarray analysis - Heart tissue was dissected from E9.5 mouse embryos and snap frozen in liquid nitrogen. RNA was extracted from pools of *Hdac3*^{Isl1KO} or *Hdac3*$^{F/F}$ control hearts using an RNeasy Mini Kit. Microarray analysis was performed in triplicate from pooled samples by the University of Massachusetts Genomics Core Facility using Affymetrix Mouse Gene 2.0 ST arrays (Affymetrix). Raw microarray data were annotated using bioconductor and oligo packages in R [219-221]. Significance of expression differences between *Hdac3*^{Isl1KO} and *Hdac3*$^{F/F}$ samples were determined using Student's *t* test. Heatmaps of microarray data were generated using the pheatmap package in R [222]. Relative expression of each transcript is reported as log-transformed expression value for

each sample, normalized to the median expression value of the transcript across all six samples. MIAME-compliant full microarray datasets can be accessed at the Gene Expression Omnibus (GEO, GSE73666).

Ingenuity pathway analysis - Microarray data from E9.5 *Hdac3*^{Isl1KO} and control hearts were analyzed using Ingenuity Pathway Analysis (IPA). IPA Diseases and Functions utility was employed to investigate phenotypes associated with the molecular changes. Hierarchical heatmaps were generated using both Diseases and Biological Functions categories and Tox Functions categories of the Diseases and Functions utility. Plots of phenotypically-relevant categories were constructed based on subcategory P-values. The Upstream Regulators utility was employed to determine potential regulators of differentially-expressed genes. Significant regulators were sorted by significance and by number of associated genes. Differentially-expressed genes associated with the upstream regulator Tgfβ1 were exported and a clustered heatmap was generated using R software.

Lentiviral infection - Lentiviral media was generated by transfecting 100mm plates of subconfluent 293T cells with 5μg of lentiviral cDNA, 5μg of pCMV-dR8.2, and 2.5μg of pCMV-VSVG, in 10ml of 2% FBS media. Media was changed to fresh 10ml of 2% FBS media 24 hours after transfection. Viral media was collected 24 hours later and filtered through a 40μm cell strainer. Isolated mouse embryonic heart tissue was infected with filtered viral media

supplemented with 10μg/ml polybrene reagent. GFP viral media was used to maintain a constant viral media volume. Infected cells were harvested for analysis 24 or 48 hours after infection.

Cell culture, transient transfection, and luciferase assay – HEK293T cells and murine endothelial cells were maintained in DMEM with 10% FBS, 100 mg/ml penicillin and 100 mM/ml streptomycin in a 37°C incubator with 5% CO_2. HEK293T cells were transfected in sub-confluent 100 mm plates with 2.5 μg of DNA and 5 μl of polyethylenamine, linear, in 10 ml of 10% FBS media. Luciferase assays were conducted by transfecting subconfluent murine endothelial cells in 6-well plates with 1μg of DNA and 2μl of polyethylenamine, linear, in 2 ml of 10% FBS media. DNA amount was maintained constant using pcDNA3.1(-) or pLJM1-EGFP DNA. Cells were lysed with passive lysis buffer 16 h after transfection, and lysates were analyzed using a dual luciferase reporter assay kit according to the manufacturer's guidelines. Luciferase activity was measured using a Berthold microplate reader according to manufacturer's guidelines.

Immunoprecipitation - Tissue samples were homogenized in immunoprecipitation buffer (50mM Tris-HCl [pH 8.0], 150mM NaCl, 0.5% Nonidet P-40, 1mM EDTA, and 1mM DTT) containing 1mM PMSF, phosphate inhibitors (Sigma), and protease inhibitors mixture (Sigma). The homogenized samples were sonicated using Branson 250 Digital Sonifier with 1s ON and 1s OFF pulses

at 40% power amplitude for 15s. Precleared lysates with beads were incubated with primary antibodies for 16hrs at 4°C. After incubation for 1hr at 4°C with beads, immune-complexes were collected, washed four times with immunoprecipitation buffer, and applied to 4-12% SDS-polyacrylamide gels for western blot analysis.

Western blotting - Tissue lysates were prepared in lysis buffer (20mM Tris HCl (pH 7.5), 15mM NaCl, 1mM Na_2EDTA, 1mM EGTA, 1% Triton X-100, 1µg.mL leupeptin, 2.5mM sodium pyrophosphate, 1mM Na_3VO_4, and 1mM β-glycerophosphate; 1mM phenylmethylsulfonyl fluoride was added before use). Protein samples were resolved on 4-12% SDS-PAGE acrylamide gel before transferring to PVDF (poly-vinylidene difluoride) membranes. We used primary antibodies to Hdac3 (1:1000) and Flag (1:1000). Primary antibodies were visualized by chemiluminescence using HRP-conjugated secondary antibodies or by infrared with IRDye®-conjugated secondary antibodies. Blots were probed with α-tubulin (1:1000) or Gapdh (1:1000) for loading control.

ELISA assay - Sandwich ELISA assay were performed according to the manufacturer's protocol. Briefly, for phospho-Smad2/3 or phospho-Hdac3 ELISA, samples were prepared using 100µl using 1x cell lysis buffer (20 mM Tris, pH 7.5, 150 mM NaCl, 1 mM EDTA, 1 mM EGTA, 1% Triton X-100, 2.5 mM sodium pyrophosphate, 1mM β-glycerophosphate, 1 mM Na_3VO_4, 1µg/ml leupeptin). 100

μl of sample diluet was added per 100 μl of sample (1:1 ratio). Samples were incubated overnight at 4°C. After four washes with 1X wash buffer, samples were incubated with detection antibody for 1 hour at 37°C. Samples were visualized using HRP-detection method at 450 nm. For phospho-Hdac3 ELISA assay, microtiter plate was coated with Hdac3 antibody (5 μg / ml) in carbonate/bicarbonate buffer (pH9.6). Sandwich ELISA for Tgf-β1 was performed according to the manufacturer's protocol. Briefly, samples were prepared using assay diluent buffer RD1-21. Samples were incubated for 2 hours at RT. After four washes with 1X wash buffer, samples were incubated with 100 μl of Tgf-β1 conjugate for 2 hour at RT. After four washes with 1X wash buffer, samples were incubated with 100 μl of substrate solution (protected from light) for 30 minutes at RT. After addition of 100 μl of stop solution, reactions were visualized at 450 nm and 540 nm. Readings at 540 nm were subtracted from readings at 450 nm to correct for optical imperfections in the plate.

Outflow tract explant assay - The outflow tract explant cultures were performed as previously described [223,224]. Briefly, a solution of rat tail collagen type I (1.5 mg/ml) containing NaOH to a final concentration of 15 mmol/L was dispensed into 24-well microculture dishes. Subsequently, gels were placed in a 37°C tissue culture incubator at 5% CO_2 and allowed to polymerize. After 30 min, collagen gels were washed several times with DMEM containing 10% fetal bovine serum, 0.1% insulin-transferrin-selenium (ITS) and 100 mg/ml penicillin and 100 mM/ml

streptomycin. Outflow tracts were carefully dissected from control and *Hdac3*^{lsl1KO} E9.5 or E10.5 or E14.5 embryonic hearts. The outflow tracts were placed endocardium face down onto collagen gels and allowed to adhere for 8h at 37°C, 5% CO_2. Eight hours after attachment, medium was added and expants were cultured for up to 24 or 48 or 72 hours. Radial migration was measured from 4X images of outflow tract explants at 45° intervals using NIS-Elements analysis software (Nikon). Explants were treated with Tgf-β antibody (1μg / ml) for 24 or 48 hours or recombinant Tgf-β (10ng / ml) for 24 or 48 hours. Explants were also detached, trypsinized, and incubated with anti-vimentin (mesenchymal marker) antibody conjugated or PECAM-1 (endothelial marker) conjugated epoxy M-450 dynabeads as per manufacturer's guidelines to isolate cells.

Chromatin immunoprecipitation (ChIP) analysis - ChIP experiments were preformed as previously described [216]. Briefly, isolated cardiac tissue or explants from E9.5 mouse embryos were cross-linked for 15 minutes in cross-linking solution (1% formaldehyde, 1.5mM EGS, 20mM Na-butyrate, 10% FBS), then quenched with 125mM glycine solution for 5 minutes followed by two washes with 1X PBS. Chromatin fragmentation was carried out by sonication in ChIP SDS lysis buffer (50mM Tris-HCl pH 8.0, 10mM EDTA, 1% SDS, 1X protease inhibitors), using the Branson Sonifier 250 (40% power amplitude, 110s). Proteins were immunoprecipitated in ChIP dilution buffer (0.01% SDS, 1.1% Triton X-100, 1.2mM EDTA, 16.7mM Tris-HCl pH 8.0, 167mM NaCl, 20mM NA-

butyrate, 1X protease inhibitor) using IgG or Hdac3 or Ncor1 or Ezh2 or H3K27me3 or H3K27ac or PolII antibody. Specificity of Hdac3 or Ncor1 or Ezh2 or H3K27me3 or H3K27ac or PolII antibody at the relevant loci was determined using IgG control antibody. Specificity of Hdac3 antibody at the relevant loci was also determined using Hdac3-null hearts compared to wild-type control. Immunoprecipitated antibody-chromatin complexes were washed twice with low salt wash buffer (20mM Tris-HCl pH 8.0, 150mM NaCl, 2mM EDTA, 0.1% SDS, and 1% Triton X-100) followed by two washes with lithium chloride wash buffer (10mM Tris-HCl pH 8.0, 250 mM LiCl, 1mM EDTA, 1% deoxycholate, and 1% Nonidet P-40) and TE buffer (10mM Tris-HCl pH 8.0, and 1mM EDTA). After removing wash buffer, cross-linking was reversed at 65C overnight in Proteinase K buffer (20mM Tris-HCl pH 7.5, 5mM EDTA, 50mM NaCl, 1% SDS, 20mM Na-butyrate, 50µg/ml Proteinase K). The following day, DNA was purified using phenol/chloroform/isoamyl alcohol. Purified precipitated DNA was analyzed by qRT-PCR as previously described. Enrichment of target sequences was determined by qRT-PCR using primers designed against Hdac3 consensus binding sites within the proximal 10kb upstream of the transcription start site of genes of interest: *Tgf-β1*, *Kpnb1*, *Sumo1*, *and Smad4*. Primer sequences are available upon request.

Statistical analysis - Statistical significance between groups was determined using two-tailed Student's *t* test or χ^2 test. A P-value < 0.05 was considered

significant.

Results

HDAC3 Is Required in the Second Heart Field for Cardiac Development

Germ line deletion of ubiquitously expressed HDAC3 results in embryonic lethality at E9.5 [125,177]. To determine the function of HDAC3 in the second heart field, we deleted HDAC3 in the second heart field progenitor cells using two Cre lines, *Isl1-Cre* (*Hdac3*^{Isl1KO}) (Fig. 3.1A–C) and *Mef2C-Cre* (*Hdac3*^{Mef2CKO}) [190,217]. *Hdac3*^{Isl1KO} embryos were identified at E18.5 (Table 3.1). However, *Hdac3*^{Isl1KO} pups displayed complete lethality at birth (P0) ($p < 0.01$; Table 3.1). *Hdac3*^{Isl1KO} embryos were characterized by malrotation of outflow tract, overriding aorta, double outlet right ventricle, membranous ventricular septal defect, ascending aortic dilatation (21–35%, $p < 0.02$), and normal outflow tract septation at E18.5 (Table 3.2 and Fig. 3.1D–I). *Hdac3*^{Isl1KO} embryos displayed aberrant distribution and expression of collagen in all layers of ascending aortic and pulmonary arterial walls (Fig. 3.1J–L). In addition, elastin fibers appeared fragmented, probably explaining aortic dilatation in *Hdac3*^{Isl1KO} embryos (Fig. 3.1K-L). *Isl1-Cre* is a knock-in allele; however, we did not observe genetic interaction between HDAC3 and ISL1 (Tables 3.1 and 3.2). *Hdac3*^{Mef2CKO} embryos revealed similar developmental cardiac defects, including double outlet

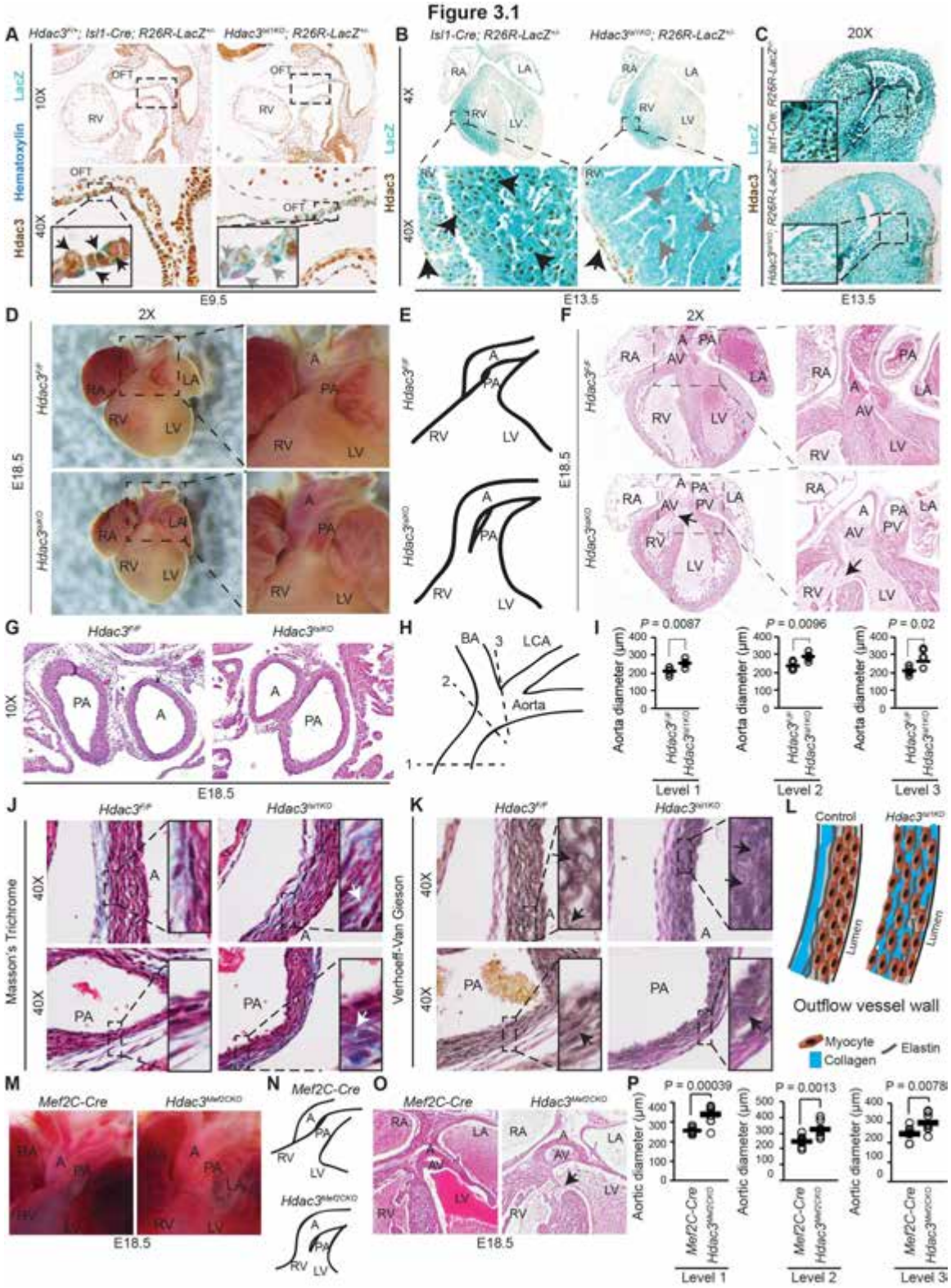
Figure 3.1
A
B
C
D
E
F
G
H
I
J
K
L
M
N
O
P
LacZ
Hematoxylin
Hdac3
10X
40X
4X
20X
2X
OFT
RV
RA
LA
LV
PA
AV
PV
BA
LCA
Aorta
E9.5
E13.5
E18.5
Level 1
Level 2
Level 3
Aorta diameter (μm)
P = 0.0087
P = 0.0096
P = 0.02
P = 0.00039
P = 0.0013
P = 0.0078
Masson's Trichrome
Verhoeff-Van Gieson
Control
Lumen
Outflow vessel wall
Myocyte
Collagen
Elastin
Mef2C-Cre

Figure 3.1: Hdac3 functions within the second heart field to regulate cardiac morphogenesis. (A-C) Hdac3 immunostaining of LacZ-stained *Hdac3*^{Isl1KO}*; R26R-LacZ*$^{+/-}$ and control embryos shows that Hdac3 protein expression (black arrows) is lost (grey arrows) in the *Isl1-Cre* expression domain in **(A)** E9.5 and **(B-C)** E13.5 *Hdac3*^{Isl1KO} hearts, including in semilunar valves **(C). (D)** Dissected and fixed E18.5 hearts show malrotation of the outflow tract in *Hdac3*^{Isl1KO} hearts. **(E)** Tracings of outflow tract vessels demonstrate abnormal, parallel orientation of the aorta and pulmonary artery in *Hdac3*^{Isl1KO} hearts. **(F)** Hematoxylin- and eosin-stained sections demonstrate double outlet right ventricle, with membranous ventricular septal defect (arrow) and an overriding aorta in *Hdac3*^{Isl1KO} E18.5 hearts. **(G)** Hematoxylin- and eosin-stained cross-sections show malrotation, but complete septation, of the aorta and pulmonary artery in E18.5 *Hdac3*^{Isl1KO} hearts. **(H-I)** Cartoon diagram of proximal aorta showing three levels: Level 1 – tubular aortic trunk, Level 2 – proximal aortic arch, Level 3 – intermediate aortic arch **(H).** Comparison of aorta diameter in *Hdac3*^{Isl1KO} and control hearts, measured at three levels from dissected, fixed hearts **(I). (J)** Masson's trichrome-stained sections of aorta and pulmonary artery demonstrate disorganized collagen (blue) in the vessel walls of *Hdac3*^{Isl1KO} E18.5 hearts. **(K)** Verhoeff-Van Gieson-stained sections of aorta and pulmonary artery demonstrate disorganized collagen (arrows, red) and fragmented elastin (arrows, black) in the vessel walls of *Hdac3*^{Isl1KO} E18.5 hearts. **(L)** Cartoon model of disorganized outflow vessel wall morphology. **(M)** Hematoxylin- and eosin-stained sections demonstrate double outlet right ventricle with aortic valve overriding a membranous ventricular septal defect (arrow) in *Hdac3*^{Mef2CKO} E18.5 hearts. **(N)** Quantification of aortic diameter shows dilation of E18.5 *Hdac3*^{Mef2CKO} aortas at three levels: Level 1 – tubular aortic trunk, Level 2 – proximal aortic arch, and Level 3 – intermediate aortic arch. **(O-P)** Hematoxylin- and eosin-stained sections show normal primary atrial septum (arrow) in **(O)** *Hdac3*^{Isl1KO} and **(P)** *Hdac3*^{Mef2CKO} E18.5 hearts. RA = right atrium, LA = left atrium, A = aorta, AV = aortic valve, PA = pulmonary artery, PV = pulmonic valve, RV = right ventricle, LV = left ventricle, BA = brachiocephalic artery, LCA = left common carotid artery, PAS = primary atrial septum.

right ventricle, ascending aortic dilatation (22–32%, $p < 0.002$), and perinatal lethality (Tables 3.2 and 3.3 and Fig. 3.1M-N). Primary atrial septum and right ventricle, in part derived by the second heart field progenitor cells, appeared normal in both *Hdac3*^{Isl1KO} and *Hdac3*^{Mef2CKO} hearts (Fig. 3.1O-P) (data not shown). Cardiomyocyte differentiation was unaffected in early *Hdac3*^{Isl1KO} embryos (data not shown).

HDAC3 Is Essential for Semilunar Valve Development

The second heart field progenitor cells are required for conotruncal cushion development, which contributes to the semilunar valves and outflow tract septum (5, 6, 8–10). *Hdac3*^{Isl1KO} embryos demonstrated dysmorphic, thickened (1.59–3-fold, $p < 0.02$), and hyperplastic (1.31–3.14-fold, $p < 0.02$) semilunar valves at E18.5 (Table 3.2 and Fig. 3.2A–N). Interestingly, aortic valves were bicuspid in *Hdac3*^{Isl1KO} hearts (Table 3.2 and Fig. 3.2E). The outflow tract septum and atrioventricular valves appeared normal in these embryos at E18.5 (Figs. 3.1G and 3.2O). Similarly, *Hdac3*^{Mef2CKO} embryos revealed defects in semilunar valve development, but not in atrioventricular valve development, at E18.5 (Table 3.2 and Fig. 3.2P–T).

The mature semilunar valves are composed of extracellular matrix, valvular interstitial cells, and endothelial cells. Remodeling of valvular interstitial

Table 3.1

Genotyping of *Isl1-Cre; Hdac3$^{F/+}$* x *Hdac3$^{F/+}$*

	observed (expected)	
	E18.5	P0
Hdac3$^{+/+}$	9 (9)	18 (11)
Hdac3$^{F/+}$	17 (18)	22 (22)
Hdac3$^{F/F}$	11 (9)	12 (11)
Isl1-Cre; Hdac3$^{+/+}$	13 (9)	17 (11)
Isl1-Cre; Hdac3$^{F/+}$	15 (18)	19 (22)
Isl1-Cre; Hdac3$^{F/F}$	7 (9)	**0** (11)
Total	72	88
Chi-square	NS	*P < 0.01*

Figure 3.2

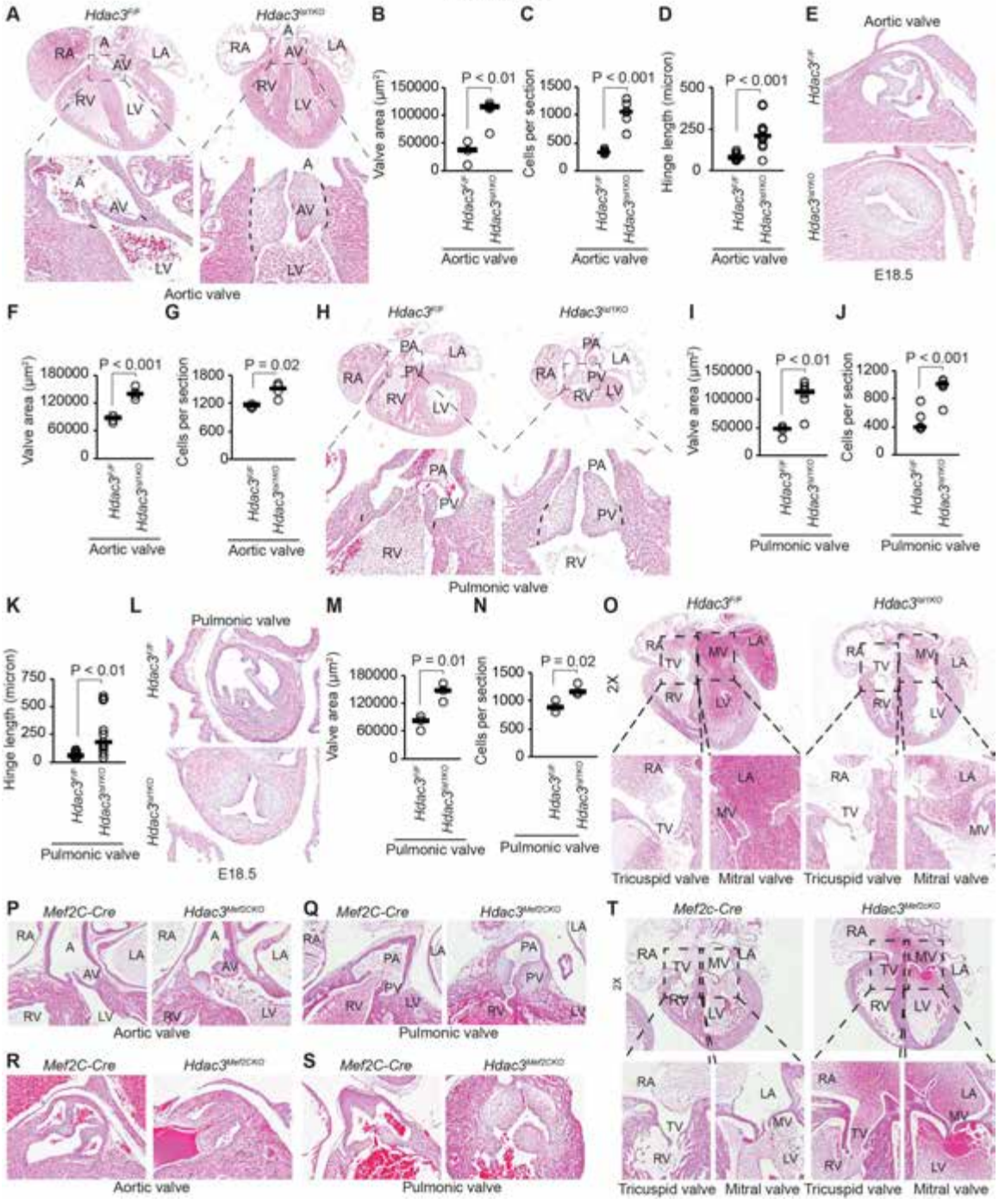
A
Hdac3f/f
Hdac3MYKO
RA
A
AV
LA
RV
LV
Aortic valve
B
Valve area (μm²)
P < 0.01
Aortic valve
C
Cells per section
P < 0.001
Aortic valve
D
Hinge length (micron)
P < 0.001
Aortic valve
E
Aortic valve
E18.5
F
Valve area (μm²)
P < 0.001
Aortic valve
G
Cells per section
P = 0.02
Aortic valve
H
PA
PV
Pulmonic valve
I
Valve area (μm²)
P < 0.01
Pulmonic valve
J
Cells per section
P < 0.001
Pulmonic valve
K
Hinge length (micron)
P < 0.01
Pulmonic valve
L
Pulmonic valve
E18.5
M
Valve area (μm²)
P = 0.01
Pulmonic valve
N
Cells per section
P = 0.02
Pulmonic valve
O
2X
TV
MV
Tricuspid valve
Mitral valve
P
Mef2C-Cre
Hdac3Mef2CKO
Aortic valve
Q
Pulmonic valve
R
Aortic valve
S
Pulmonic valve
T
Mef2c-Cre
Tricuspid valve
Mitral valve

Figure 3.2: Hdac3 is required for semilunar valve development. (A) Hematoxylin- and eosin-stained sections demonstrate thick, hyperplastic, and dysmorphic aortic valve in *Hdac3*^{lsl1KO} E18.5 hearts. **(B)** Quantification of aortic valve area, measured from frontal sections of E18.5 hearts. **(C)** Quantification of number of nuclei per aortic valve section, counted from hematoxylin- and eosin-stained frontal sections of E18.5 hearts. **(D)** Quantification of width of junction between aortic valve and cardiac wall, measured from frontal sections of E18.5 hearts. **(E)** Hematoxylin- and eosin-stained sections demonstrate thick, hyperplastic, dysmorphic, and bicuspid aortic valve in *Hdac3*^{lsl1KO} E18.5 hearts. **(F)** Quantification of aortic valve area, measured from cross-sections of E18.5 hearts. **(G)** Quantification of number of nuclei per aortic valve section, counted from hematoxylin- and eosin-stained cross sections of E18.5 hearts. **(H)** Hematoxylin- and eosin-stained sections demonstrate thick, hyperplastic, and dysmorphic pulmonic valve in *Hdac3*^{lsl1KO} E18.5 hearts. **(I)** Quantification of pulmonic valve area, measured from frontal sections of E18.5 hearts. **(J)** Quantification of number of nuclei per pulmonic valve section, counted from hematoxylin- and eosin-stained frontal sections of E18.5 hearts. **(K)** Width of hinge region in pulmonic valve measured from frontal sections of E18.5 hearts. **(L)** Hematoxylin- and eosin-stained sections demonstrate thick, hyperplastic, dysmorphic, and tricuspid pulmonic valve in *Hdac3*^{lsl1KO} E18.5 hearts. **(M)** Quantification of pulmonic valve area, measured from cross-sections of E18.5 hearts. **(N)** Quantification of number of nuclei per pulmonic valve section, counted from hematoxylin- and eosin-stained cross sections of E18.5 hearts. **(O)** Hematoxylin- and eosin-stained sections demonstrate normal tricuspid and mitral valve morphology in *Hdac3*^{lsl1KO} E18.5 hearts. **(P-Q)** Hematoxylin- and eosin-stained sections show thickened, hyperplastic **(P)** aortic and **(Q)** pulmonic valves in E18.5 *Hdac3*^{Mef2CKO} hearts. **(R)** Hematoxylin- and eosin-stained sections show hyperplastic, bicuspid aortic valve in E18.5 *Hdac3*^{Mef2CKO} E18.5 hearts. **(S)** Hematoxylin- and eosin-stained sections show hyperplastic, tricuspid pulmonic valve in E18.5 *Hdac3*^{Mef2CKO} hearts. **(T)** Hematoxylin- and eosin-stained sections demonstrate normal mitral and tricuspid valves in E18.5 *Hdac3*^{Mef2CKO} hearts. RA = right atrium, LA = left atrium, A = aorta, AV = aortic valve, PA = pulmonary artery, PV = pulmonic valve, RV = right ventricle, LV = left ventricle, MV = mitral valve, TV = tricuspid valve.

cells and extracellular matrix, mainly collagens, proteoglycans, and elastin, is essential for maturation of the semilunar valves [65]. *Hdac3*^{Isl1KO} hearts displayed loss of extracellular matrix trilaminar stratification and valvular interstitial cell compartmentalization in the semilunar valves at various stages of development (Fig. 3.3A–F, L, and M). Specifically, loss of HDAC3 resulted in aberrant expression of collagen and proteoglycan in all layers, probably explaining enlarged and thickened semilunar valves (Fig. 3.3A–F, L, and M). Elastin fibers appeared disorganized and fragmented in *Hdac3*^{Isl1KO} semilunar valves (Fig. 3.3, A, B, E, F, L, and M). Similarly, *Hdac3*^{Mef2CKO} embryos revealed aberrant expression of collagen and proteoglycan in all layers of the semilunar valves (Fig. 3.3G-H). Remodeling of the semilunar valves is associated with an increase in apoptosis [198]. *Hdac3*^{Isl1KO} semilunar valve interstitial cells displayed a 55– 65% decrease in apoptosis compared with controls ($p < 0.02$) during valve remodeling (Fig. 3.3I–K).

HDAC3 Regulates TGF-β Signaling Pathway

Transcriptional analysis of early embryonic *Hdac3*^{Isl1KO} hearts revealed significant expression changes indicative of the congenital heart defects observed in late stage *Hdac3*^{Isl1KO} embryos (Fig. 3.4A-B). Upstream regulator analysis identified marked changes in TGF- β1 pathway genes (Fig. 3.4C–E). Positive regulators of the TGF- β1 pathway, including *Sumo1*, *Nrp2*, *Smad4*,

Table 3.2

Phenotypes of mice, aged E18.5 - P0

Genotype	Incidence	Total	p Value (χ^2 Test)	
Outflow tract malrotation				
Hdac3$^{Isl1\text{-}KO}$	6	6	*Hdac3*$^{Isl1\text{-}KO}$ (6/6): *Hdac3*$^{F/F}$ (0/6)	p = 0.014
Hdac3$^{Mef2c\text{-}KO}$	8	9	*Hdac3*$^{Mef2c\text{-}KO}$ (8/9): *Hdac3*$^{F/F}$ (0/6)	p = 0.0209
Hdac3$^{Tagln\text{-}KO}$	3	3	*Hdac3*$^{Tagln\text{-}KO}$ (3/3): *Hdac3*$^{F/F}$ (0/4)	p = 0.045
Hdac3$^{F/+}$; *Isl1-Cre*	0	4	*Hdac3*$^{F/+}$;*Isl1-Cre* (0/4): *Hdac3*$^{F/F}$ (0/6)	p = 1
Double outlet right ventricle				
Hdac3$^{Isl1\text{-}KO}$	5	6	*Hdac3*$^{Isl1\text{-}KO}$ (5/6): *Hdac3*$^{F/F}$ (0/6)	p = 0.0253
Hdac3$^{Mef2c\text{-}KO}$	3	3	*Hdac3*$^{Mef2c\text{-}KO}$ (3/3): *Hdac3*$^{F/F}$ (0/6)	p = 0.014
Hdac3$^{Tagln\text{-}KO}$	3	3	*Hdac3*$^{Tagln\text{-}KO}$ (3/3): *Hdac3*$^{F/F}$ (0/4)	p = 0.045
Hdac3$^{F/+}$; *Isl1-Cre*	0	4	*Hdac3*$^{F/+}$;*Isl1-Cre* (0/4): *Hdac3*$^{F/F}$ (0/6)	p = 1
Ventricular septal defect				
Hdac3$^{Isl1\text{-}KO}$	6	6	*Hdac3*$^{Isl1\text{-}KO}$ (6/6): *Hdac3*$^{F/F}$ (0/6)	p = 0.014
Hdac3$^{Mef2c\text{-}KO}$	5	5	*Hdac3*$^{Mef2c\text{-}KO}$ (5/5): *Hdac3*$^{F/F}$ (0/6)	p = 0.014
Hdac3$^{Tagln\text{-}KO}$	3	3	*Hdac3*$^{Tagln\text{-}KO}$ (3/3): *Hdac3*$^{F/F}$ (0/4)	p = 0.045
Hdac3$^{F/+}$; *Isl1-Cre*	0	4	*Hdac3*$^{F/+}$;*Isl1-Cre* (0/4): *Hdac3*$^{F/F}$ (0/6)	p = 1
Over-riding aorta				
Hdac3$^{Isl1\text{-}KO}$	5	6	*Hdac3*$^{Isl1\text{-}KO}$ (5/6): *Hdac3*$^{F/F}$ (0/6)	p = 0.0253
Hdac3$^{Mef2c\text{-}KO}$	3	3	*Hdac3*$^{Mef2c\text{-}KO}$ (3/3): *Hdac3*$^{F/F}$ (0/6)	p = 0.014
Hdac3$^{Tagln\text{-}KO}$	3	3	*Hdac3*$^{Tagln\text{-}KO}$ (3/3): *Hdac3*$^{F/F}$ (0/4)	p = 0.045
Hdac3$^{F/+}$; *Isl1-Cre*	0	4	*Hdac3*$^{F/+}$;*Isl1-Cre* (0/4): *Hdac3*$^{F/F}$ (0/6)	p = 1
Hyperplastic aortic valve				
Hdac3$^{Isl1\text{-}KO}$	12	12	*Hdac3*$^{Isl1\text{-}KO}$ (12/12): *Hdac3*$^{F/F}$ (0/12)	p = 0.00053
Hdac3$^{Mef2c\text{-}KO}$	9	9	*Hdac3*$^{Mef2c\text{-}KO}$ (9/9): *Hdac3*$^{F/F}$ (0/12)	p = 0.00053
Hdac3$^{Tagln\text{-}KO}$	3	3	*Hdac3*$^{Tagln\text{-}KO}$ (3/3): *Hdac3*$^{F/F}$ (0/4)	p = 0.045
Hdac3$^{F/+}$; *Isl1-Cre*	0	8	*Hdac3*$^{F/+}$;*Isl1-Cre* (0/8): *Hdac3*$^{F/F}$ (0/12)	p = 1
Hyperplastic pulmonic valve				
Hdac3$^{Isl1\text{-}KO}$	12	12	*Hdac3*$^{Isl1\text{-}KO}$ (12/12): *Hdac3*$^{F/F}$ (0/12)	p = 0.00053
Hdac3$^{Mef2c\text{-}KO}$	9	9	*Hdac3*$^{Mef2c\text{-}KO}$ (9/9): *Hdac3*$^{F/F}$ (0/12)	p = 0.00053
Hdac3$^{Tagln\text{-}KO}$	3	3	*Hdac3*$^{Tagln\text{-}KO}$ (3/3): *Hdac3*$^{F/F}$ (0/4)	p = 0.045
Hdac3$^{F/+}$; *Isl1-Cre*	0	8	*Hdac3*$^{F/+}$;*Isl1-Cre* (0/8): *Hdac3*$^{F/F}$ (0/12)	p = 1
Bicuspid aortic valve				
Hdac3$^{Isl1\text{-}KO}$	4	4	*Hdac3*$^{Isl1\text{-}KO}$ (4/4): *Hdac3*$^{F/F}$ (0/6)	p = 0.014
Hdac3$^{Mef2c\text{-}KO}$	3	3	*Hdac3*$^{Mef2c\text{-}KO}$ (3/3): *Hdac3*$^{F/F}$ (0/6)	p = 0.014
Hdac3$^{F/+}$; *Isl1-Cre*	0	4	*Hdac3*$^{F/+}$;*Isl1-Cre* (0/4): *Hdac3*$^{F/F}$ (0/6)	p = 1

Figure 3.3

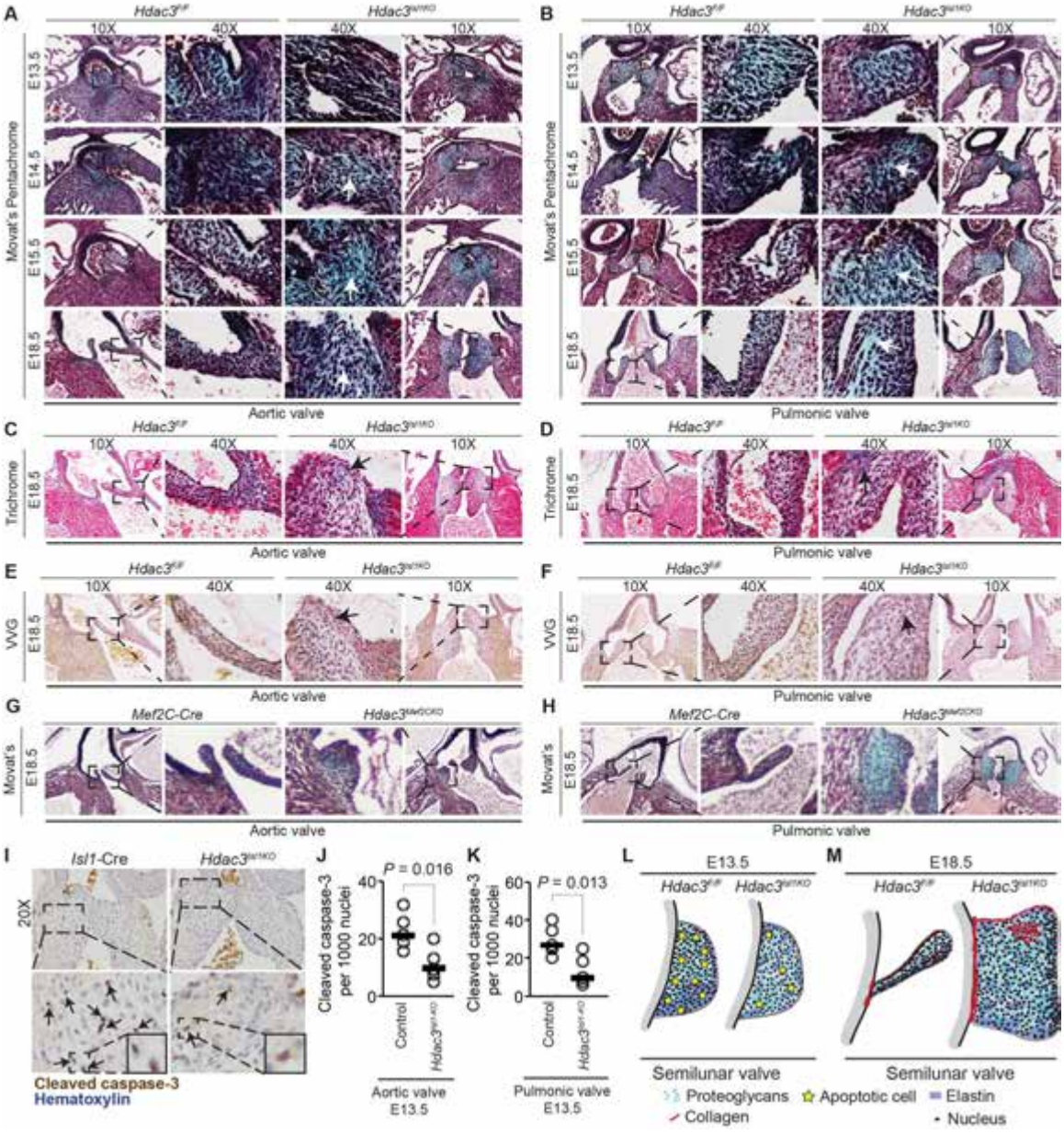
A
B
C
D
E
F
G
H
I
J
K
L
M
Hdac3f/f
Hdac3IWKO
10X
40X
Movat's Pentachrome
E13.5
E14.5
E15.5
E18.5
Aortic valve
Pulmonic valve
Trichrome
VVG
Movat's
Mef2C-Cre
Hdac3MWDKO
Isl1-Cre
20X
Cleaved caspase-3
Hematoxylin
Cleaved caspase-3 per 1000 nuclei
P = 0.016
P = 0.013
Control
Aortic valve E13.5
Pulmonic valve E13.5
Semilunar valve
Proteoglycans
Apoptotic cell
Elastin
Collagen
Nucleus

Figure 3.3: Hdac3 is required for extracellular matrix homeostasis and remodeling of semilunar valves. (A) Movat's pentachrome staining of remodeling aortic valve shows an increase in proteoglycans (arrows, blue) from E13.5 to E18.5 in *Hdac3*^{Isl1KO} aortic valves with a reduction and remodeling of proteoglycans in control valves. **(B)** Movat's pentachrome staining of remodeling pulmonic valve shows an increase in proteoglycans (arrows, blue) from E13.5 to E18.5 in *Hdac3*^{Isl1KO} pulmonic valves with a reduction and remodeling of proteoglycans in control valves. **(C)** Masson's trichrome staining demonstrates disorganized collagen expression (arrow, blue) in *Hdac3*^{Isl1KO} E18.5 aortic valve. **(D)** Masson's trichrome staining demonstrates disorganized collagen expression (arrow, blue) in *Hdac3*^{Isl1KO} E18.5 pulmonic valve. **(E)** Verhoeff-Van Gieson (VVG) staining shows disorganized collagen expression (arrow, red) in *Hdac3*^{Isl1KO} E18.5 aortic valve. **(F)** Verhoeff-Van Gieson (VVG) staining shows disorganized collagen expression (arrow, red) in *Hdac3*$^{Isl1-KO}$ E18.5 aortic valve. **(G)** Movat's pentachrome-stained sections show increased proteoglycans (blue) in aortic valve cusps of E18.5 *Hdac3*^{Mef2CKO} hearts. **(H)** Movat's pentachrome staining reveals increased proteoglycans (blue) in E18.5 *Hdac3*^{Mef2CKO} pulmonic valve. **(I)** Representative images of cleaved caspase-3 immunostaining in E13.5 semilunar valves. Arrows indicate positive staining. **(J)** Quantification of cleaved caspase-3 positive cells in E13.5 control and *Hdac3*^{Isl1KO} aortic valves. **(K)** Quantification of cleaved caspase-3 positive cells in E13.5 control and *Hdac3*^{Isl1KO} pulmonic valves. **(L)** Cartoon model depicting disorganized extracellular matrix and reduced apoptosis in *Hdac3*^{Isl1KO} E13.5 semilunar valves. **(M)** Cartoon model showing hyperplastic, enlarged, and disorganized *Hdac3*^{Isl1KO} E18.5 semilunar valves.

Snai1, *Tgf- β1*, and *Kpnb1* were 3–9- fold up-regulated ($p < 0.02$) in *Hdac3*^{Isl1KO} hearts (Fig. 3.4*F*). ChIP-qPCR analysis confirmed chromatin occupancy of HDAC3 (0.15–0.5%, $p < 0.002$) on identified sites in the conserved noncoding regions within 10 kb upstream of TGF-β pathway genes, including *Smad4*, *Sumo1*, *Tgf- β1*, and *Kpnb1* (Fig. 3.4G–J). We also observed ~3.5-fold higher TGF-β levels in *Hdac3*^{Isl1KO} outflow tracts compared with control ($p < 0.015$; Fig. 3.4K). Loss of HDAC3 resulted in ~2.7-fold activation of SMAD2/3 phosphorylation ($p < 0.02$), suggesting enhanced TGF-β signaling (Fig. 3.4L-M). These results suggest that HDAC3 represses TGF-β signaling pathway during early cardiogenesis.

TGF-β Mediates Aberrant EndMT and Extracellular Matrix Remodeling in Hdac3^{Isl1KO} *Heart*

TGF-β signaling and its downstream target genes, such as *Snai1*, are critical factors that induce EndMT in the developing outflow tract cushions [213]. EndMT is characterized by loss of endothelial markers, such as TEK, and gain of mesenchymal markers, such as TAGLN [206]. *Hdac3*^{Isl1KO} hearts exhibited robust down-regulation of *Tek* and up-regulation of *Snai1* and *Tagln* (Figs. 3.4F and 3.5A). *Hdac3*^{Isl1KO} outflow tract cushion explants showed ~3-fold induction of EndMT ($p < 0.005$; Fig. 3.5B-C), and these changes were largely abolished by TGF-β-neutralizing antibody ($p < 0.009$; Fig. 3.5B–F). Aberrant TGF-β signaling

Table 3.3

Genotyping of *Mef2c-Cre; Hdac3$^{F/+}$* x *Hdac3$^{F/+}$*

	observed (expected)	
	E18.5	P0
Hdac3$^{+/+}$	14 (8)	10 (12)
Hdac3$^{F/+}$	12 (16)	23 (24)
Hdac3$^{F/F}$	6 (8)	12 (12)
Mef2c-Cre; Hdac3$^{+/+}$	10 (8)	18 (12)
Mef2c-Cre; Hdac3$^{F/+}$	13 (16)	30 (24)
Mef2c-Cre; Hdac3$^{F/F}$	9 (8)	3 (12)
Total	64	96
Chi-square	NS	*P = 0.04*

Figure 3.4

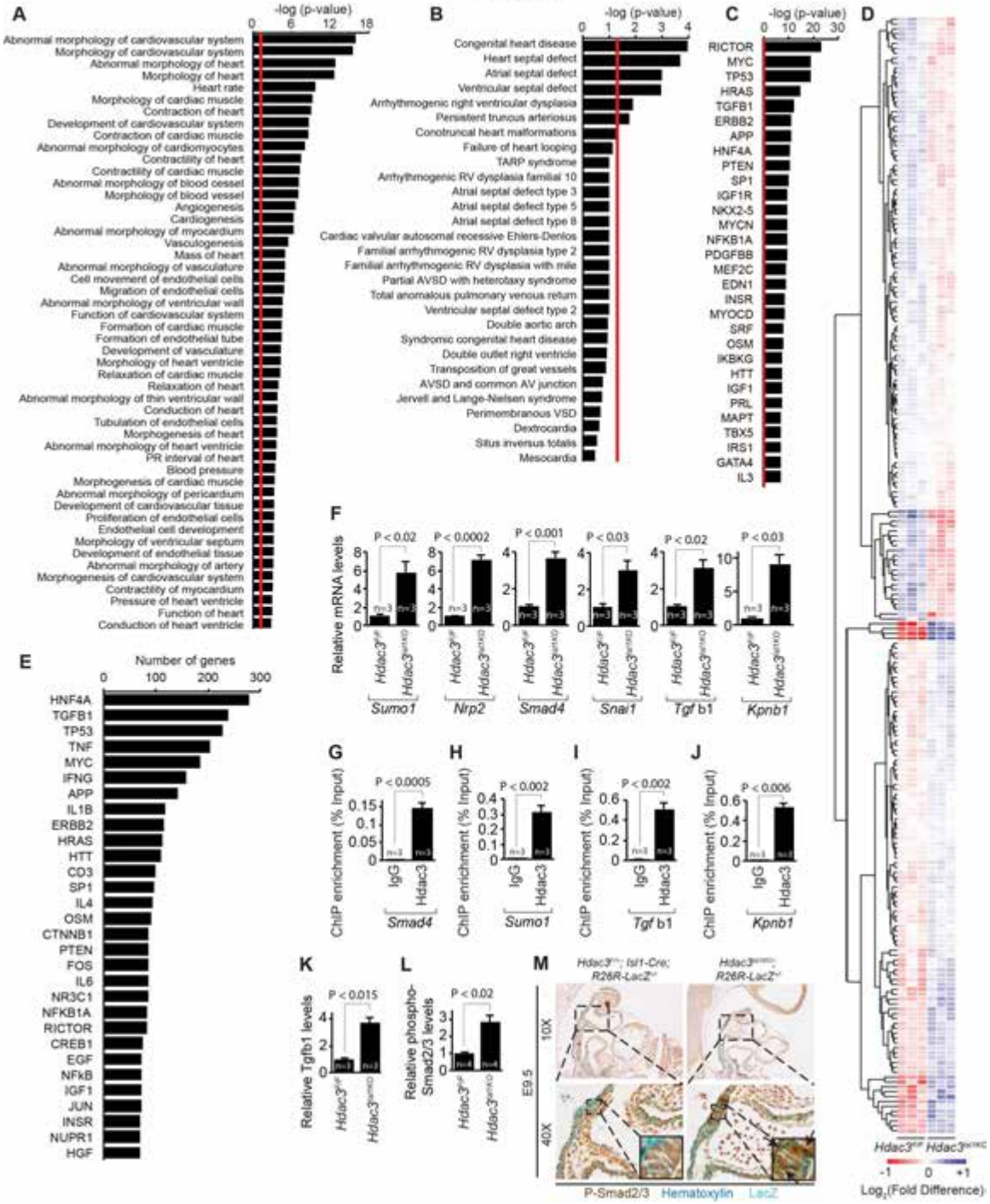
A
-log (p-value)
0 6 12 18
Abnormal morphology of cardiovascular system
Morphology of cardiovascular system
Abnormal morphology of heart
Morphology of heart
Heart rate
Morphology of cardiac muscle
Contraction of heart
Development of cardiovascular system
Contraction of cardiac muscle
Abnormal morphology of cardiomyocytes
Contractility of heart
Contractility of cardiac muscle
Abnormal morphology of blood cessel
Morphology of blood vessel
Angiogenesis
Cardiogenesis
Abnormal morphology of myocardium
Vasculogenesis
Mass of heart
Abnormal morphology of vasculature
Cell movement of endothelial cells
Migration of endothelial cells
Abnormal morphology of ventricular wall
Function of cardiovascular system
Formation of cardiac muscle
Formation of endothelial tube
Development of vasculature
Morphology of heart ventricle
Relaxation of cardiac muscle
Relaxation of heart
Abnormal morphology of thin ventricular wall
Conduction of heart
Tubulation of endothelial cells
Morphogenesis of heart
Abnormal morphology of heart ventricle
PR interval of heart
Blood pressure
Morphogenesis of cardiac muscle
Abnormal morphology of pericardium
Development of cardiovascular tissue
Proliferation of endothelial cells
Endothelial cell development
Morphology of ventricular septum
Development of endothelial tissue
Abnormal morphology of artery
Morphogenesis of cardiovascular system
Contractility of myocardium
Pressure of heart ventricle
Function of heart
Conduction of heart ventricle
B
-log (p-value)
0 1 2 3 4
Congenital heart disease
Heart septal defect
Atrial septal defect
Ventricular septal defect
Arrhythmogenic right ventricular dysplasia
Persistent truncus arteriosus
Conotruncal heart malformations
Failure of heart looping
TARP syndrome
Arrhythmogenic RV dysplasia familial 10
Atrial septal defect type 3
Atrial septal defect type 5
Atrial septal defect type 8
Cardiac valvular autosomal recessive Ehlers-Danlos
Familial arrhythmogenic RV dysplasia type 2
Familial arrhythmogenic RV dysplasia with mile
Partial AVSD with heterotaxy syndrome
Total anomalous pulmonary venous return
Ventricular septal defect type 2
Double aortic arch
Syndromic congenital heart disease
Double outlet right ventricle
Transposition of great vessels
AVSD and common AV junction
Jervell and Lange-Nielsen syndrome
Perimembranous VSD
Dextrocardia
Situs inversus totalis
Mesocardia
C
-log (p-value)
0 10 20 30
RICTOR
MYC
TP53
HRAS
TGFB1
ERBB2
APP
HNF4A
PTEN
SP1
IGF1R
NKX2-5
MYCN
NFKB1A
PDGFBB
MEF2C
EDN1
INSR
MYOCD
SRF
OSM
IKBKG
HTT
IGF1
PRL
MAPT
TBX5
IRS1
GATA4
IL3
D
Hdac3F/F Hdac3Nx/Cx
-1 0 +1
Log2(Fold Difference)
E
Number of genes
0 100 200 300
HNF4A
TGFB1
TP53
TNF
MYC
IFNG
APP
IL1B
ERBB2
HRAS
HTT
CD3
SP1
IL4
OSM
CTNNB1
PTEN
FOS
IL6
NR3C1
NFKB1A
RICTOR
CREB1
EGF
NFkB
IGF1
JUN
INSR
NUPR1
HGF
F
Relative mRNA levels
P < 0.02
P < 0.0002
P < 0.001
P < 0.03
P < 0.02
P < 0.03
n=3
Hdac3F/F
Hdac3Nx/Cx
Sumo1
Nrp2
Smad4
Snai1
Tgf b1
Kpnb1
G
ChIP enrichment (% Input)
P < 0.0005
IgG
Hdac3
Smad4
H
ChIP enrichment (% Input)
P < 0.002
IgG
Hdac3
Sumo1
I
ChIP enrichment (% Input)
P < 0.002
IgG
Hdac3
Tgf b1
J
ChIP enrichment (% Input)
P < 0.006
IgG
Hdac3
Kpnb1
K
Relative Tgfb1 levels
P < 0.015
Hdac3F/F
Hdac3Nx/Cx
L
Relative phospho-Smad2/3 levels
P < 0.02
Hdac3F/F
Hdac3Nx/Cx
M
Hdac3+/-; Isl1-Cre; R26R-LacZ+/-
Hdac3Nx/Cx; R26R-LacZ+/-
E9.5
10X
40X
P-Smad2/3
Hematoxylin
LacZ

Figure 3.4: Hdac3 is a critical regulator of Tgf-β signaling pathway. (A-E) Ingenuity Pathway Analysis (IPA) of microarray data from E9.5 *Hdac3*^{Isl1KO} hearts. **(A)** Cardiovascular development and functions subcategories significantly dysregulated in E9.5 *Hdac3*^{Isl1KO} hearts, sorted by significance, from IPA diseases and functions analysis. **(B)** Classes of congenital heart anomalies affected in E9.5 *Hdac3*^{Isl1KO} hearts, sorted by significance, from IPA diseases and functions analysis. **(C)** Top 30 most significant upstream regulators from IPA upstream analysis of E9.5 *Hdac3*^{Isl1KO} microarray data. **(D)** Clustered heatmap of differentially-expressed genes related to upstream regulator Tgf-β1 from IPA upstream analysis of *Hdac3*^{Isl1KO} microarray data. **(E)** Top 30 upstream regulators, based on number of associated genes differentially-expressed in E9.5 *Hdac3*^{Isl1KO} hearts from IPA upstream analysis. **(F)** Transcripts for *Sumo1*, *Nrp2*, *Smad4*, *Snai1*, *Tgf-β1*, and *Kpnb1* were detected by real-time qPCR in *Hdac3*$^{F/F}$ and *Hdac3*^{Isl1KO} outflow tract with right ventricle derived from E9.5 embryos (mean ± SEM, n=3). **(G-J)** ChIP-qPCR analysis of Hdac3 recruitment to promoter-proximal regions of Tgf-β pathway genes performed in wild-type E9.5 outflow tract (mean ± SEM, n=3). **(K-L)** ELISA for Tgf-β1 **(K)** and phospho-Smad2/3 **(L)** was performed in *Hdac3*$^{F/F}$ and *Hdac3*^{Isl1KO} outflow tracts (mean ± SEM, n=3 **(K)**, n=4 **(L)**). **(M)** Phospho-Smad2/3 immunostaining (arrows) in E9.5 *Hdac3*^{Isl1KO}*; R26R-LacZ*$^{+/-}$ hearts.

activates valvular interstitial cells, which in turn, express smooth muscle genes and produce extracellular matrix scaffold proteins to remodel valvular matrix [201]. *Hdac3*^{Isl1KO} hearts revealed significant expression changes in smooth muscle and extracellular matrix genes (Fig. 3.5A and 3.5G–M). Smooth muscle genes, including *Tagln*, *Myh11*, and *Cnn2*, were up-regulated in *Hdac3*^{Isl1KO} hearts and semilunar valves (Fig. 3.5A and 3.5G-H). Simultaneously, expression of proteoglycans, including *Dcn*, *Bgn*, *Fmod*, and *Vcan*, and collagens, including *Col2a1*, *Col11a2*, *Col9a2*, *Col1a2*, and *Col3a1*, were significantly altered in *Hdac3*^{Isl1KO} hearts and semilunar valves (Fig. 3.5A and 3.5I–M). We next examined the requirement of TGF-β for aberrant expression of extracellular matrix genes in *Hdac3*^{Isl1KO} valvular interstitial cells. Loss of HDAC3 resulted in 6–10-fold expression changes in proteoglycans, collagen, and smooth muscle genes ($p < 0.006$), and these changes were largely abolished by TGF-β-neutralizing antibody (Fig. 3.5H–M). Taken together, these results suggest that aberrant EndMT and extra- cellular matrix remodeling in *Hdac3*^{Isl1KO} hearts are mediated by TGF-β signaling.

HDAC3 Functions within Mesenchymal or Smooth Muscle Cells to Regulate Semilunar Valve and Outflow Tract Development

The second heart field progenitor cells give rise to cardiomyocytes, endothelial cells, and mesenchymal cells or smooth muscle cells [156,225]. Genetic

Figure 3.5

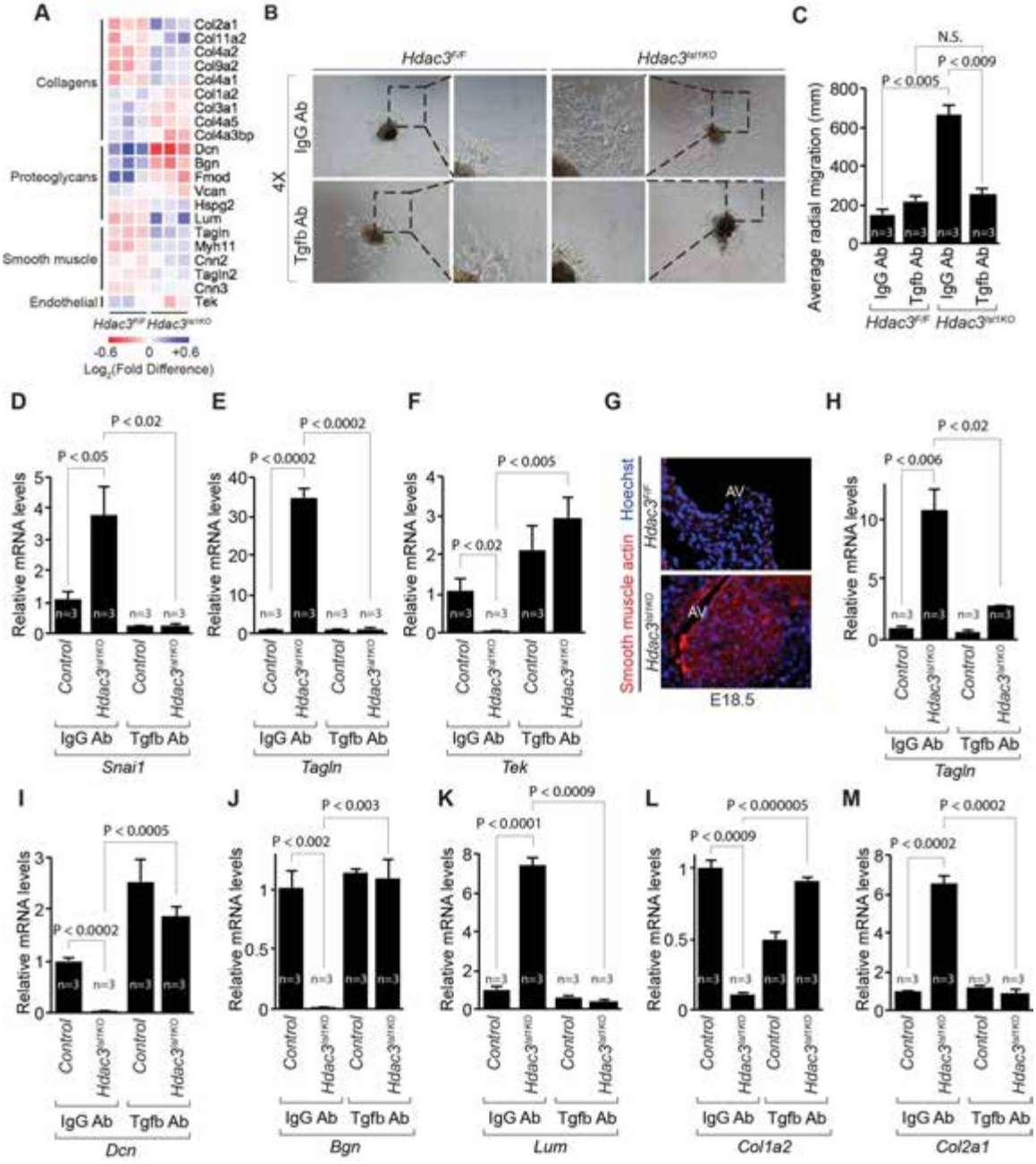
A
Collagens
Proteoglycans
Smooth muscle
Endothelial
Col2a1
Col11a2
Col4a2
Col9a2
Col4a1
Col1a2
Col3a1
Col4a5
Col4a3bp
Dcn
Bgn
Fmod
Vcan
Hspg2
Lum
Tagln
Myh11
Cnn2
Tagln2
Cnn3
Tek
Hdac3F/F Hdac3SMKO
-0.6 0 +0.6
Log2(Fold Difference)
B
Hdac3F/F
Hdac3SMKO
IgG Ab
Tgfb Ab
4X
C
N.S.
P < 0.009
P < 0.005
Average radial migration (mm)
IgG Ab
Tgfb Ab
Hdac3F/F Hdac3SMKO
D
P < 0.02
P < 0.05
Relative mRNA levels
Control
Hdac3SMKO
IgG Ab
Tgfb Ab
Snai1
E
P < 0.0002
Tagln
F
P < 0.005
P < 0.02
Tek
G
Smooth muscle actin
Hoechst
AV
E18.5
H
P < 0.02
P < 0.006
Tagln
I
P < 0.0005
P < 0.0002
Dcn
J
P < 0.003
P < 0.002
Bgn
K
P < 0.0009
P < 0.0001
Lum
L
P < 0.000005
P < 0.0009
Col1a2
M
P < 0.0002
P < 0.0002
Col2a1

Figure 3.5: Tgf-β mediates aberrant expression of EndMT and extracellular matrix genes in *Hdac3*^{Isl1KO} heart. (A) Heatmap of microarray data shows differential expression of extracellular matrix, smooth muscle, and endothelial-related genes in *Hdac3*^{Isl1KO} E9.5 hearts. **(B)** EndMT assay of Tgf-β antibody-treated or IgG antibody-treated outflow tract cushion explants 24 hours after isolation from *Hdac3*^{Isl1KO} and *Hdac3*$^{F/F}$ E10.5 hearts. **(C)** Quantification of average radial migration, measured in 8 directions, from Tgf-β antibody-treated or IgG antibody-treated outflow tract cushion explants from *Hdac3*^{Isl1KO} and *Hdac3*$^{F/F}$ E10.5 hearts, measured 24 hours after isolation. **(D-F)** Transcripts for *Snai1* **(D)**, *Tagln* **(E)**, and *Tek* **(F)** were detected by real-time qPCR in IgG or Tgf-β antibody treated control and *Hdac3*^{Isl1KO} outflow tract explants derived from E9.5 hearts (mean ± SEM, n=3). **(G)** Immunostaining for smooth muscle actin in *Hdac3*^{Isl1KO} and control E18.5 aortic valves (AV). **(H-M)** Transcripts for *Tagln* **(H)**, *Dcn* **(I)**, *Bgn* **(J)**, *Lum* **(K)**, *Col1a2* **(L)**, and *Col2a1* **(M)** were detected by real-time qPCR in IgG or Tgf-β antibody treated control and *Hdac3*^{Isl1KO} proximal outflow tract explants with semilunar valves derived from E14.5 embryos (mean ± SEM, n=3).

deletion of *Hdac3* using *Cdh5-Cre* (*Hdac3*^{Cdh5KO}), which is expressed in differentiated endothelial and endocardial cells at E8.0 [218], and *Myh6-Cre* (*Hdac3*^{Myh6KO}), which is expressed in differentiated cardiomyocytes at E8.5 [178], did not reveal malrotation of outflow tract, overriding aorta, double outlet right ventricle, or valve defects observed in *Hdac3*^{Isl1KO} or *Hdac3*^{Mef2CKO} embryos (Fig. 3.6A–O). Importantly, genetic deletion of *Hdac3* using *Tagln- Cre* (*Hdac3*^{TaglnKO}), which is expressed in differentiated mesenchymal or smooth muscle cells at E8.5 [226], recapitulated outflow tract malrotation, overriding aorta, double outlet right ventricle, aberrant semilunar valve development, membranous ventricular septal defect, disorganized collagen, and fragmented elastin in great vessel walls and showed hyperplastic semilunar valves with expanded proteoglycans and aberrant collagen deposition, as observed in *Hdac3*^{Isl1KO} and *Hdac3*^{Mef2CKO} embryos (Fig. 3.7A–L). Expression of positive regulators of TGF-β pathway genes, smooth muscle markers, proteoglycans, and collagens were 4 –20-fold up-regulated in *Hdac3*^{TaglnKO} semilunar valves ($p < 0.03$; Fig. 3.7M). *Hdac3*^{TaglnKO} outflow tract cushion explants displayed an ~3-fold increase in EndMT ($p < 0.03$) and ~20 – 40-fold expression changes in proteoglycans and smooth muscle genes ($p < 0.004$; Fig. 3.7N–Q). Importantly, these changes were largely abolished by TGF-β-neutralizing antibody ($p < 0.004$), suggesting that aberrant EndMT and extracellular matrix remodeling in *Hdac3*^{TaglnKO} hearts are mediated by TGF-β signaling (Fig. 3.7N–Q). Together,

these data suggest a primary role of HDAC3 in the second heart field-derived mesenchymal or smooth muscle cells during early cardiac development.

HDAC3 Epigenetically Silences TGF-β1 within Mesenchymal Cells by Recruiting EZH2 to the NCOR Complex

During EndMT, endothelial cells lose their endothelium-specific markers and morphology and acquire a mesenchymal cell-like phenotype [206]. In this process, endothelium-derived mesenchymal cells displayed >90% repression of TGF-β1 expression compared with endothelial cells ($p < 0.003$); however, this repression was completely absent in mesenchymal cells lacking HDAC3 (Fig. 3.8A-B). We observed ~0.6 –1.8% enrichment of HDAC3 at a regulatory region upstream of TGF-β1 within mesenchymal cells compared with endothelial cells ($p < 0.02$; Fig. 3.8C-D). We evaluated chromatin occupancy of various histone marks to determine the regulatory mechanism of the HDAC3-enriched region upstream of TGF-β1 within mesenchymal cells. ChIP-qPCR analysis revealed loss of trimethylation of Lys-27 on histone H3 (H3K27me3) and ~8% enrichment of acetylation of Lys-27 on histone H3 (H3K27ac) at the TGF-β1 regulatory region in $Hdac3^{Isl1KO}$ semilunar valves compared with control ($p < 0.04$, Fig. 3.8E-F). Consistent with these findings, $Hdac3^{Isl1KO}$ semilunar valves displayed ~0.9 – 3% enrichment of RNA polymerase II and CREBBP ($p < 0.006$) and abolished occupancy of EZH2, EED, and SUZ12, the H3K27 methyltransferase components of PRC2 complex, at the TGF-β1 regulatory region (Fig. 3.8G–K).

NCOR1 was required for recruitment of HDAC3 to the TGF-β1 locus (Fig. 3.8L). Interestingly, NCOR1 occupancy remained unchanged at this locus in *Hdac3*^{Isl1KO} semilunar valves, suggesting that HDAC3 is not required for NCOR1 recruitment to the TGF-β1 regulatory region (Fig. 3.8M). Co-ChIP-qPCR analysis revealed co-occupancy of HDAC3 with either EZH2, H3K27me3, or NCOR1 at the TGF-β1 locus in wild-type semilunar valves (Fig. 3.8N). HDAC3 interacts with EZH2 within mesenchymal cells of semilunar valves (Fig. 3.8O). Importantly, EZH2 and NCOR1 are required for deposition of the H3K27me3 mark at the TGF-β1 locus within valvular mesenchymal cells (Fig. 3.8P). These data suggest that HDAC3 is required to mediate epigenetic silencing of TGF-β1 within mesenchymal cells of semilunar valves.

Deacetylase Activity of HDAC3 Is Dispensable for EndMT and Epigenetic Silencing of TGF-β1

Approximately 10% of mammalian enzymes are catalytically inactive [227]. These "dead" enzymes or pseudoenzymes are biologically functional; however, their enzyme-independent functions remain largely undefined. A recent study [144] describes a deacetylase-independent function of HDAC3 in lipid metabolism. To determine whether deacetylase activity of HDAC3 is required to regulate EndMT, expression of *Tgf-β1*, and recruitment of EZH2 to the TGF-β1 locus, we generated a previously described mutant form of HDAC3 in which two highly conserved tandem His residues, 134 and 135, are mutated to alanine

Figure 3.6

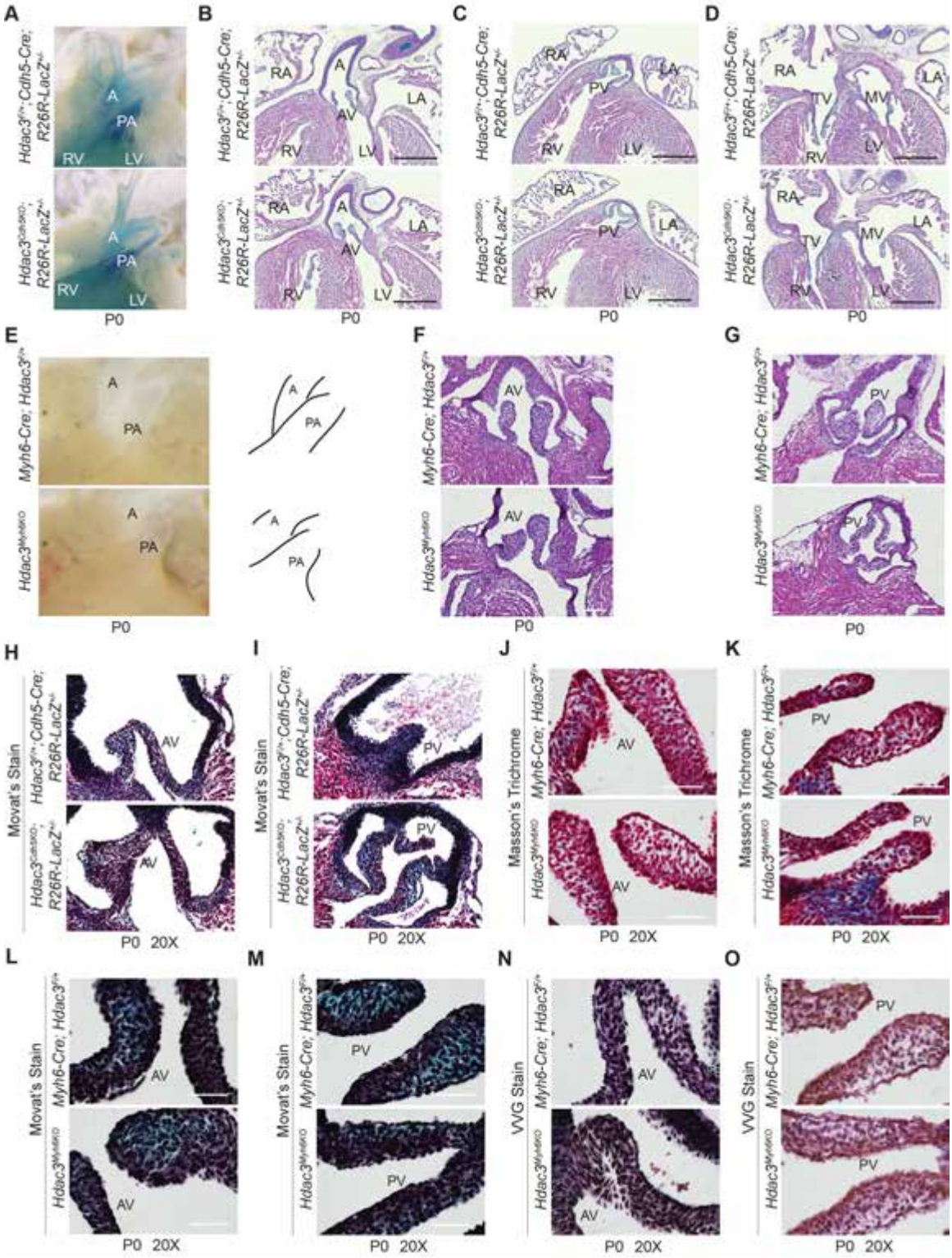
A
B
C
D
E
F
G
H
I
J
K
L
M
N
O
Hdac3f/+;Cdh5-Cre; R26R-LacZ+/-
Hdac3Cdh5KO; R26R-LacZ+/-
Myh6-Cre; Hdac3f/+
Hdac3MyhKO
RA
LA
RV
LV
A
PA
AV
PV
TV
MV
P0
P0 20X
Movat's Stain
Masson's Trichrome
VVG Stain

Figure 3.6: Endocardial or myocardial Hdac3 is dispensable for morphogenesis of second heart field-derived structures. (A-D) *Hdac3*^{Cdh5KO} hearts appear normal at birth. **(A)** Position of aorta and pulmonary artery appear normal in *Hdac3*^{Cdh5KO} mice hearts at birth (P0). **(B-D)** Hematoxylin, eosin and LacZ stained sections of hearts from control and *Hdac3*^{Cdh5KO} mice. **(B)** Aortic valve, **(C)** pulmonic valve, **(D)** tricuspid valve, and mitral valve appear normal in size and shape *Hdac3*^{Cdh5KO} hearts. **(E-G)** *Hdac3*^{Myh6KO} hearts appear normal at birth. **(E)** Position of aorta and pulmonary artery appear normal in *Hdac3*^{Myh6KO} hearts at birth. **(F-G)** Hematoxylin- and eosin-stained sections of hearts from control and *Hdac3*^{Myh6KO} mice. **(F)** Aortic valves and **(G)** pulmonic valves appear normal in size and shape in *Hdac3*^{Myh6KO} hearts as compared to control. **(H-I)** Movat's pentachrome staining show normal extracellular matrix organization in *Hdac3*^{Cdh5KO} P0 **(H)** aortic valves and **(I)** pulmonic valves. **(J-O)** *Hdac3*^{Myh6KO} extracellular matrix appears normal. **(J-K)** Masson's trichrome staining of **(J)** aortic valve and **(K)** pulmonic valve, **(L-M)** Movat's pentachrome staining of **(L)** aortic valve and **(M)** pulmonic valve, and **(N-O)** Verhoeff-van Gieson staining of **(N)** aortic valve and **(O)** pulmonic valve show normal extracellular matrix in semilunar valve cusps of P0 *Hdac3*^{Myh6KO} hearts. A = aorta, PA = pulmonary artery, RA = right atrium, LA = left atrium, RV = right ventricle, LV = left ventricle, PV = pulmonic valve, AV = aortic valve, TV = tricuspid valve, MV = mitral valve. Scale bars are 50μm respectively.

Figure 3.7

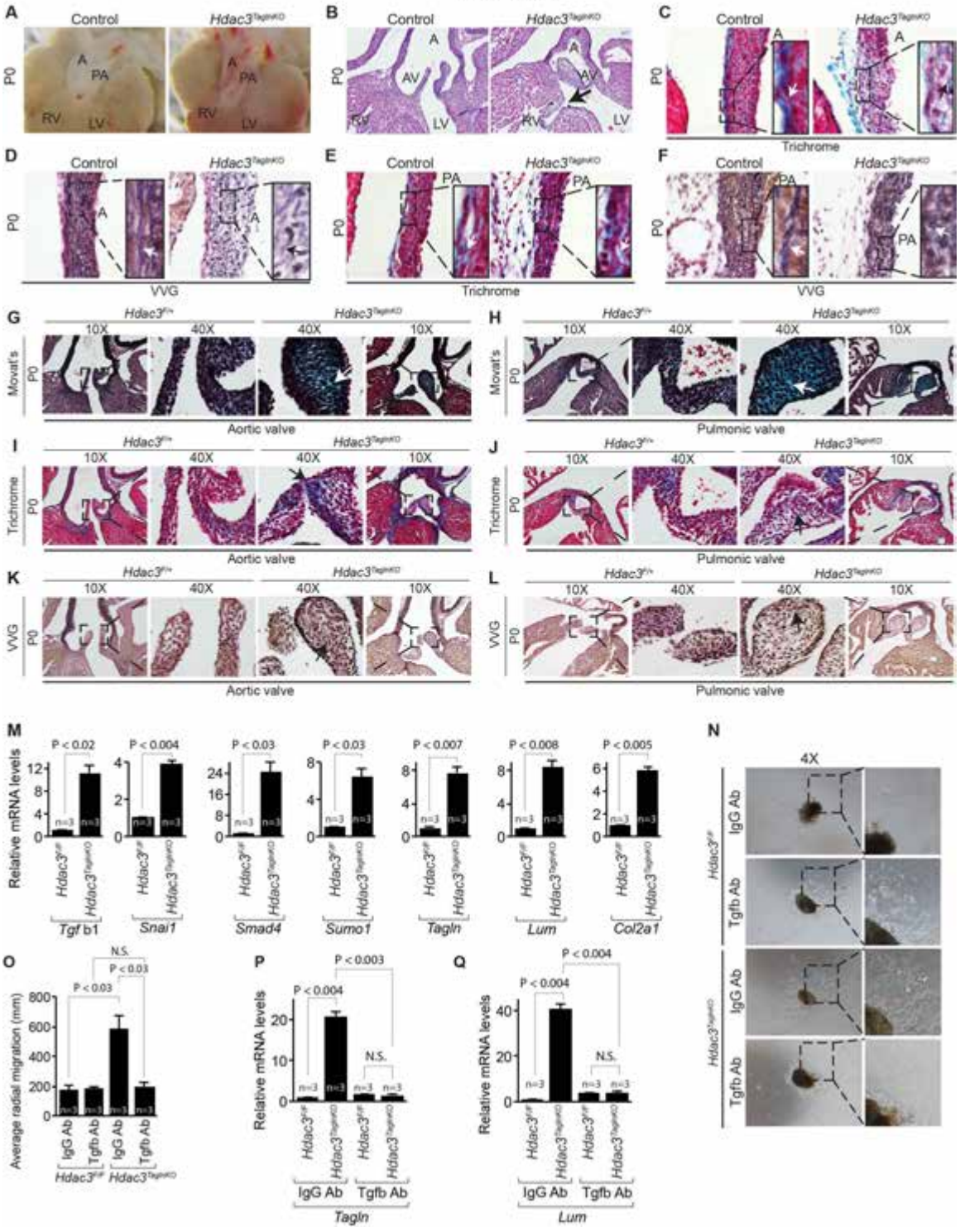
A
Control
Hdac3TagInKO
P0
A
PA
RV
LV
B
AV
C
Trichrome
D
VVG
E
F
G
Hdac3f/+
10X
40X
Movat's
Aortic valve
H
Pulmonic valve
I
J
K
L
M
Relative mRNA levels
P < 0.02
P < 0.004
P < 0.03
P < 0.007
P < 0.008
P < 0.005
n=3
Tgf b1
Snai1
Smad4
Sumo1
Tagln
Lum
Col2a1
N
4X
IgG Ab
Tgfb Ab
O
Average radial migration (mm)
N.S.
P
Q

Figure 3.7: Hdac3 functions within mesenchymal or smooth muscle cells to regulate outflow tract and semilunar valve development. (A) Dissected, fixed P0 hearts show malrotation of the aorta and pulmonary artery in *Hdac3*^{TaglnKO} hearts. (B) Hematoxylin- and eosin-stained sections show double outlet right ventricle with aortic valve (AV) overriding a ventricular septal defect (arrow) in *Hdac3*^{TaglnKO} P0 hearts. **(C)** Masson's trichrome staining of P0 aortic vessel wall shows collagen on the outer surface of control aortic walls (white arrow, blue staining) and aberrant collagen expression throughout the vessel wall (black arrow, blue staining) in *Hdac3*^{TaglnKO} aortic walls. **(D)** Verhoeff-Van Gieson (VVG) staining of P0 aortic vessel wall shows thick, continuous elastin fibers (white arrow, grey staining) in control aortas and thin, fragmented elastin fibers (black arrow, grey staining) in *Hdac3*^{TaglnKO} aortas. **(E)** Masson's trichrome staining of P0 pulmonic artery wall shows collagen on the outer surface of control pulmonic artery walls (white arrow, blue staining) and aberrant collagen expression throughout the vessel wall (white arrow, blue staining) in *Hdac3*^{TaglnKO} pulmonic artery walls. **(F)** Verhoeff-Van Gieson (VVG) staining of P0 pulmonic artery wall shows thick, continuous elastin fibers (white arrow, grey staining) in control aortas and thin, fragmented elastin fibers (white arrow, grey staining) in *Hdac3*^{TaglnKO} pulmonic arteries. **(G)** Movat's pentachrome staining of P0 aortic valve shows expanded proteoglycans (arrow, blue) in *Hdac3*^{TaglnKO} aortic valve compared to *Hdac3*$^{F/+}$ control. **(H)** Movat's pentachrome staining of P0 pulmonic valve shows expanded proteoglycans (arrow, blue) in *Hdac3*^{TaglnKO} pulmonic valve compared to *Hdac3*$^{F/+}$ control. **(I)** Masson's trichrome staining of P0 aortic valves shows disorganized collagen expression (arrow, blue) in *Hdac3*^{TaglnKO} aortic valve. **(J)** Masson's trichrome staining of P0 pulmonic valves shows disorganized collagen expression (arrow, blue) in *Hdac3*^{TaglnKO} pulmonic valve. **(K)** Verhoeff-Van Gieson (VVG) stain of P0 aortic valves demonstrates disorganized collagen expression (arrow, red) in *Hdac3*^{TaglnKO} aortic valve. **(L)** Verhoeff-Van Gieson (VVG) stain of P0 pulmonic valves demonstrates disorganized collagen expression (arrow, red) in *Hdac3*^{TaglnKO} pulmonic valve. **(M)** Relative mRNA levels of *Tgf-β1*, *Snai1*, *Smad4*, *Sumo1*, *Tagln*, *Lum*, and *Col2a1* show increased expression in *Hdac3*^{TaglnKO} E14.5 hearts. **(N)** EndMT assay of Tgf-β antibody-treated or IgG antibody-treated outflow tract cushion explants from *Hdac3*^{TaglnKO} and *Hdac3*$^{F/F}$ E10.5 hearts, 24 hours after isolation. **(O)** Quantification of average radial migration, measured in 8 directions, from Tgf-β antibody-treated or IgG antibody-treated outflow tract cushion explants from *Hdac3*^{TaglnKO} and *Hdac3*$^{F/F}$ E10.5 hearts, measured 24 hours after isolation. **(P-Q)** Transcripts for *Tagln* **(P)** and *Lum* **(Q)** were detected by real-time qPCR in IgG or Tgf-β antibody treated control and *Hdac3*^{TaglnKO} outflow tract cushion explants derived from E10.5 hearts (mean ± SEM, n=3).

(HDAC3^{H134A,H135A}). These mutations do not affect its expression (Fig. 3.9A-B), chromatin recruitment, and interaction with NCOR1 [144]; however, they render HDAC3 completely inactive (Fig. 3.9C). HDAC3-null outflow tract cushion explants showed an ~2-fold increase in EndMT ($p < 0.05$), and these changes were largely rescued by either wild-type HDAC3 or HDAC3^{H134A,H135A} expression ($p < 0.04$; Fig. 3.9D-E). Similarly, either wild-type HDAC3 or HDAC3^{H134A,H135A} rescued aberrant *Tgf-β1* transcription within cultured HDAC3-null semilunar valve mesenchymal cells ($p < 0.0004$; Fig. 3.9F). Hence, we generated a mutant TGF-β1 promoter luciferase reporter lacking the HDAC3 enriched regulatory region (-42 to -1 upstream of ATG). Transfection of HDAC3 or HDAC3^{H134A,H135A} resulted in >90% repression of the wild-type TGF-β1 reporter ($p < 0.002$); however, it failed to repress the mutant TGF-β1 reporter (Fig. 3.9G). The mutant TGF-β1 promoter luciferase reporter displayed transcriptional activity similar to control (Fig. 3.9G). Interestingly, valvular mesenchymal cells expressing HDAC3^{H134A,H135A} showed similar levels of H3K27ac at the TGF-β1 locus compared with those expressing wild-type HDAC3, although HDAC3^{H134A,H135A} lacks the ability to actively deacetylate histones (Fig. 3.9H). Either wild-type HDAC3 or HDAC3^{H134A,H135A} expression restored chromatin occupancy of EZH2, EED, and SUZ12 and thereby deposition of the H3K27me3 mark at the TGF-β1 locus in cultured HDAC3- null semilunar valve mesenchymal cells (Fig. 3.9I–L). Taken together,

Figure 3.8

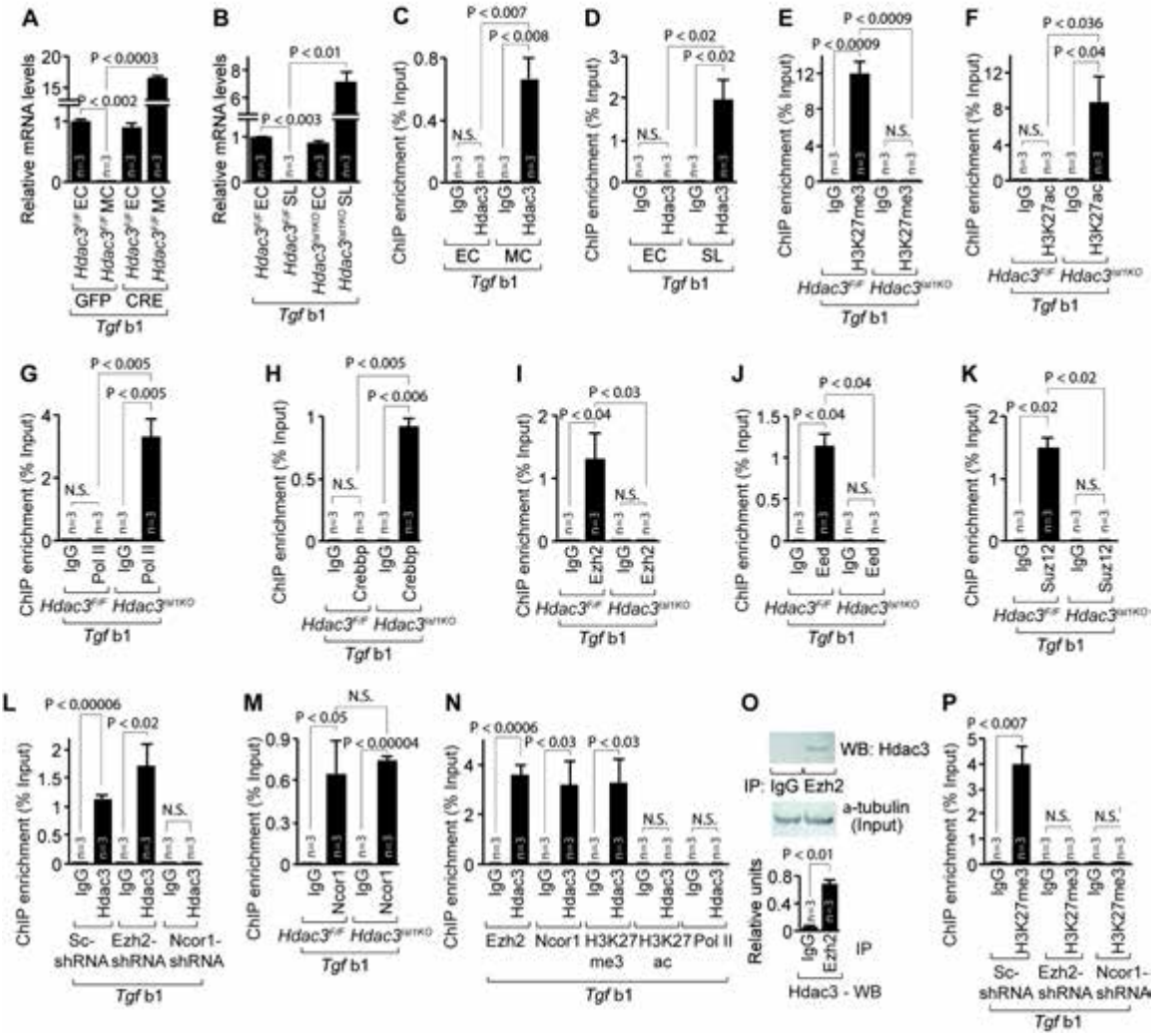
A
Relative mRNA levels
P < 0.0003
P < 0.002
Hdac3F/F EC
Hdac3F/F MC
Hdac3F/F EC
Hdac3F/F MC
GFP
CRE
Tgf b1
B
Relative mRNA levels
P < 0.01
P < 0.003
Hdac3F/F EC
Hdac3F/F SL
Hdac3W1KO EC
Hdac3W1KO SL
Tgf b1
C
ChIP enrichment (% Input)
P < 0.007
P < 0.008
N.S.
IgG
Hdac3
EC
MC
Tgf b1
D
ChIP enrichment (% Input)
P < 0.02
P < 0.02
N.S.
EC
SL
Tgf b1
E
ChIP enrichment (% Input)
P < 0.0009
P < 0.0009
N.S.
H3K27me3
Hdac3F/F
Hdac3W1KO
Tgf b1
F
ChIP enrichment (% Input)
P < 0.036
P < 0.04
N.S.
H3K27ac
Hdac3F/F
Hdac3W1KO
Tgf b1
G
ChIP enrichment (% Input)
P < 0.005
P < 0.005
N.S.
Pol II
Hdac3F/F
Hdac3W1KO
Tgf b1
H
ChIP enrichment (% Input)
P < 0.005
P < 0.006
N.S.
Crebbp
Hdac3F/F
Hdac3W1KO
Tgf b1
I
ChIP enrichment (% Input)
P < 0.03
P < 0.04
N.S.
Ezh2
Hdac3F/F
Hdac3W1KO
Tgf b1
J
ChIP enrichment (% Input)
P < 0.04
P < 0.04
N.S.
Eed
Hdac3F/F
Hdac3W1KO
Tgf b1
K
ChIP enrichment (% Input)
P < 0.02
P < 0.02
N.S.
Suz12
Hdac3F/F
Hdac3W1KO
Tgf b1
L
ChIP enrichment (% Input)
P < 0.00006
P < 0.02
N.S.
Hdac3
Sc-shRNA
Ezh2-shRNA
Ncor1-shRNA
Tgf b1
M
ChIP enrichment (% Input)
N.S.
P < 0.05
P < 0.00004
Ncor1
Hdac3F/F
Hdac3W1KO
Tgf b1
N
ChIP enrichment (% Input)
P < 0.0006
P < 0.03
P < 0.03
N.S.
N.S.
Ezh2
Ncor1
H3K27me3
H3K27ac
Pol II
Tgf b1
O
WB: Hdac3
IP: IgG Ezh2
a-tubulin (Input)
Relative units
P < 0.01
IgG
Ezh2
IP
Hdac3 - WB
P
ChIP enrichment (% Input)
P < 0.007
N.S.
N.S.
H3K27me3
Sc-shRNA
Ezh2-shRNA
Ncor1-shRNA
Tgf b1

Figure 3.8: Hdac3 epigenetically silences Tgf-β1 within valvular mesenchymal cells by recruiting Ezh2 to the Ncor complex. (A) Relative mRNA levels of Tgf-β1 in isloated cardiac endothelial cells (EC) or cardiac mesenchymal cells (MC) from E10.5 *Hdac3*$^{F/F}$ outflow tract cushion explants, infected either with CRE or GFP control lentivirus. **(B)** Relative mRNA levels of Tgf-β1 in isolated cardiac endothelial cells (EC) or dissected semilunar vales (SL) derived from *Hdac3*^{Isl1KO} and *Hdac3*$^{F/F}$ E14.5 hearts. **(C)** ChIP-qPCR analysis of Hdac3 occupancy upstream of Tgf-β1 in isolated cardiac endothelial cells (EC) or cardiac mesenchymal cells (MC) from E10.5 outflow tract cushion explants. **(D)** ChIP-qPCR analysis of Hdac3 occupancy upstream of Tgf-β1 in isolated cardiac endothelial cells (EC) or dissected semilunar valves (SL) from E14.5 hearts. **(E-K)** ChIP-qPCR analysis of **(E)** H3K27 tri-methylation, **(F)** H3K27 acetylation, **(G)** RNA polymerase II, **(H)** Crebbp, **(I)** Ezh2, **(J)** Eed, and **(K)** Suz12 upstream of Tgf-β1 in *Hdac3*^{Isl1KO} and control E14.5 semilunar valves. **(L)** ChIP-qPCR analysis of Hdac3 occupancy upstream of Tgf-β1 in E14.5 valvular mesenchymal cells infected with either control shRNA (sc-shRNA), Ezh2-shRNA, or Ncor1-shRNA. **(M)** ChIP-qPCR analysis of Ncor1 upstream of Tgf-β1 in *Hdac3*^{Isl1KO} and control E14.5 semilunar valves **(N)** Co-ChIP for Hdac3 and either Ezh2, Ncor1, H3K27me3, H3K27ac, or Pol II upstream of Tgf-β1 in E14.5 wild-type dissected semilunar valves. **(O)** Total lysates from E14.5 wild-type pooled semilunar valves were immunoprecipitated by Ezh2 antibody, and western blot was performed using Hdac3 antibody. α-tubulin is shown as an input control. Hdac3 was quantified and normalized to total input α-tubulin using ImageJ software (mean ± SEM, n=3). **(P)** ChIP-qPCR analysis of H3K27me3 upstream of Tgf-β1 in E14.5 valvular mesenchymal cells infected with either control shRNA (sc-shRNA), Ezh2-shRNA, or Ncor1-shRNA.

these findings demonstrate that HDAC3-mediated epigenetic silencing of TGF-β1 within second heart field-derived mesenchymal cells is essential for termination of EndMT (Fig. 3.10A-B). In the absence of HDAC3, aberrant expression of TGF-β within mesenchymal cells leads to perpetual activation of mesenchymal cells to myofibroblasts, altered extracellular matrix homeostasis, and enhanced EndMT, which in turn, leads to congenital cardiac anomalies resembling those seen in patients with mutations causing activation of the TGF-β signaling pathway (Fig. 3.10A-B).

Discussion

Previous studies from our group and others have demonstrated that HDACs are critical regulators of various develop- mental processes, including cardiogenesis [122,216]. Among class I HDACs (HDAC1, -2, -3, and -8), global loss of HDAC2 or HDAC8 in mice does not affect morphogenesis of second heart field-derived structures at birth [123,140,215]. Interestingly, murine embryos lacking HDAC1 within the second heart field (*Hdac1*^{Isl1KO}) display normal cardiogenesis, including development of the outflow tract and semilunar valves (Z. Milstone and C.M. Trivedi, unpublished results). Similarly, second heart field-derived structures appear normal in mice lacking class II HDACs, such as HDAC4, -5, -6, or -9 at birth [119]. Taken together, our data reveal a unique and a specific role for HDAC3 in regulation of second heart field morphogenesis.

Figure 3.9

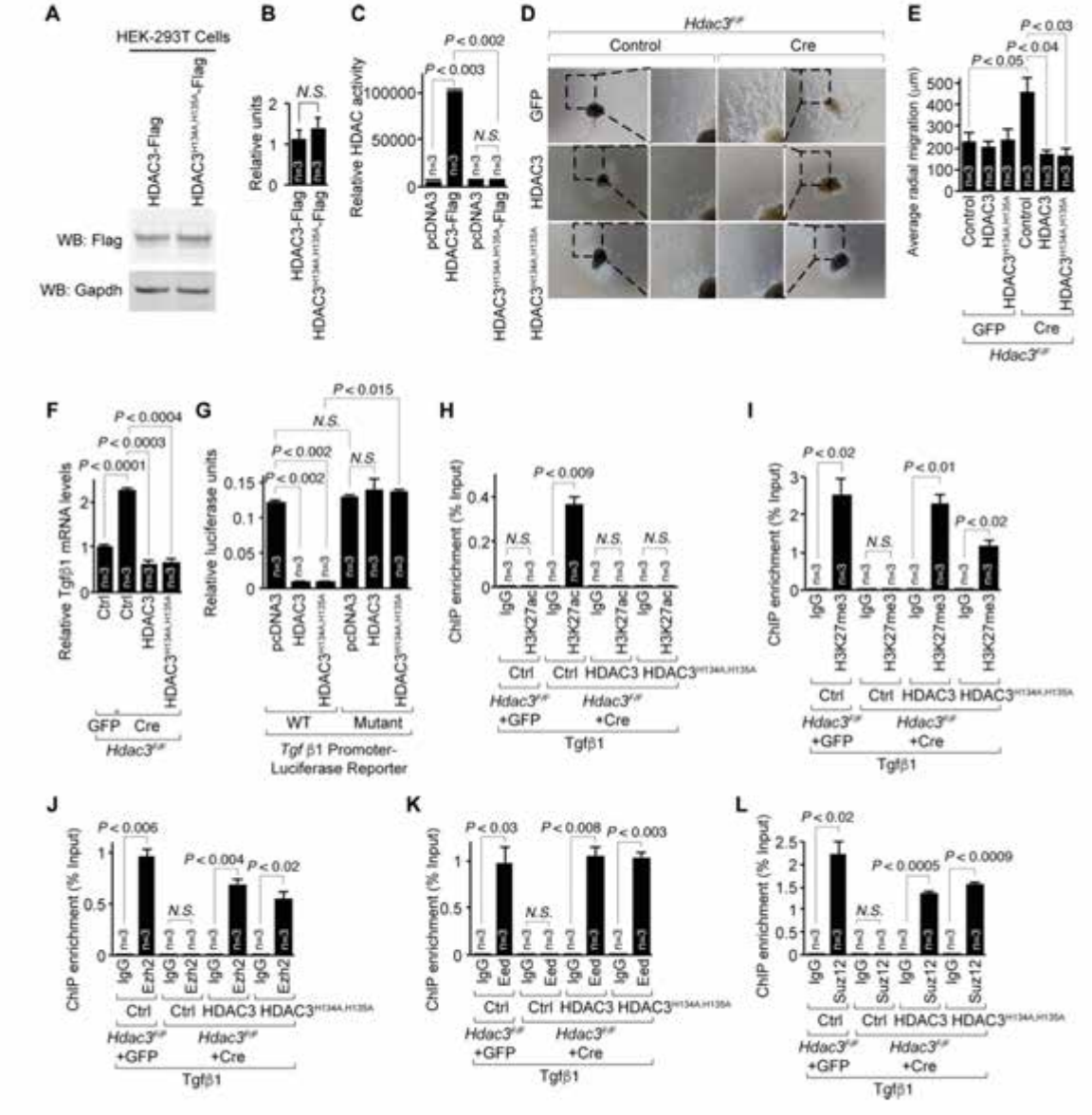
A
HEK-293T Cells
HDAC3-Flag
HDAC3H134A,H135A-Flag
WB: Flag
WB: Gapdh
B
Relative units
N.S.
C
Relative HDAC activity
P < 0.002
P < 0.003
N.S.
pcDNA3
HDAC3-Flag
HDAC3H134A,H135A-Flag
D
Hdac3f/f
Control
Cre
GFP
HDAC3
HDAC3H134A,H135A
E
Average radial migration (μm)
P < 0.03
P < 0.04
P < 0.05
Control
HDAC3
HDAC3H134A,H135A
GFP
Cre
Hdac3f/f
F
Relative Tgfβ1 mRNA levels
P < 0.0004
P < 0.0003
P < 0.0001
Ctrl
HDAC3
HDAC3H134A,H135A
GFP
Cre
Hdac3f/f
G
Relative luciferase units
P < 0.015
N.S.
P < 0.002
P < 0.002
N.S.
pcDNA3
HDAC3
HDAC3H134A,H135A
WT
Mutant
Tgf β1 Promoter-Luciferase Reporter
H
ChIP enrichment (% Input)
P < 0.009
N.S.
IgG
H3K27ac
Ctrl
HDAC3
HDAC3H134A,H135A
Hdac3f/f
+GFP
+Cre
Tgfβ1
I
ChIP enrichment (% Input)
P < 0.02
P < 0.01
P < 0.02
N.S.
IgG
H3K27me3
Ctrl
HDAC3
HDAC3H134A,H135A
Hdac3f/f
+GFP
+Cre
Tgfβ1
J
ChIP enrichment (% Input)
P < 0.006
P < 0.004
P < 0.02
N.S.
IgG
Ezh2
Ctrl
HDAC3
HDAC3H134A,H135A
Hdac3f/f
+GFP
+Cre
Tgfβ1
K
ChIP enrichment (% Input)
P < 0.03
P < 0.008
P < 0.003
N.S.
IgG
Eed
Ctrl
HDAC3
HDAC3H134A,H135A
Hdac3f/f
+GFP
+Cre
Tgfβ1
L
ChIP enrichment (% Input)
P < 0.02
P < 0.0005
P < 0.0009
N.S.
IgG
Suz12
Ctrl
HDAC3
HDAC3H134A,H135A
Hdac3f/f
+GFP
+Cre
Tgfβ1

Figure 3.9: Hdac3 functions in a deacetylase-independent manner to regulate EndMT and epigenetic silencing of Tgf-β1. (A) HDAC3-Flag and HDAC3^{H134A,H135A}-Flag expression constructs were transfected in HEK-293T cells. Expression was detected by western blot from whole cell lysates using Flag antibody. Gapdh is shown as a loading control. **(B)** HDAC3-Flag and HDAC3^{H134A,H135A}-Flag expression was quantified and normalized to total input Gapdh using ImageJ software (mean ± S.D., n=3). **(C)** HDAC activity of HDAC3-Flag and HDAC3^{H134A,H135A}-Flag expression was quantified against a pseudosubstrate. **(D)** EndMT assay of control- or Cre-infected E10.5 *Hdac3$^{F/F}$* outflow tract cushion explants co-infected with GFP, HDAC3-Flag, or HDAC3^{H134A,H135A}-Flag lentiviruses, imaged 24 hours after isolation. **(E)** Quantification of average radial migration, measured in 8 directions, of control- or Cre-infected E10.5 *Hdac3$^{F/F}$* outflow tract cushion explants co-infected with GFP, HDAC3-Flag, or HDAC3^{H134A,H135A}-Flag lentiviruses, measured 24 hours after isolation (mean ± SEM, n=3). **(F)** Relative mRNA levels of *Tgf-β1* in control- or Cre-infected E14.5 *Hdac3$^{F/F}$* valvular mesenchymal cells co-infected with control, HDAC3-Flag, or HDAC3^{H134A,H135A}-Flag lentiviruses (mean ± SEM, n=3). **(G)** A 1309bp Tgf-β1 promoter luciferase reporter (WT) or a truncated, 1267bp Tgf-β1 promoter luciferase reporter, lacking a Hdac3 enriched region (mutant) were transfected in murine endothelial cells with and without an Hdac3 or HDAC3^{H134A,H135A} expression plasmid. Induction is represented as a ratio of firefly and renilla luciferase activity. **(H-J)** ChIP-qPCR analysis of **(H)** H3K27 acetylation, **(I)** H3K27 tri-methylation, and **(J)** Ezh2 upstream of Tgf-β1 in control- or Cre-infected E14.5 *Hdac3$^{F/F}$* valvular mesenchymal cells co-infected with control, HDAC3-Flag, or HDAC3^{H134A,H135A}-Flag lentiviruses (mean ± SEM, n=3).

Figure 3.10

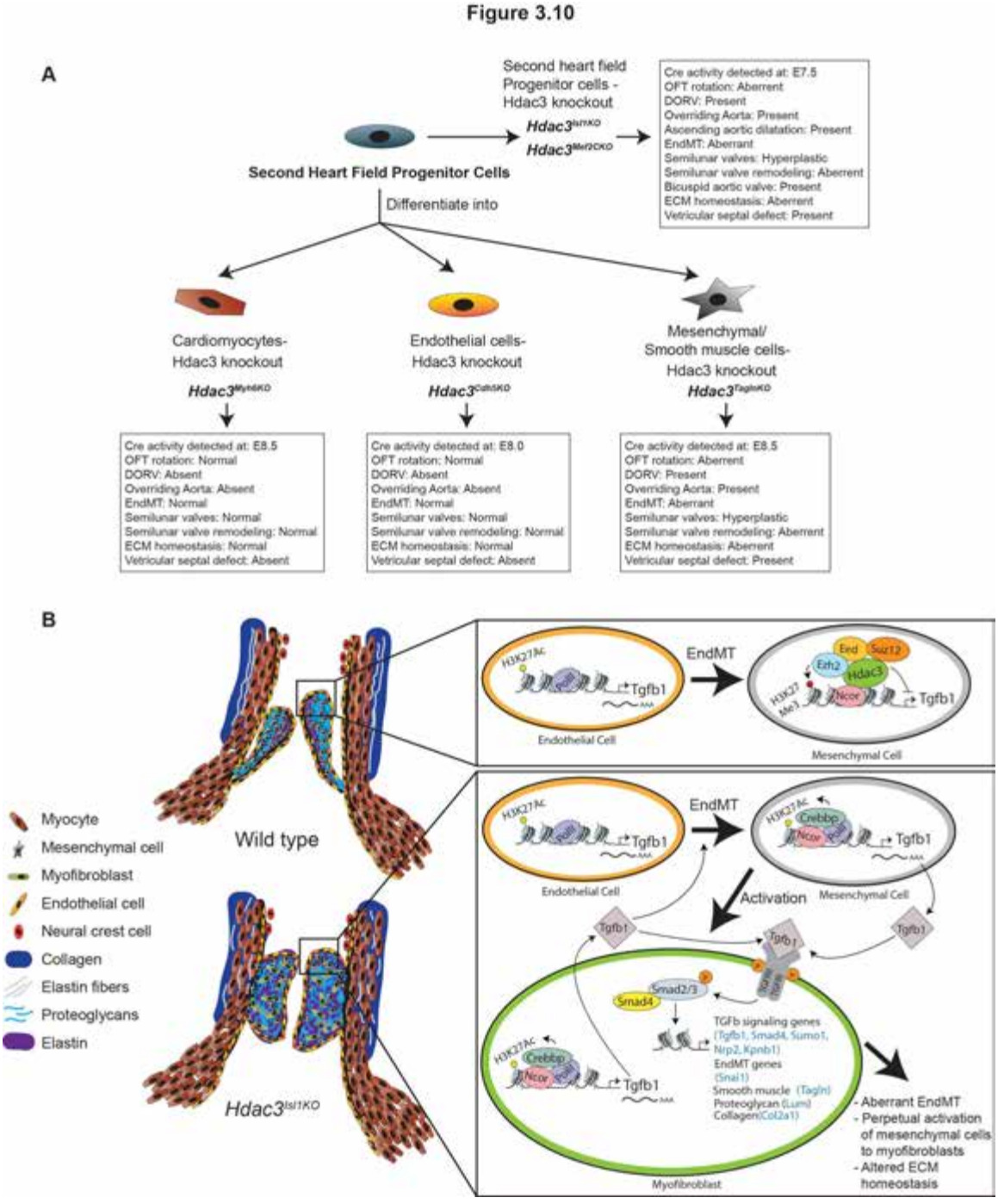
A
Second heart field Progenitor cells - Hdac3 knockout
Hdac3Isl1KO
Hdac3Mef2CKO
Cre activity detected at: E7.5
OFT rotation: Aberrent
DORV: Present
Overriding Aorta: Present
Ascending aortic dilatation: Present
EndMT: Aberrant
Semilunar valves: Hyperplastic
Semilunar valve remodeling: Aberrent
Bicuspid aortic valve: Present
ECM homeostasis: Aberrent
Vetricular septal defect: Present
Second Heart Field Progenitor Cells
Differentiate into
Cardiomyocytes- Hdac3 knockout
Hdac3MyhKO
Endothelial cells- Hdac3 knockout
Hdac3CdhKO
Mesenchymal/ Smooth muscle cells- Hdac3 knockout
Hdac3TaglnKO
Cre activity detected at: E8.5
OFT rotation: Normal
DORV: Absent
Overriding Aorta: Absent
EndMT: Normal
Semilunar valves: Normal
Semilunar valve remodeling: Normal
ECM homeostasis: Normal
Vetricular septal defect: Absent
Cre activity detected at: E8.0
OFT rotation: Normal
DORV: Absent
Overriding Aorta: Absent
EndMT: Normal
Semilunar valves: Normal
Semilunar valve remodeling: Normal
ECM homeostasis: Normal
Vetricular septal defect: Absent
Cre activity detected at: E8.5
OFT rotation: Aberrent
DORV: Present
Overriding Aorta: Present
EndMT: Aberrant
Semilunar valves: Hyperplastic
Semilunar valve remodeling: Aberrent
ECM homeostasis: Aberrent
Vetricular septal defect: Present
B
Myocyte
Mesenchymal cell
Myofibroblast
Endothelial cell
Neural crest cell
Collagen
Elastin fibers
Proteoglycans
Elastin
Wild type
Hdac3Isl1KO
H3K27AC
Tgfb1
EndMT
Endothelial Cell
Mesenchymal Cell
Eed
Suz12
Ezh2
Hdac3
H3K27 Me3
Ncor
Crebbp
Activation
Smad2/3
Smad4
TGFb signaling genes (Tgfb1, Smad4, Sumo1, Nrp2, Kpnb1)
EndMT genes (Snai1)
Smooth muscle (Tagln)
Proteoglycan (Lum)
Collagen(Col2a1)
Myofibroblast
- Aberrant EndMT
- Perpetual activation of mesenchymal cells to myofibroblasts
- Altered ECM homeostasis

Figure 3.10: Summary of phenotypes and proposed model of Hdac3 function within second heart field progenitor cells and second heart field-derived mesenchymal cells. (A) Loss of Hdac3 in second heart field progenitor cells leads to outflow tract and semilunar valve pathologies. Strikingly, genetic deletion of Hdac3 in differentiated mesenchymal and smooth muscle cells (*Hdac3*^{TaglnKO}) recapitulates the majority of these phenotypes. However, deletion of Hdac3 in differentiated cardiomyocytes (*Hdac3*^{Myh6KO}) or endothelial cells (*Hdac3*^{Cdh5KO}) did not recapitulate the cardiovascular defects observed in *Hdac3*^{Isl1KO} embryos. **(B)** *Hdac3*^{Isl1KO} hearts exhibit disorganized collagen and elastin within dilated aortic walls and hyperplastic semilunar valves containing activated myofibroblasts and disorganized extracellular matrix. In both control and *Hdac3*^{Isl1KO} cardiac endothelial cells, the upstream regulatory region of Tgf-β1 is occupied by RNA polymerase II and Crebbp and exhibits H3K27 acetylation, concomitant with Tgf-β1 expression. In control semilunar valves, endothelial cells undergo EndMT to become mesenchymal cells. In these mesenchymal cells, Ncor1, Hdac3, and PRC2 complex (Ezh2, Eed, and Suz12) are recruited to the upstream regulatory region of Tgf-β1, which becomes tri-methylated on histone H3K27, and Tgf-β1 expression is epigenetically silenced. In *Hdac3*^{Isl1KO} hearts, Ezh2, Eed, and Suz12 are not recruited to the Tgf-β1 regulatory region, RNA polymerase II and Crebbp are present, and histone H3K27 remains acetylated, favoring aberrant expression of Tgf-β1 in mesenchymal cells. Tgf-β1 activates mesenchymal cells to become myofibroblasts, which perpetuate EndMT and activation of mesenchymal cells through continued induction of Tgf-β1 and aberrant expression of extracellular matrix, including proteoglycans and collagen.

Second heart field progenitor cells progressively and restrictively differentiate into various cardiac cell types, including cardiomyocytes, endothelial cells, and mesenchymal or smooth muscle cells [24]. Genetic ablation of HDAC3 in the second heart field progenitor cells using either *Isl1-Cre* or *Mef2c*-AHF-Cre resulted in ascending aortic dilatation, outflow tract malrotation, overriding aorta, double outlet right ventricle, semilunar valve stenosis, bicuspid aortic valve, and membranous ventricular septal defects that closely resembled those seen in patients with congenital cardiovascular diseases. Strikingly, genetic deletion of HDAC3 in mesenchymal or smooth muscle cells ($Hdac3^{TaglnKO}$) recapitulated the cardiovascular anomalies observed in $Hdac3^{Isl1KO}$ and $Hdac3^{Mef2CKO}$ embryos; however, genetic deletion of HDAC3 in differentiated cardiomyocytes ($Hdac3^{Myh6KO}$) or endothelial cells($Hdac3^{Cdh5KO}$) did not recapitulate these defects. These observations define a spatiotemporal function of HDAC3 within mesenchymal or smooth muscle cells of second heart field-derived structures that is required for arterial pole morphogenesis (Fig. 3.10A-B).

The anterior part of the second heart field contributes to the arterial pole of the heart, myocardial, and endothelial layers of the outflow tract, right ventricle, ventricular septum, and endocardial cushion mesenchyme of the outflow tract. The posterior part of the second heart field contributes to the venous pole of the heart, atria, dorsal mesenchymal protrusion, and atrial septum [189]. $Isl1^{Cre}$ marks both the anterior and posterior part of the second heart field [24]. However, genetic

deletion of ubiquitously expressed HDAC3 in the *Isl1*^{Cre} expression domain only affected morphogenesis of the anterior heart field-derived structures. Indeed, embryos lacking HDAC3 in the anterior second heart field (*Mef2C*-AHF-Cre) recapitulated these defects. Thus, HDAC3 mainly functions within the anterior part of the second heart field. Interestingly, embryos lacking HDAC3 in the second heart field display normal ventricular myocardium (data not shown). Previously, we demonstrated that HDAC3 is required in the primary heart field (*Nkx2-5* enhancer-Cre) for development of the ventricular myocardium at the early stages of cardiogenesis [216]. Taken together, these findings suggest that once the primary heart field progenitors have adopted a cardiac fate to form the nascent heart tube, the second heart field-derived ventricular myocardium can develop independently of HDAC3. This is consistent with prior evidence that the ventricular myocardium remains unaffected after genetic manipulations or ablation of the second heart field progenitor cells [34,192].

Outflow tract malrotation in tandem with ventricular septal defect is one of the most common cyanotic congenital heart defects at birth [7]. Proper alignment, orientation, and septation of the cardiac outflow tract into the aorta and the pulmonary artery require intricate coordination and interaction among multiple cell types, including neural crest and second heart field [228]. Cardiac neural crest cell-dependent processes, such as outflow tract septation and distal outflow tract morphogenesis, appeared normal in embryos lacking HDAC3 in the second heart field (Fig. 3.1G). Previously, we demonstrated that neural crest-specific genetic

deletion of HDAC3 resulted in anomalous outflow tract septation and distal outflow tract morphogenesis; however, outflow tract rotation and semilunar valve development were unaffected [147]. Instead, second heart field-derived myocardium at the base of the outflow tract governs the normal outflow tract rotation [229]. Prior studies also suggest that aberrant EndMT and remodeling of the outflow tract cushions give rise to structural outflow tract defects, particularly outflow tract malrotation [228]. Our data establish that loss of HDAC3 triggers EndMT in the outflow tract cushion that can be markedly reduced by inhibiting TGF-β. Indeed, TGF-β and its downstream target genes are critical regulators of EndMT [197]. In particular, TGF-β-activated SMAD proteins directly stimulate the expression of zinc finger transcription factor Snai1 within the outflow tract cushion [213]. Studies in chicken and mice have shown that transcriptional repressor Snai1 is both sufficient and required for EndMT [230]. Consistent with these findings, embryos lacking HDAC3 in the second heart field or valvular mesenchymal cells display a marked increase in Snai1 expression within the developing outflow tract and semilunar valves. Overall, our data demonstrate that genetic deletion of HDAC3 in the second heart field or in valvular mesenchymal cells augments TGF-β bioavailability, which, in turn, promotes aberrant EndMT and remodeling of the outflow tract cushion, and this, in part, may modulate outflow tract rotation. Importantly, our results highlight the underlying fact that outflow tract rotation and septation are independent processes regulated by distinct second heart field and cardiac neural crest lineages.

Our data reveal that HDAC3 is a critical regulator of extracellular matrix homeostasis within the second heart field-derived structures. Aberrant extracellular matrix is often an underlying pathology in semilunar valve stenosis, bicuspid aortic valve, and aortic dilatation [62,85,211]. Patients with connective tissue disorders often exhibit altered composition and distribution of extracellular matrix within thickened semilunar valves and ascending aorta, resembling those seen in *Hdac3*^{Isl1KO} and *Hdac3*^{Mef2CKO} embryos. We demonstrate that HDAC3 is required to maintain proper composition of both proteoglycans and collagen in the developing semilunar valves and ascending aorta. The small leucine-rich proteoglycans, such as biglycan, decorin, and fibromodulin, sequester TGF-β to limit its bioavailability and thereby regulate proper remodeling of the hinge region of the semilunar valves and ascending aorta [210,212]. Without this sequestration, an increase of TGF-β bioavailability manifests as dilatation of ascending aorta, bicuspid aortic valves, and thickened semilunar valves in connective tissue disorders. Consistent with this model, our data demonstrate that genetic deletion of HDAC3 in the second heart field or valvular mesenchymal cells leads to significant down-regulation of biglycan, decorin, and fibromodulin, probably explaining increased TGF-β bioavailability, enlarged hinge region of semilunar valves, bicuspid aortic valves, and dilation of ascending aorta in *Hdac3*^{Isl1KO} and *Hdac3*^{Mef2CKO} embryos. Interestingly, we observed striking up-regulation of lumican, a small leucine-rich proteoglycan, in the outflow tract and developing

semilunar valves of *Hdac3*^{Isl1KO} embryos, probably explaining thickened semilunar valves. Patients with bicuspid aortic valve, the most common congenital heart defect, are at increased risk for ascending aortic dilatation [231]. Proteoglycans facilitate collagen assembly and synthesis, a critical process for the development of semilunar valves and ascending aorta [210]. Indeed, patients with mutations in collagen genes, such as *Col1a2* or *Col3a1*, are often predisposed to bicuspid aortic valves and aortic dilatation. Consistent with these observations, significantly reduced expression of *Col1a2* and *Col3a1* in *Hdac3*^{Isl1KO} embryos might explain bicuspid aortic valves and ascending aortic dilatation.

Recent elegant studies [232] clearly demonstrate that in addition to their complex roles in early development, TGF-β signaling pathways are involved in many human diseases as a result of mutations in components of the pathways or aberrant regulation of signaling. Our study identifies HDAC3 as a novel and specific regulator of the TGF-β signaling pathway at the extra- cellular, membrane, cytoplasmic, and nuclear levels. For instance, our data demonstrate that loss of HDAC3 augments expression of extracellular agonist ligands of the TGF-β pathway, such as TGF-β1. Simultaneously, expression of extracellular antagonists of these ligands, such as decorin, biglycan, fibromodulin, and collagen, is strikingly diminished in the absence of HDAC3, probably explaining increased TGF-β bioavailability in *Hdac3*^{Isl1KO} embryos. Similarly, gain of

NRP2, SUMO1, KPNB1, and SMAD4 expression in *Hdac3*^{Isl1KO} embryos would probably explain amplification of TGF-β signaling at the membrane, cytoplasmic, and nuclear levels.

Our findings demonstrate that HDAC3 is required to maintain quiescence of valvular mesenchymal cells, the most prevalent cells of valvular cusps. Pathologic conditions promote activation and differentiation of valvular interstitial cells into myofibroblasts, smooth muscle-like fibroblasts that are observed in patients with semilunar valve disease [202]. Myofibroblasts express smooth muscle-specific genes and secrete strikingly higher levels of TGF-β, proteoglycans, and collagen that alter the composition of the extracellular matrix [85]. Hence, semilunar valve pathologies augment TGF-β bioavailability, which in turn promotes aberrant EndMT and transcriptional activation of smooth muscle and extracellular matrix genes within the myofibroblasts [201]. TGF-β activation and aberrant extracellular matrix further promote the activation and differentiation of new valvular mesenchymal cells derived via EndMT [202]. Consistent with these observations, our data demonstrate that loss of HDAC3 leads to strikingly higher expression of TGF-β1, smooth muscle genes, and aberrant expression of extracellular matrix genes within the valvular mesenchymal cells, and these changes were largely abolished by TGF-β-neutralizing antibody. Taken together, our findings support a model in which HDAC3-mediated repression of TGF-β1 within valvular mesenchymal cells is required to prevent perpetual activation of EndMT and to maintain extracellular matrix homeostasis in the semilunar valves.

Catalytically inactive enzymes or “pseudoenzymes” are clearly widespread, occurring in most enzyme families, including HDACs [227]. For instance, class II HDACs, such as HDAC4, -5, -7, and -9, lack deacetylase activity due to a His substitution at the key Tyr residue [233]. These pseudoenzymes function as scaffolding proteins to recruit various co-factors in a signal-de- pendent manner [119]. Similarly, HDAC1 and -3, class I HDACs, and their deacetylase-dead mutants have the same degree of *in vivo* effect on cardiomyopathy [92]. During endothelial-to-mesenchymal transition, epigenetic mechanisms regulating gene activation and silencing remain largely undefined [234]. The present study provides the mechanistic basis of a deacetylase-independent function of HDAC3 as a scaffold to recruit methyltransferase components of PRC2 (polycomb repressive complex 2) to epigenetically silence TGF-β1. Repressor complex-mediated gene silencing is critical to maintain cellular identity of differentiated cells through multiple divisions [121]. Recent evidence suggests that PRC2-mediated epigenetic silencing is maintained for many cell generations. EZH2, the major H3K27 methyltransferase of the PRC2 complex, supported by EED and SUZ12, catalyzes methylation of H3K27 to mediate chromatin compaction and thereby regulate differentiation and cell identity [235]. Consistent with this model, our data demonstrate that HDAC3 recruits EZH2, EED, and SUZ12 to the NCOR complex in a deacetylase-independent manner and thereby mediates epigenetic silencing of TGF-β1 within valvular mesenchymal cells. In the absence of HDAC3, the NCOR complex fails to recruit

PRC2 complex, resulting in aberrant recruitment of CREBBP, which catalyzes acetylation of H3K27 to mediate activation of TGF-β1 expression, which in turn promotes perpetual transdifferentiation of valvular mesenchymal cells to myofibroblasts. Subsequently, activated myofibroblasts secrete higher levels of extracellular matrix proteins and promote aberrant EndMT. Future investigations dissecting the modes of interaction among HDAC3, EZH2, EED, and SUZ12 will be important to determine PRC2-independent functions of HDAC3. Similarly, murine models expressing catalytically inactive HDAC3 would further define deacetylase-independent functions of HDAC3 during cardiogenesis.

Elucidation of the role of HDAC3 in the second heart field is directly relevant to human congenital heart disease. Marfan syndrome, Ehlers-Danlos syndrome, and Loeys-Dietz syndrome, caused by mutations and activation of TGF-β signaling genes, are associated with congenital cardiovascular anomalies resembling those seen in *Hdac3*^{Isl1KO}, *Hdac3*^{Mef2CKO}, or *Hdac3*^{TaglnKO} embryos. Our data suggest that many of these cardiovascular defects, such as aortic dilatation, outflow tract defects, bicuspid aortic valve, semilunar valve stenosis, and membranous ventricular septal defects, are likely to be caused by defective morphogenesis of the second heart field and aberrant extracellular matrix as a result of anomalous epigenetic silencing of TGF-β.

Acknowledgements

We gratefully acknowledge Dr. Sylvia Evans (University of California, San Diego) for providing *Isl1*-Cre mice, Dr. Brian Black (University of California, San Francisco) for providing *Mef2C*-AHF-Cre mice, and Dr. Mitchell Lazar (University of Pennsylvania) for providing *Hdac3*^{Flox} mice.

Chapter IV: Discussion and future directions

Despite the prevalence and severity of congenital heart disease, the molecular mechanisms of normal and pathogenic cardiac development are not well understood. Recent studies highlighting roles of chromatin-modifying enzymes and related teratogens, including Hdac inhibitors, in congenital heart disease pathogenesis stressed the importance of investigating basic functions of epigenetic enzymes in cardiac progenitor cells [112-114,236]. This thesis aimed to determine the functions of Hdac3 in the major mesodermal cardiac progenitor populations: the primary heart field and the second heart field.

Prior to this work, Hdac3 was shown to have developmental roles in the cardiac neural crest and cardiac conduction system and distinct developmental and postnatal functions cardiomyocytes [147-150]. Deletion studies in murine cardiomyocytes demonstrated that loss of Hdac3 in cardiomyocytes embryonically lead to postnatal defects in cardiac metabolism and lethal cardiac hypertrophy by four months of age [177]. Conversely, under normal diet conditions, postnatal deletion of Hdac3 in cardiomyocytes produced no phenotype or lethality [150]. Metabolic deficiencies and heart failure were only observed in these mice in response to high fat diet. This divergence in phenotype between prenatal and postnatal loss of Hdac3 in the same cell type hinted at stage-specific requirements for Hdac3 during cardiac development. Our work extended this investigation of stage-specific functions of Hdac3 back to the mesoderm-derived

first heart field and second heart field progenitor cells. The findings presented in this thesis demonstrate clear embryonic requirements for Hdac3 in both of these early progenitor populations. Importantly, these progenitor-specific functions of Hdac3 offer new insights into potential mechanisms underlying multiple forms of human congenital heart disease, including Holt-Oram Syndrome, connective tissue disorders, and teratogenic effects of Hdac inhibition. Such findings could inform clinical efforts to treat or prevent cardiac defects.

Stage-specific importance of Hdac3 in cardiomyocyte differentiation

In support of the stage-specific nature of Hdac3 function in cardiac development, we found that Hdac3 has roles in the primary heart field distinct from those in the second heart field or differentiated cardiac lineages. Loss of Hdac3 in the primary heart field results in precocious differentiation of cardiac progenitors into cardiomyocytes. The affected hearts exhibit ventricular septal defects and hypoplastic walls, leading to mid-gestational embryonic lethality.

The precocious cardiomyocyte differentiation and hypoplastic wall phenotype observed in *Hdac3*$^{Nkx2\text{-}5KO}$ hearts were not observed upon loss of Hdac3 in either differentiated cardiomyocytes or second heart field progenitors. This implies that although Hdac3 is required in primary heart field progenitor cells for cardiomyocyte differentiation, once this initial specification event has occurred, the second heart field can differentiate appropriately in the absence of

Hdac3. The specific requirement for Hdac3 in primary heart field, but not second heart field, cardiomyocyte differentiation provides a new example of a difference in regulation between these two progenitor pools.

Within the primary heart field progenitor cells, we showed that Hdac3 interacts with, deacetylates, and suppresses the activity of the primary heart field transcription factor Tbx5. Tbx5 is known to promote differentiation of primary heart field progenitors, inducing expression of cardiac differentiation genes, including those aberrantly expressed in *Hdac3*$^{Nkx2\text{-}5KO}$ hearts [42,44]. The deacetylase function of Hdac3 opposes EP300, an acetyltransferase, which we showed acetylates Tbx5 *in vitro* and *in vivo* and enhances its transcriptional activity. In this manner, Hdac3 functions as a brake, tempering the activation of Tbx5-induced cardiac differentiation genes. Loss of Hdac3 allows for increased Tbx5 acetylation and aberrant induction of its target genes. Mutating suspected acetylation sites in TBX5 abolishes its transcriptional activity, supporting the correlation between TBX5 acetylation and activity. Importantly, these findings showed, for the first time, acetylation of a T-box protein and regulation of T-box protein activity by a histone deacetylase, thereby establishing a novel post-translational regulatory mechanism for T-box proteins. Further mass-spectrometry experiments could more precisely describe the post-translational modifications of Tbx5 and allow for more in-depth investigation into regulation of Tbx5 activity.

T-box proteins are critical developmental regulators in nearly every organ system, including cardiac, limb, and craniofacial development [237]. Within the heart, T-box genes show specific, overlapping expression patterns from the time of cardiac specification through late stages of cardiac remodeling [237]. These proteins are conserved through evolution and expression patterns of Tbx5 are correlated with chamber septation, suggesting an evolutionary role of Tbx5 in the development of the four-chambered heart and dual circulatory systems [11,237]. The importance of T-box proteins in cardiac development is further evidenced by the causative links between mutations in T-box genes, including Tbx1 and Tbx5, and human congenital heart disease [29,30,50,52]. The proposed acetylation sites that we identified in TBX5 are conserved across the T-box family and throughout evolution. This suggests that other T-box family members may share a similar mechanism of regulation by acetylation, as described between Tbx5, Hdac3, and EP300 in this dissertation. Further investigation into regulation of other T-box proteins, such as Tbx1, by acetylation is thus warranted.

More than 40 TBX5 mutations have been identified in patients with Holt-Oram Syndrome, one of which is believed to result in a gain-of-function [45,47]. Deletion analysis revealed that this gain-of-function mutation, $TBX5^{G125R}$, lies within a critical domain for interaction with Hdac3. Notably, this point mutation disrupts the physical interaction between HDAC3 and TBX5. $TBX5^{G125R}$ exhibits increased acetylation and transcriptional activity that cannot be efficiently suppressed by Hdac3. Mutation of suspected acetylation sites ameliorates this

aberrant activity. This suggests a potential mechanistic role of TBX5 acetylation and disrupted interaction between HDAC3 and the TBX5^{G125R} gain-of-function mutant relevant to congenital heart disease, highlighting the importance of post-translational modifications in insuring proper protein function. Fulcoli and colleagues have demonstrated proof of principle for prenatal pharmaceutical interventions for congenital heart disease in mice, specifically DiGeorge Syndrome, by targeting proteins involved in post-translational modification of Tbx1 [109]. The disruption in acetylation and interaction with Hdac3 by the TBX5^{G125R} gain-of-function mutation presents a novel therapeutic target for prenatal treatment of Holt-Oram Syndrome.

Hdac3 functions in second heart field-derived lineages

In contrast to the primary heart field, deletion of Hdac3 in the second heart field progenitors leads to later lethality, around the time of birth, with no obvious ventricular wall hypoplasia. Instead, deletion of Hdac3 in second heart field progenitors results in outflow tract rotation defects, double outlet right ventricle, ventricular septal defect, and semilunar valve defects, including pulmonary valve hyperplasia, aortic valve hyperplasia, and bicuspid aortic valve. These defects are highly penetrant in second heart field Hdac3 knockouts. Importantly, loss of Hdac3 in differentiated endothelial or myocardial cells do not recapitulate these

defects, however loss of Hdac3 in mesenchymal smooth muscle cells manifests as a similar spectrum of outflow tract defects and semilunar valve hyperplasia. We determined that *Hdac3*^{Isl1KO} semilunar valves fail to undergo normal remodeling, instead exhibiting excessive EndMT, reduced apoptosis, and expanded, disorganized extracellular matrix deposition. Within valvular mesenchymal cells, Hdac3 suppresses expression of Tgfβ1 and Tgfβ1 pathway components, which are known to regulate valve development and extracellular matrix organization [238-241]. Upon loss of Hdac3, Tgfβ1 expression increases, the Tgfβ1 pathway is activated, and valvular mesenchymal cells take on a pathogenic myofibroblast phenotype. This is accompanied by extracellular matrix disorganization within the outflow tract vessels and semilunar valves. The disorganized extracellular matrix and dilatation of the aorta in *Hdac3*^{Isl1KO} hearts resemble cardiac phenotypes observed in humans with connective tissue disorders such as Marfan Syndrome, Ehlers-Denlos Syndrome, and Loeys-Dietz Syndrome [60-62,70-73]. Patients with these syndromes often show elevated Tgfβ1 expression levels, consistent with observations in *Hdac3*^{Isl1KO} hearts [61,74,75].

Our model proposes that Hdac3 acts at the Tgfβ1 promoter in mesenchymal cells to epigenetically regulate Tgfβ1 transcription. We show that Hdac3 and the N-CoR complex are required to recruit the PRC2 methyltransferase complex to the Tgfβ1 promoter, resulting in histone H3K27 tri-methylation and transcriptional repression. In the absence of Hdac3, the Tgfβ1 promoter becomes occupied by Crebbp and polymerase, and exhibits histone

H3K27 acetylation, all hallmarks of gene activation. Indeed, increased Tgfb1 gene expression is observed in Hdac3 knockout semilunar valves and outflow tracts, along with gene expression changes and protein expression indicative of Tgfb1 pathway activation. This is accompanied by changes in cell behavior, including enhanced EndMT and an activated myofibroblast phenotype of valve interstitial cells.

Importantly, we found that Hdac3's recruitment of the PRC2 complex and epigenetic repression of Tgfβ1 does not require Hdac3's catalytic activity. A catalytically dead point mutant version of Hdac3, HDAC3$^{H134A, H135A}$ could rescue PRC2 complex recruitment, Tgfβ1 promoter H3K27 tri-methylation, and EndMT defects in explant experiments. These findings support a new, deacetylase-independent role for Hdac3 as a scaffold to coordinate gene regulation in second heart field development.

Clinically, these discoveries establish a novel mechanism for regulation of Tgfβ1 expression that could serve as a therapeutic target for treatment of disorders involving aberrant Tgfβ1 expression. Tgfβ1 expression is elevated in patients with connective tissue disorders, such as Marfan Syndrome, Ehlers-Denlos Syndrome, and Loeys-Dietz Syndrome, and reactivation of Tgfβ1 in valvular interstitial cells is associated with adult valve disease [61,74,75,197,201,242,243]. Pharmaceutical interventions targeting Tgfβ1 expression and activation are in clinical trials for treatment of such diseases [243]. We propose that suppression of Tgfβ1 expression that occurs naturally in mesenchymal cells during development

requires recruitment of the PRC2 complex to the Tgfβ1 promoter, facilitated by Hdac3. Strategies to suppress Tgfβ1 expression in patients with connective tissue disorders or adult valve pathologies may explore targeting Hdac3-mediated recruitment of the PRC2 complex, Tgfβ1 promoter methylation, or Tgfβ1 promoter deacetylation as alternate strategies to induce suppression of pathogenic Tgfβ1 expression.

Although bicuspid aortic valve is the most prevalent congenital cardiac defect, animal models with highly penetrant bicuspid aortic valve phenotypes have not been established. We show, for the first time, a genetic mouse model that reproducibly exhibits bicuspid aortic valve. This model will facilitate investigations into the cellular and molecular etiologies of this common human malformation.

Interestingly, while mesenchymal cell deletion of Hdac3 partially recapitulated the outflow tract defects and valve hyperplasia observed in *Hdac3*^{Isl1KO} hearts, these hearts did not exhibit bicuspid aortic valve (Appendix A). In fact, neither mesenchymal, myocardial, nor endothelial deletion of Hdac3 resulted in bicuspid aortic valve (Appendix A). This implies that the mechanism of bicuspid aortic valve development is independent of the aortic valve hyperplasia and outflow tract rotation defects observed in *Hdac3*^{Isl1KO}, *Hdac3*^{Mef2cKO}, and *Hdac3*^{TaglnKO} hearts. Furthermore, the mechanism of bicuspid aortic valve development in *Hdac3*^{Isl1KO} and *Hdac3*^{Mef2cKO} requires Hdac3 function either

specifically within the second heart field progenitor cells or in multiple interacting derivative cell types.

In humans, bicuspid aortic valve arises either due to fusion of two adjacent cusps or due to developmental abnormalities resulting in a failure of one cusp to form [65,82,244,245]. Previous work has suggested that separate genetic mechanisms are responsible for different subtypes of bicuspid aortic valve [245]. Preliminary analysis of the developing aortic valve in *Hdac3*^{Isl1KO} hearts suggests abnormal formation of the noncoronary cusp, with morphology mimicking the right-noncoronary bicuspid aortic valve subtype (data not shown). Further investigation into this phenotype, its developmental origins, cellular basis, and molecular mechanism will define additional functions of Hdac3 in aortic valve biology and may provide insights into the causes of human bicuspid aortic valve development and associated pathologies.

Future directions – expanding investigation into early roles of Hdac3 in cardiac development

This thesis described critical, stage-specific roles of Hdac3 in mesoderm-derived cardiac progenitors: the primary heart field and second heart field, with important human disease associations. These findings, together with prior work demonstrating separate embryonic and postnatal requirements for Hdac3 in cardiomyocytes, clearly established that the essential functions of Hdac3 evolve

as development progresses from the primary and second heart field progenitors to the differentiated postnatal lineages [150,177].

Extending this investigation one step further back in development, preliminary analysis of mesodermal knockouts of Hdac3 (*Hdac3*^{Mesp1KO}) suggests requirements for Hdac3 in cardiogenic mesoderm distinct from those in the primary heart field, second heart field, or differentiated cardiac cells (Appendix B). *Hdac3*^{Mesp1KO} embryos exhibit embryonic lethality prior to E12.5, earlier than the lethality of any of the Hdac3 knockouts described in this thesis. These embryos show heart looping defects, hypoplastic endocardial cushions, extracellular matrix disorganization, and gene expression changes in developmental signaling pathways and cell lineage markers (Appendix B).

These preliminary findings warrant further analysis, including phenotypic and molecular characterization of *Hdac3*^{Mesp1KO} embryos at earlier developmental time points to determine the origin of the observed defects and identify the mechanisms of Hdac3's functions at these earliest stages of cardiac development. Tracing the differences in gene expression observed by microarray analysis at E9.5 back to their time of onset would help to distinguish primary from secondary changes in gene expression in response to loss of Hdac3, facilitating the identification of the direct gene targets for Hdac3 in cardiogenic mesoderm. Dual-staining and *in situ* analyses of early embryos could investigate the specific effects of mesodermal Hdac3 deletion on individual derivative populations, such as the primary heart field or second heart field progenitors. Such work, combined

with the existing literature on cardiac roles of Hdac3, including the work in this dissertation, would provide a more complete picture of the important functions of Hdac3 from cardiac specification through maintenance of cardiac health in the mature, adult heart.

Regulation of Hdac3 activity – key to stage specific functions?

Considering the evolving roles of Hdac3 throughout cardiac development, interactions and regulation of Hdac3 activities must be dynamically regulated as development progresses through progenitor stages and into differentiated cardiac cell types. Hdac3 appears ubiquitously expressed throughout the heart and body during the period of cardiac development, which argues against transcriptional regulation of Hdac3 as a mechanism for differences in requirements across stages of differentiation. Interestingly, expression of interacting factors, for example co-expression of Hdac3 and Tbx5, may not be sufficient for their interaction.

While we observed interaction between Hdac3 and Tbx5 in E8.5 hearts by endogenous co-IP, a recent Tbx5 interactome study conducted in E9.5 hearts did not identify Hdac3 as a binding partner of Tbx5, despite overlapping cardiac expression of both proteins at this stage [246]. The interactome study utilized an Avitag Tbx5 mouse model, but reported no adverse affects of the genetic manipulation on embryonic development, suggesting conserved function of

Avitag Tbx5. This raises the question of whether the interaction between Hdac3 and Tbx5 is developmentally transient. Hdac3 acts as a suppressor of Tbx5 activity in cardiac progenitor cells, preventing activation of myocardial differentiation genes. A lifting of this repression by dissociation of Hdac3 and Tbx5 may be required to allow differentiation to proceed at the appropriate developmental stage. Regulation of this interaction may, therefore, be important in directing the correct timing of differentiation. Further study into the mechanism regulating Hdac3 interaction with Tbx5 could reveal whether this interaction serves as a downstream effector of a differentiation signal to induce cardiomyocyte differentiation.

Much like the interaction between Hdac3 and Tbx5, Hdac2 has been shown to interact with, deacetylate, and functionally repress Gata4 in embryonic cardiomyocytes [140]. This interaction is dependent on the phosphorylation status of Hdac2. Although a phospho-mutant version of Hdac2 retains deacetylase activity comparable to that of wild-type Hdac2, it exhibits an 87% reduction in its interaction with Gata4 and is unable to repress Gata4 activity [140]. Studies in other systems have described post-translational regulation of Hdac3 by phosphorylation [247,248]. Investigation into the role of post-translational modifications of either Tbx5 or Hdac3, such as Hdac3 phosphorylation, on their association with one another could provide insight into the regulation of stage-specific roles of Hdac3 during cardiac development.

Concluding remarks

Overall, the work presented here expands our understanding of the developmental roles of histone deacetylases, specifically Hdac3, in cardiac progenitor cells. We show that Hdac3 is required in cardiac progenitor cells for survival of the embryo and describe clinically relevant interactions that may serve as therapeutic targets for congenital heart disease or related conditions. For example, we found that Hdac3 interacts with and deacetylates Tbx5, a relationship that is disrupted by a point mutation in Tbx5 found in patients with congenital heart disease. This disrupted regulatory relationship between Hdac3 and Tbx5 highlights the relevance of Hdac3 activities in human disease etiology. Furthermore, this mechanism establishes a novel therapeutic target for a subset of Holt-Oram Syndrome patients, with the potential for similar mechanisms among other T-box-associated diseases, such as DiGeorge Syndrome.

Within cardiac progenitors, we describe both deacetylase-dependent and deacetylase-independent mechanisms by which Hdac3 regulates cardiac gene expression and distinct cell-type and stage-specific roles of Hdac3. This work opens new questions into the nature and regulation of Hdac3 activity, such as when and where is Hdac3 enzymatically active during cardiac development, are its interactions with other proteins or DNA regulatory sequences transient, and, if so, do these dynamic interactions serve as downstream effectors of developmental signaling cascades? Further studies utilizing deacetylase-

deficient and phosphorylation mutants of Hdac3 in the context of cardiac development will expand our understanding of the functions and regulation of Hdac3 in cardiogenesis. Such work, together with the findings presented in this dissertation, will establish the clinical importance of Hdac3 in congenital heart disease pathology and help to inform development of preventative and therapeutic approaches to combat this prevalent and devastating disease.

Appendix A – incidence of bicuspid aortic valve and valve hyperplasia in tissue-specific Hdac3 knockout mice

Appendix A

Incidence of bicuspid aortic valve and valve hyperplasia in tissue-specific Hdac3 knockout mice

		Defect present (incidence/total examined)		
Knockout genotype	Age	BAV*	AV** hyperplasia	OFT[X] malrotation
Isl1-Cre;Hdac3$^{F/F}$	E18.5	yes (6/6)	yes (12/12)	yes (4/4)
Mef2c-Cre;Hdac3$^{F/F}$	E18.5	yes (3/3)	yes (9/9)	yes (8/9)
Tagln-Cre;Hdac3$^{F/F}$	P0	no (0/3)	yes (3/3)	yes (3/3)
αMHC-Cre;Hdac3$^{F/F}$	P0	no (0/3)	no (0/3)	no (0/3)
Cdh5-Cre;Hdac3$^{F/F}$	P0	no (0/3)	no (0/3)	no (0/3)
Tie2-Cre;Hdac3$^{F/F}$	E12.5	no (0/3)	no (0/3)	no (0/3)

*BAV - bicuspid aortic valve
**AV - aortic valve
[X] OFT - outflow tract

Appendix B – Mesodermal deletion of Hdac3

Overview

This dissertation describes stage- and cell type-specific requirements for Hdac3 during cardiac development. Based on these findings, I have conducted preliminary analysis to determine the effects of loss of Hdac3 in the mesoderm, which is a precursor to both the primary heart field and second heart field, which are examined in the main body of this dissertation. Using Mesp1-Cre, I deleted Hdac3 in the mesoderm (Figure B1 A) and discovered complete lethality of *Hdac3*^{Mesp1KO} embryos between E9.5 and E12.5 (Table B1). *Hdac3*^{Mesp1KO} embryos exhibited heart looping defects at E9.5 (Figure B1 B-G), associated with shortening of the outflow tract when measured at E10.5 (Figure B1 H-J). The abnormally looped *Hdac3*^{Mesp1KO} hearts show Hdac3 deletion within the outflow tract and atrioventricular cushions and both sets of cushions appear significantly hypoplastic (Figure B2 A-E). These hearts also exhibit a deficiency in Mesp1-negative cells in the outflow tract and potential defects in epicardium formation or integrity (Figure B2 F-H). Preliminary microarray analysis of E9.5 control and *Hdac3*^{Mesp1KO} hearts, along with staining, indicates defects in extracellular matrix and cytoskeletal-related genes in *Hdac3*^{Mesp1KO} hearts (Figure B3). Comparison with other stage-specific knockouts of Hdac3 suggests that these defects are specific to the mesoderm or to multiple interacting derivative cell populations (Table B2). Further work is required to address the origin and mechanisms of the defects observed.

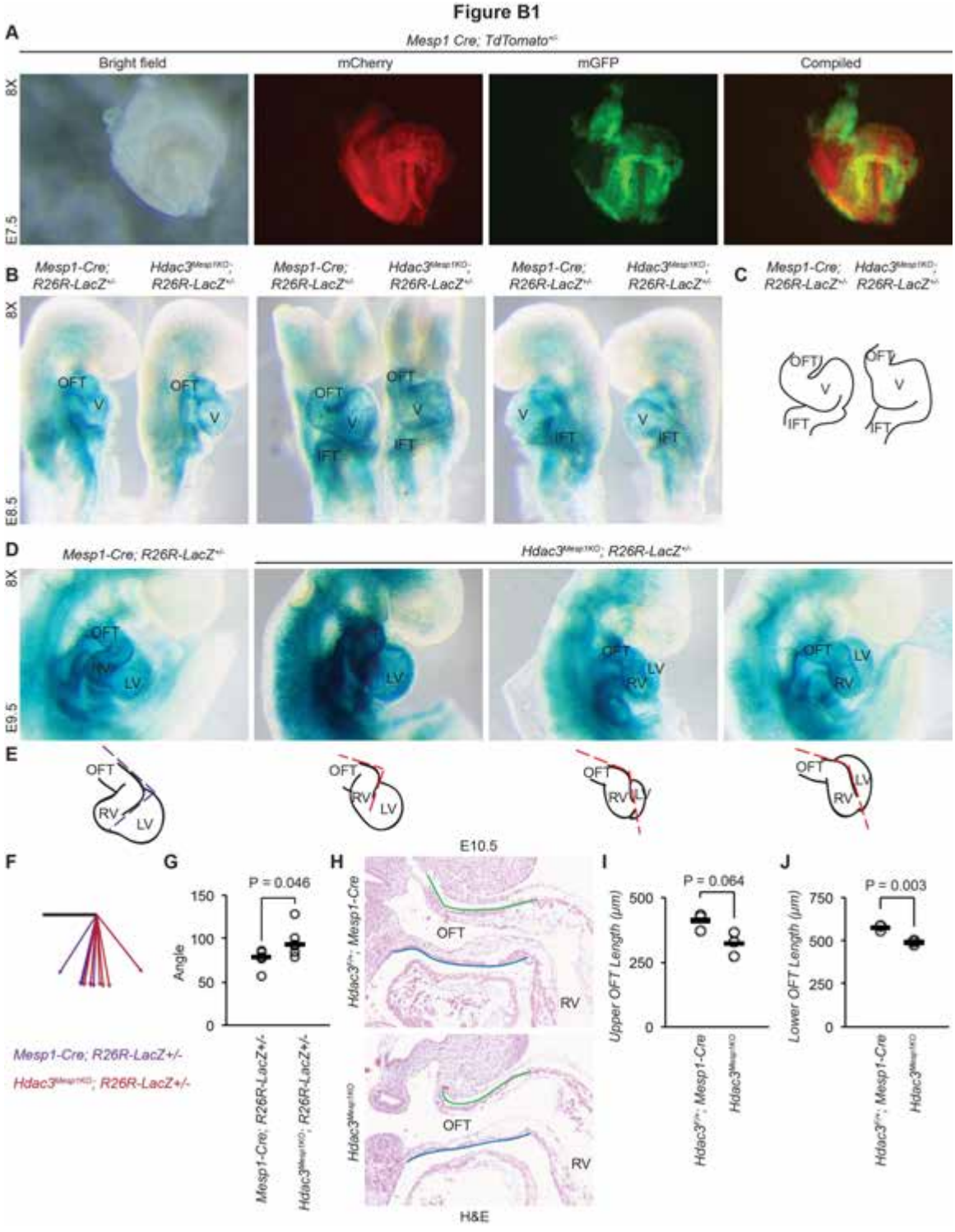
Figure B1
A
Mesp1 Cre; TdTomato+/-
Bright field
mCherry
mGFP
Compiled
8X
E7.5
B
Mesp1-Cre; R26R-LacZ+/-
Hdac3Mesp1KO; R26R-LacZ+/-
8X
E8.5
OFT
V
IFT
C
D
Mesp1-Cre; R26R-LacZ+/-
Hdac3Mesp1KO; R26R-LacZ+/-
8X
E9.5
OFT
RV
LV
E
F
G
P = 0.046
Angle
150
100
50
0
Mesp1-Cre; R26R-LacZ+/-
Hdac3Mesp1KO; R26R-LacZ+/-
H
E10.5
Hdac3+/+; Mesp1-Cre
Hdac3Mesp1KO
OFT
RV
H&E
I
P = 0.064
Upper OFT Length (μm)
500
250
0
J
P = 0.003
Lower OFT Length (μm)
750
500
250
0

Figure B1. Abnormal heart looping upon mesoderm-specific deletion of Hdac3. **(A)** Bright field and fluorescence images of a *Mesp1-Cre; TdTomato*$^{+/-}$ E7.5 embryo show Mesp1-Cre expression in the cardiac crescent. **(B)** LacZ-stained *Hdac3*^{Mesp1KO}*; R26R-LacZ*$^{+/-}$ and control E8.5 embryos demonstrate abnormal looping between the outflow tract and ventricle of *Hdac3*^{Mesp1KO}*; R26R-LacZ*$^{+/-}$ hearts. **(C)** Tracing of *Hdac3*^{Mesp1KO}*; R26R-LacZ*$^{+/-}$ and control E8.5 heart tubes from the frontal perspective. **(D)** LacZ-stained *Hdac3*^{Mesp1KO}*; R26R-LacZ*$^{+/-}$ and control E9.5 embryos demonstrate a spectrum of severity of outflow tract to right ventricle looping angle defects. **(E)** Tracing of LacZ-stained *Hdac3*^{Mesp1KO}*; R26R-LacZ*$^{+/-}$ and control E9.5 hearts depict the spectrum of increasing outflow tract to right ventricle looping angle (dashed red lines) compared to control heart looping (purple dashed lines). **(F)** Purple (control) and red (*Hdac3*^{Mesp1KO}*; R26R-LacZ*$^{+/-}$) arrows reflect the angle of right ventricle orientation relative to the outflow tract (black line) measured from images of individual LacZ-stained E9.5 embryos. **(G)** Comparison of the angle between the outflow tract and right ventricle measured from images LacZ-stained *Hdac3*^{Mesp1KO}*; R26R-LacZ*$^{+/-}$ and control E9.5 embryos. **(H)** Hematoxylin- and eosin-stained sections of the outflow tract of *Hdac3*^{Mesp1KO} and control E10.5 hearts. Green and blue lines show the upper and lower lengths, respectively, of the outflow tract. **(I-J)** Quantification of outflow tract length, measured on the **(I)** upper surface and **(J)** lower surface of the outflow tract in hematoxylin- and eosin-stained sagittal sections of *Hdac3*^{Mesp1KO} and control E10.5 hearts.

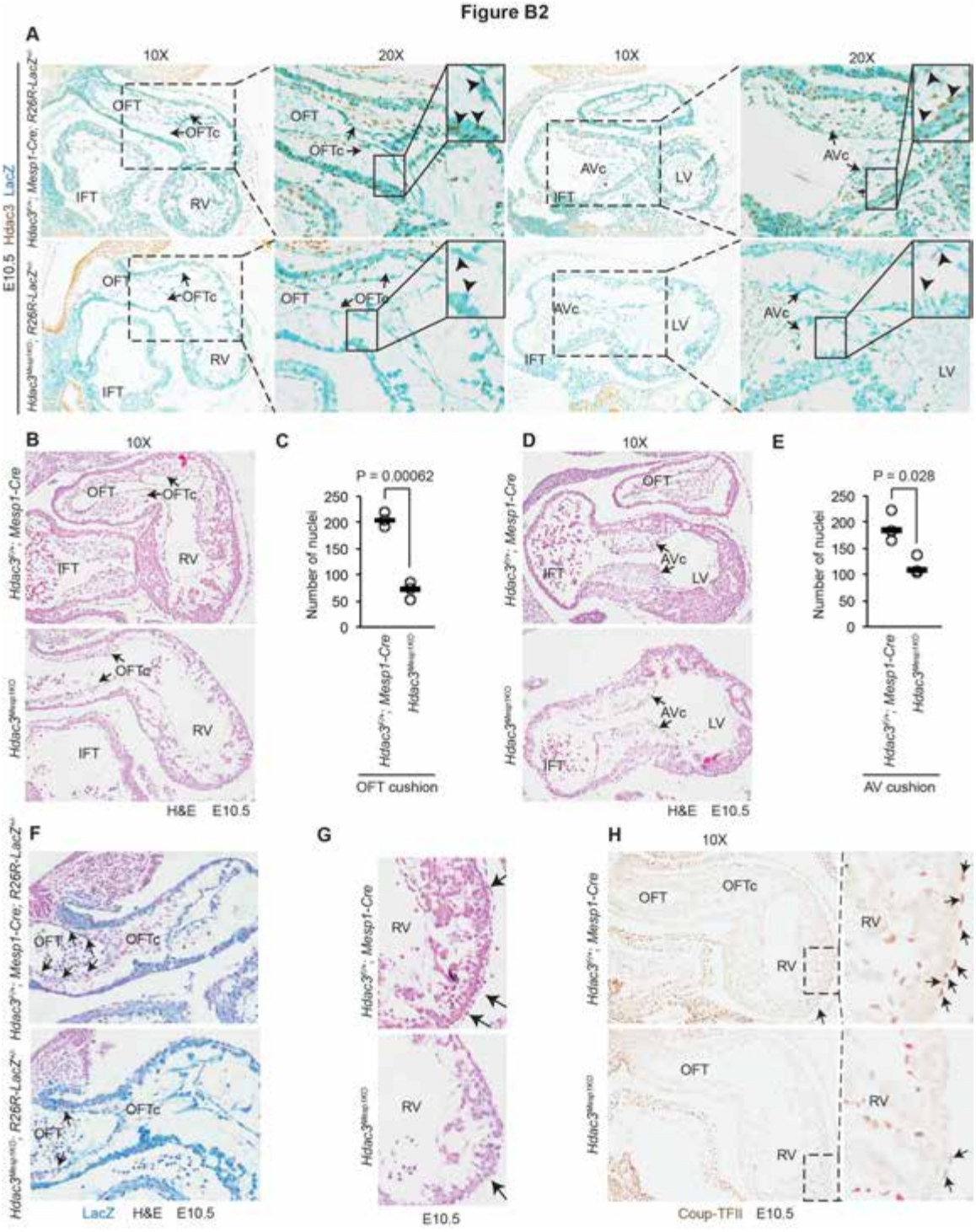
Figure B2
A
10X
20X
10X
20X
E10.5 Hdac3 LacZ
Hdac3f/+; Mesp1-Cre; R26R-LacZ+/-
Hdac3Mesp1KO; R26R-LacZ+/-
OFT
OFTc
IFT
RV
AVc
LV
B
10X
Hdac3f/+; Mesp1-Cre
Hdac3Mesp1KO
H&E E10.5
C
P = 0.00062
Number of nuclei
Hdac3f/+; Mesp1-Cre
Hdac3Mesp1KO
OFT cushion
D
10X
H&E E10.5
E
P = 0.028
AV cushion
F
LacZ H&E E10.5
G
E10.5
H
10X
Coup-TFII E10.5

Figure B2. Developmental defects in *Hdac3^{Mesp1KO}* embryos. (A) HDAC3 immunostaining of LacZ-stained *Hdac3^{Mesp1KO}; R26R-LacZ$^{+/-}$* and control embryos shows that HDAC3 protein expression is lost in the Mesp1-Cre expression domain, including outflow tract and atrioventricular canal in E10.5 hearts. **(B)** Hematoxylin- and eosin-stained sagittal sections demonstrate malformed, hypoplastic outflow tract cushions in E10.5 *Hdac3^{Mesp1KO}* hearts. **(C)** Quantification of number of nuclei per outflow tract cushion section, counted from hematoxylin- and eosin-stained sagittal sections from E10.5 embryos. **(D)** Hematoxylin- and eosin-stained sagittal sections demonstrate hypoplastic atrioventricular cushions in E10.5 *Hdac3^{Mesp1KO}* hearts. **(E)** Quantification of number of nuclei per atrioventricular cushion section, counted from hematoxylin- and eosin-stained sagittal sections from E10.5 embryos. **(F)** Hematoxylin- and eosin-stained sagittal sections of LacZ-stained *Hdac3^{Mesp1KO}; R26R-LacZ$^{+/-}$* and control E10.5 embryos demonstrate a reduction in Mesp1-Cre-negative cells in the outflow tract and outflow tract cushions in *Hdac3^{Mesp1KO}; R26R-LacZ$^{+/-}$* hearts. **(G)** Hematoxylin- and eosin-stained sections show an uninterrupted epicardial layer around the right ventricle in control E10.5 hearts, which is incomplete and fragmented in *Hdac3^{Mesp1KO}* E10.5 hearts. **(H)** COUP-TFII immunostaining shows epicardial expression in control E10.5 hearts, which is discontinuous in *Hdac3^{Mesp1KO}* E10.5 hearts.

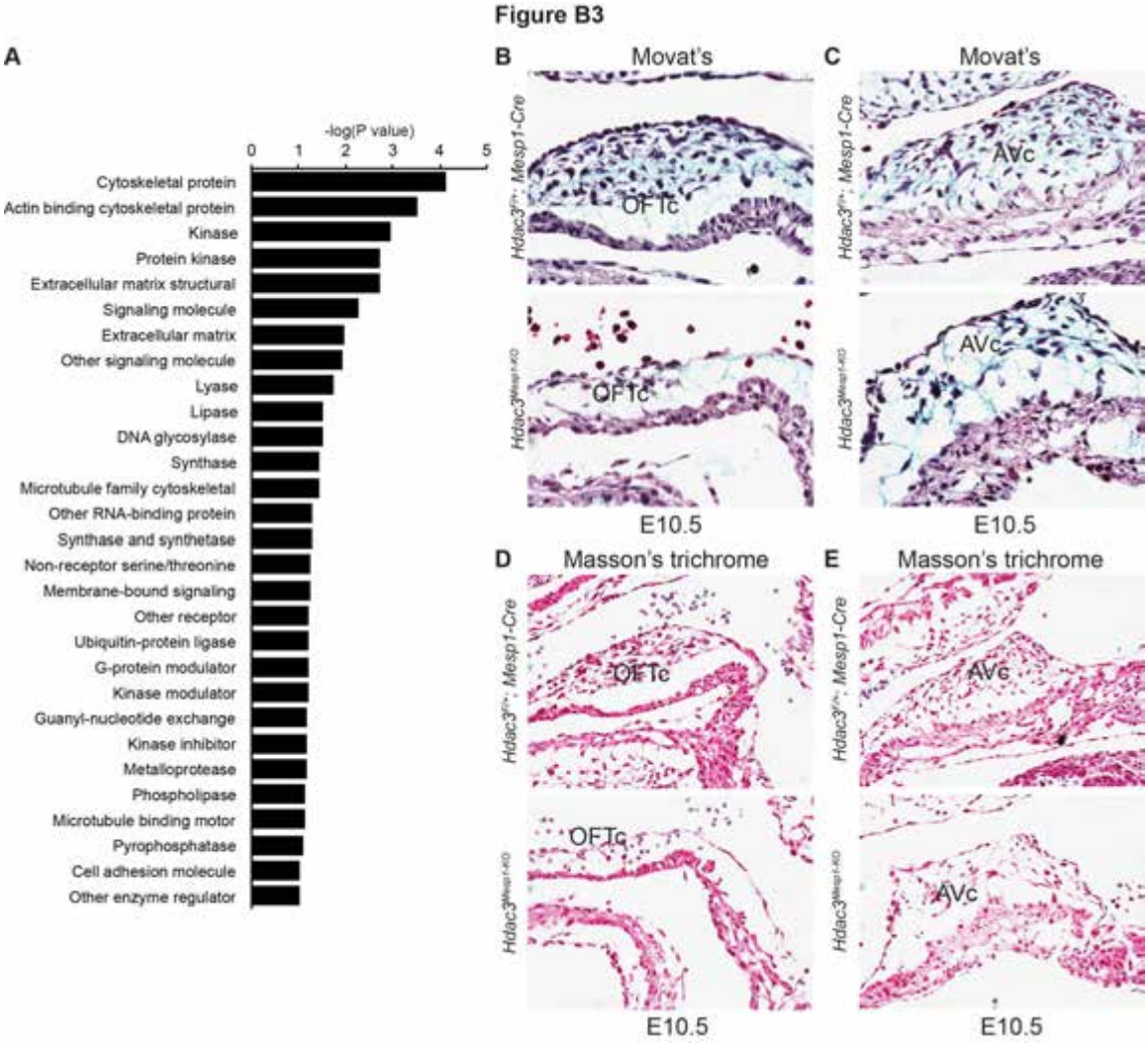

Figure B3. Gene expression and related extracellular matrix changes in *Hdac3*^{Mesp1KO} hearts. (A) DAVID analysis of microarray data from pooled E9.5 *Hdac3*$^{F/F}$ and *Hdac3*^{Mesp1KO} hearts indicate changes in cytoskeletal, signaling, and extracellular matrix genes. **(B-C)** Movat's pentachrome staining of E10.5 hearts show abnormal proteoglycan content (blue) in the outflow tract **(B)** and atrioventricular cushions **(C)** of *Hdac3*^{Mesp1KO} hearts**. (D-E)** Masson's trichrome staining of E10.5 hearts shows abnormal tissue architecture in the myocardium of the outflow tract **(D)** and atrioventricular canal **(E)** in *Hdac3*^{Mesp1KO} hearts.

Table B2

Incidence of developmental defects in tissue-specific Hdac3 knockout embryos
Age E9.5-E10.5

	Defect present (incidence/total examined)			
Knockout genotype	OFTc* hypoplasia	AVc** hypoplasia	Looping defect	Epicardium defect
Mesp1-Cre;Hdac3$^{F/F}$	yes (6/6)	yes (6/6)	yes (6/6)	yes (6/6)
Nkx2-5-IRES-Cre;Hdac3$^{F/F}$	no (0/3)	no (0/3)	no (0/3)	no (0/3)
Isl1-Cre;Hdac3$^{F/F}$	no (0/3)	no (0/3)	no (0/3)	no (0/3)
Tie2-Cre;Hdac3$^{F/F}$	no (0/3)	no (0/3)	no (0/3)	no (0/3)

*OFTc - outflow tract cushion
**AVc - atrioventricular cushion

References

1. Hoffman, J. I. Incidence of congenital heart disease: I. Postnatal incidence. *Pediatr Cardiol* **16,** 103–113 (1995).
2. Hoffman, J. I. Incidence of congenital heart disease: II. Prenatal incidence. *Pediatr Cardiol* **16,** 155–165 (1995).
3. Hoffman, J. I. E. & Kaplan, S. The incidence of congenital heart disease. *Journal of the American College of Cardiology* **39,** 1890–1900 (2002).
4. Hoffman, J. I. The global burden of congenital heart disease. *Cardiovasc J Afr* **24,** 141–145 (2013).
5. Chinn, A., Fitzsimmons, J., Shepard, T. H. & Fantel, A. G. Congenital heart disease among spontaneous abortuses and stillborn fetuses: prevalence and associations. *Teratology* **40,** 475–482 (1989).
6. Jorgensen, M., McPherson, E., Zaleski, C., Shivaram, P. & Cold, C. Stillbirth: The heart of the matter. *Am. J. Med. Genet. A* **164,** 691–699 (2014).
7. van der Linde, D. *et al.* Birth Prevalence ofCongenital Heart Disease Worldwide. *Journal of the American College of Cardiology* **58,** 2241–2247 (2011).
8. Sayasathid, J., Sukonpan, K. & Somboonna, N. *Epidemiology and Etiology of Congenital Heart Diseases*. (2012).
9. Marelli, A. J., Mackie, A. S., Ionescu-Ittu, R., Rahme, E. & Pilote, L. Congenital heart disease in the general population: changing prevalence and age distribution. *Circulation* **115,** 163–172 (2007).
10. Fahed, A. C., Gelb, B. D., Seidman, J. G. & Seidman, C. E. Genetics of congenital heart disease: the glass half empty. *Circ. Res.* **112,** 707–720 (2013).
11. Koshiba-Takeuchi, K. *et al.* Reptilian heart development and the molecular basis of cardiac chamber evolution. *Nature* **461,** 95–98 (2009).
12. Pandur, P., Sirbu, I. O., Kühl, S. J., Philipp, M. & Kühl, M. Islet1-expressing cardiac progenitor cells: a comparison across species. *Dev. Genes Evol.* **223,** 117–129 (2013).
13. Jensen, B., Wang, T., Christoffels, V. M. & Moorman, A. F. M. Biochimica et Biophysica Acta. *BBA - Molecular Cell Research* **1833,** 783–794 (2013).
14. Argüello, C., la Cruz, de, M. V. & Gómez, C. S. Experimental study of the formation of the heart tube in the chick embryo. *J Embryol Exp Morphol* **33,** 1–11 (1975).
15. Yutzey, K. E. & Kirby, M. L. Wherefore heart thou? Embryonic origins of cardiogenic mesoderm. *Dev. Dyn.* **223,** 307–320 (2002).
16. Brade, T., Pane, L. S., Moretti, A., Chien, K. R. & Laugwitz, K. L. Embryonic Heart Progenitors and Cardiogenesis. *Cold Spring Harbor*

Perspectives in Medicine **3,** a013847–a013847 (2013).
17. Keyte, A. & Hutson, M. R. The neural crest in cardiac congenital anomalies. *Differentiation* **84,** 25–40 (2012).
18. Keyte, A. L., Alonzo-Johnsen, M. & Hutson, M. R. Evolutionary and developmental origins of the cardiac neural crest: Building a divided outflow tract. *Birth Defects Res. C Embryo Today* **102,** 309–323 (2014).
19. Vincent, S. D. & Buckingham, M. E. in *sciencedirect.com* **90,** 1–41 (Elsevier, 2010).
20. Bruneau, B. G. *et al.* A murine model of Holt-Oram syndrome defines roles of the T-box transcription factor Tbx5 in cardiogenesis and disease. *Cell* **106,** 709–721 (2001).
21. Bruneau, B. G. E. A. Chamber-Specific Cardiac Expression of Tbx5 and Heart Defects in Holt–Oram Syndrome. 1–9 (1999).
22. Hatcher, C. J., Goldstein, M. M., Mah, C. S., Delia, C. S. & Basson, C. T. Identification and localization of TBX5 transcription factor during human cardiac morphogenesis. *Dev. Dyn.* **219,** 90–95 (2000).
23. Brown, D., Samsa, L., Qian, L. & Liu, J. Advances in the Study of Heart Development and Disease Using Zebrafish. *Journal of cardiovascular development and disease* **3,** 13 (2016).
24. Evans, S. M., Yelon, D., Conlon, F. L. & Kirby, M. L. Myocardial Lineage Development. *Circ. Res.* **107,** 1428–1444 (2010).
25. Harvey, R. P. Organogenesis: Patterning the vertebrate heart. *Nat. Rev. Genet.* **3,** 544–556 (2002).
26. Benson, D. W. *et al.* Mutations in the cardiac transcription factor NKX2.5 affect diverse cardiac developmental pathways. *J. Clin. Invest.* **104,** 1567–1573 (1999).
27. Risebro, C. A. & Riley, P. R. Formation of the Ventricles. *The Scientific World JOURNAL* **6,** 1862–1880 (2006).
28. Lalani, S. R. & Belmont, J. W. Genetic basis of congenital cardiovascular malformations. *European Journal of Medical Genetics* **57,** 402–413 (2014).
29. Li, Q. Y. *et al.* Holt-Oram syndrome is caused by mutations in TBX5, a member of the Brachyury (T) gene family. *Nat. Genet.* **15,** 21–29 (1997).
30. Basson, C. T. *et al.* Mutations in human TBX5 [corrected] cause limb and cardiac malformation in Holt-Oram syndrome. *Nat. Genet.* **15,** 30–35 (1997).
31. Mjaatvedt, C. H. *et al.* The Outflow Tract of the Heart Is Recruited from a Novel Heart-Forming Field. *Dev. Biol.* **238,** 97–109 (2001).
32. Waldo, K. L. *et al.* Conotruncal myocardium arises from a secondary heart field. *Development* **128,** 3179–3188 (2001).
33. Cai, C.-L. *et al.* Isl1 identifies a cardiac progenitor population that proliferates prior to differentiation and contributes a majority of cells to

the heart. *Dev. Cell* **5,** 877–889 (2003).
34. Ward, C., Stadt, H., Hutson, M. & Kirby, M. L. Ablation of the secondary heart field leads to tetralogy of Fallot and pulmonary atresia. *Dev. Biol.* **284,** 72–83 (2005).
35. Moorman, A. F. M., Christoffels, V. M., Anderson, R. H. & van den Hoff, M. J. B. The heart-forming fields: one or multiple? *Philosophical Transactions of the Royal Society of London B: Biological Sciences* **362,** 1257–1265 (2007).
36. Stevens, K. N. *et al.* Common Variation in ISL1 Confers Genetic Susceptibility for Human Congenital Heart Disease. *PLoS ONE* **5,** e10855 (2010).
37. Bruneau, B. G. The developmental genetics of congenital heart disease. *Nature* **451,** 943–948 (2008).
38. Bajolle, F. *et al.* Conotruncal defects associated with anomalous pulmonary venous connections. *Archives of Cardiovascular Diseases* **102,** 105–110 (2009).
39. Dees, E., Lin, H., Cotton, R. B., Graham, T. P. & Dodd, D. A. Outcome of preterm infants with congenital heart disease. *The Journal of Pediatrics* **137,** 653–659 (2000).
40. Andrews, R. E., Simpson, J. M., Sharland, G. K., Sullivan, I. D. & Yates, R. W. M. Outcome after preterm delivery of infants antenatally diagnosed with congenital heart disease. *The Journal of Pediatrics* **148,** 213–216 (2006).
41. Bruneau, B. G. *et al.* Chamber-specific cardiac expression of Tbx5 and heart defects in Holt-Oram syndrome. *Dev. Biol.* **211,** 100–108 (1999).
42. Hiroi, Y. *et al.* Tbx5 associates with Nkx2-5 and synergistically promotes cardiomyocyte differentiation. *Nat. Genet.* **28,** 276–280 (2001).
43. Plageman, T. F. & Yutzey, K. E. Microarray analysis of Tbx5-induced genes expressed in the developing heart. *Dev. Dyn.* **235,** 2868–2880 (2006).
44. Herrmann, F., Bundschu, K., Kühl, S. J. & Kühl, M. Tbx5 overexpression favors a first heart field lineage in murine embryonic stem cells and in Xenopus laevis embryos. *Dev. Dyn.* **240,** 2634–2645 (2011).
45. Heinritz, W., Shou, L., Moschik, A. & Froster, U. G. The human TBX5 gene mutation database. *Hum. Mutat.* **26,** 397 (2005).
46. Brassington, A.-M. E. *et al.* Expressivity of Holt-Oram syndrome is not predicted by TBX5 genotype. *Am. J. Hum. Genet.* **73,** 74–85 (2003).
47. Postma, A. V. *et al.* A gain-of-function TBX5 mutation is associated with atypical Holt-Oram syndrome and paroxysmal atrial fibrillation. *Circ. Res.* **102,** 1433–1442 (2008).
48. Momma, K. Cardiovascular Anomalies Associated With Chromosome

22q11.2 Deletion Syndrome. *The American Journal of Cardiology* **105,** 1617–1624 (2010).
49. Choudhry, P. & Trede, N. S. DiGeorge Syndrome Gene tbx1 Functions through wnt11r to Regulate Heart Looping and Differentiation. *PLoS ONE* **8,** e58145 (2013).
50. Scambler, P. J. 22q11 Deletion Syndrome: A Role for TBX1 in Pharyngeal and Cardiovascular Development. *Pediatr Cardiol* **31,** 378–390 (2010).
51. Yagi, H. *et al.* Role of TBX1 in human del22q11.2 syndrome. *Lancet* **362,** 1366–1373 (2003).
52. Merscher, S. *et al.* TBX1 is responsible for cardiovascular defects in velo-cardio-facial/DiGeorge syndrome. *Cell* **104,** 619–629 (2001).
53. Xu, H. Tbx1 has a dual role in the morphogenesis of the cardiac outflow tract. *Development* **131,** 3217–3227 (2004).
54. Gong, W. *et al.* Mutation analysis of TBX1 in non-deleted patients with features of DGS/VCFS or isolated cardiovascular defects. *Journal of Medical Genetics* **38,** E45 (2001).
55. Xu, H., Cerrato, F. & Baldini, A. Timed mutation and cell-fate mapping reveal reiterated roles of Tbx1 during embryogenesis, and a crucial function during segmentation of the pharyngeal system via regulation of endoderm expansion. *Development* **132,** 4387–4395 (2005).
56. Guo, T. *et al.* Genotype and cardiovascular phenotype correlations with TBX1 in 1,022 velo-cardio-facial/digeorge/22q11.2 deletion syndrome patients. *Hum. Mutat.* **32,** 1278–1289 (2011).
57. Torres-Juan, L. *et al.* Mutations in TBX1 genocopy the 22q11.2 deletion and duplication syndromes: a new susceptibility factor for mental retardation. *Eur. J. Hum. Genet.* **15,** 658–663 (2007).
58. Yobb, T. M. *et al.* Microduplication and triplication of 22q11.2: a highly variable syndrome. *Am. J. Hum. Genet.* **76,** 865–876 (2005).
59. Zweier, C., Sticht, H., Aydin-Yaylagül, I., Campbell, C. E. & Rauch, A. Human TBX1 Missense Mutations Cause Gain of Function Resulting in the Same Phenotype as 22q11.2 Deletions. *The American Journal of Human Genetics* **80,** 510–517 (2007).
60. MacCarrick, G. *et al.* Loeys–Dietz syndrome: a primer for diagnosis and management. *Genet Med* **16,** 576–587 (2014).
61. Loeys, B. L. *et al.* A syndrome of altered cardiovascular, craniofacial, neurocognitive and skeletal development caused by mutations in TGFBR1 or TGFBR2. *Nat. Genet.* **37,** 275–281 (2005).
62. Loeys, B. L. *et al.* Aneurysm Syndromes Caused by Mutations in the TGF-β Receptor. *N Engl J Med* **355,** 788–798 (2006).
63. Arjunon, S., Rathan, S., Jo, H. & Yoganathan, A. P. Aortic Valve: Mechanical Environment and Mechanobiology. *Ann Biomed Eng* **41,** 1331–1346 (2013).
64. Dupuis, L. E. & Kern, C. B. Small leucine-rich proteoglycans exhibit

unique spatiotemporal expression profiles during cardiac valve development. *Dev. Dyn.* **243,** 601–611 (2014).
65. Hinton, R. B. & Yutzey, K. E. Heart Valve Structure and Function in Development and Disease. *Annu. Rev. Physiol.* **73,** 29–46 (2011).
66. Lockhart, M., Wirrig, E., Phelps, A. & Wessels, A. Extracellular matrix and heart development. *Birth Defects Res. Part A Clin. Mol. Teratol.* **91,** 535–550 (2011).
67. Doyle, J. J., Gerber, E. E. & Dietz, H. C. Matrix-dependent perturbation of TGFβ signaling and disease. *FEBS Lett.* **586,** 2003–2015 (2012).
68. Verma, S. & Siu, S. C. Aortic Dilatation in Patients with Bicuspid Aortic Valve. *N Engl J Med* **370,** 1920–1929 (2014).
69. Jones, J. A., Spinale, F. G. & Ikonomidis, J. S. Transforming growth factor-beta signaling in thoracic aortic aneurysm development: a paradox in pathogenesis. *J. Vasc. Res.* **46,** 119–137 (2009).
70. Byers, P. H. & Murray, M. L. Ehlers-Danlos syndrome: a showcase of conditions that lead to understanding matrix biology. *Matrix Biol.* **33,** 10–15 (2014).
71. Cooper, T. K. *et al.* The Haploinsufficient Col3a1 Mouse as a Model for Vascular Ehlers-Danlos Syndrome. *Veterinary Pathology* **47,** 1028–1039 (2010).
72. Robinson, P. N. *et al.* The molecular genetics of Marfan syndrome and related disorders. *Journal of Medical Genetics* **43,** 769–787 (2006).
73. Verstraeten, A., Alaerts, M., Van Laer, L. & Loeys, B. Marfan Syndrome and Related Disorders: 25 Years of Gene Discovery. *Hum. Mutat.* n/a–n/a (2016). doi:10.1002/humu.22977
74. Neptune, E. R. *et al.* Dysregulation of TGF-β activation contributes to pathogenesis in Marfan syndrome. *Nat. Genet.* **33,** 407–411 (2003).
75. Morissette, R. *et al.* Transforming growth factor-β and inflammation in vascular (type IV) Ehlers-Danlos syndrome. *Circulation: Cardiovascular Genetics* **7,** 80–88 (2014).
76. Mátyás, G. *et al.* Identification and in silico analyses of novelTGFBR1 andTGFBR2 mutations in Marfan syndrome-related disorders. *Hum. Mutat.* **27,** 760–769 (2006).
77. Langlois, D. *et al.* Conditional inactivation of TGF-β type II receptor in smooth muscle cells and epicardium causes lethal aortic and cardiac defects. *Transgenic Res.* **19,** 1069–1082 (2010).
78. Jiang, X., Rowitch, D. H., Soriano, P., McMahon, A. P. & Sucov, H. M. Fate of the mammalian cardiac neural crest. *Development* **127,** 1607–1616 (2000).
79. Majesky, M. W. Developmental Basis of Vascular Smooth Muscle Diversity. *Arteriosclerosis, Thrombosis, and Vascular Biology* **27,** 1248–1258 (2007).

80. Topouzis, S. & Majesky, M. W. Smooth muscle lineage diversity in the chick embryo. Two types of aortic smooth muscle cell differ in growth and receptor-mediated transcriptional responses to transforming growth factor-beta. *Dev. Biol.* **178,** 430–445 (1996).
81. Girdauskas, E., Schulz, S., Borger, M. A., Mierzwa, M. & Kuntze, T. Transforming growth factor-beta receptor type II mutation in a patient with bicuspid aortic valve disease and intraoperative aortic dissection. *The Annals of Thoracic Surgery* **91,** e70–1 (2011).
82. Laforest, B. & Nemer, M. Genetic Insights into Bicuspid Aortic Valve Formation. *Cardiology Research and Practice* **2012,** 1–8 (2012).
83. Grewal, N. *et al.* Normal and abnormal development of the aortic wall and valve: correlation with clinical entities. *Neth Heart J* **22,** 363–369 (2014).
84. Jian, B., Narula, N., Li, Q.-Y., Mohler, E. R. & Levy, R. J. Progression of aortic valve stenosis: TGF-beta1 is present in calcified aortic valve cusps and promotes aortic valve interstitial cell calcification via apoptosis. *The Annals of Thoracic Surgery* **75,** 457–65– discussion 465–6 (2003).
85. Hinton, R. B. *et al.* Extracellular matrix remodeling and organization in developing and diseased aortic valves. *Circ. Res.* **98,** 1431–1438 (2006).
86. Ferencz, C. *et al.* Congenital cardiovascular malformations associated with chromosome abnormalities: an epidemiologic study. *The Journal of Pediatrics* **114,** 79–86 (1989).
87. Ferencz, C. *et al.* Congenital cardiovascular malformations: Questions on inheritance. *Journal of the American College of Cardiology* **14,** 756–763 (1989).
88. Ko, J. M. Genetic Syndromes associated with Congenital Heart Disease. *Korean Circ J* **45,** 357 (2015).
89. Li, H. *et al.* Genetic modifiers predisposing to congenital heart disease in the sensitized Down syndrome population. *Circulation: Cardiovascular Genetics* **5,** 301–308 (2012).
90. Azhar, M. & Ware, S. M. Genetic andDevelopmental Basis of Cardiovascular Malformations. *Clinics in Perinatology* **43,** 39–53 (2016).
91. Maynard, T. M. *et al.* 22q11 Gene dosage establishes an adaptive range for sonic hedgehog and retinoic acid signaling during early development. *Hum. Mol. Genet.* **22,** 300–312 (2012).
92. Chen, T. & Dent, S. Y. R. Chromatin modifiers and remodellers: regulators of cellular differentiation. *Nat. Rev. Genet.* **15,** 93–106 (2013).
93. Mirabella, A. C., Foster, B. M. & Bartke, T. Chromatin deregulation in disease. *Chromosoma* **125,** 75–93 (2015).
94. Choudhary, C. *et al.* Lysine acetylation targets protein complexes and

co-regulates major cellular functions. *Science* **325,** 834–840 (2009).
95. Guo, T. *et al.* Histone Modifier Genes Alter Conotruncal Heart Phenotypes in 22q11.2 Deletion Syndrome. *Am. J. Hum. Genet.* **97,** 869–877 (2015).
96. Sanlaville, D. *et al.* Phenotypic spectrum of CHARGE syndrome in fetuses with CHD7 truncating mutations correlates with expression during human development. *Journal of Medical Genetics* **43,** 211–217 (2006).
97. Hsu, P. *et al.* CHARGE syndrome: A review. *J Paediatr Child Health* (2014). doi:10.1111/jpc.12497
98. Schulz, Y. *et al.* CHD7, the gene mutated in CHARGE syndrome, regulates genes involved in neural crest cell guidance. *Hum Genet* (2014). doi:10.1007/s00439-014-1444-2
99. Basson, M. A. & van Ravenswaaij-Arts, C. Functional Insights into Chromatin Remodelling from Studies on CHARGESyndrome. *Trends Genet.* **31,** 600–611 (2015).
100. Bouazoune, K. & Kingston, R. E. Chromatin remodeling by the CHD7 protein is impaired by mutations that cause human developmental disorders. *Proceedings of the National Academy of Sciences* **109,** 19238–19243 (2012).
101. Payne, S. *et al.* Developmental Biology. *Dev. Biol.* **405,** 82–95 (2015).
102. Liu, Y. *et al.* CHD7 interacts with BMP R-SMADs to epigenetically regulate cardiogenesis in mice. *Hum. Mol. Genet.* **23,** 2145–2156 (2014).
103. Boyle, M. I., Jespersgaard, C., Brøndum-Nielsen, K., Bisgaard, A. M. & Tümer, Z. Cornelia de Lange syndrome. *Clinical Genetics* **88,** 1–12 (2014).
104. Decroos, C. *et al.* Biochemical and Structural Characterization of HDAC8 Mutants Associated with Cornelia de Lange Syndrome Spectrum Disorders. *Biochemistry* **54,** 6501–6513 (2015).
105. Decroos, C. *et al.* Compromised Structure and Function of HDAC8 Mutants Identified in Cornelia de Lange Syndrome Spectrum Disorders. *ACS Chem. Biol.* **9,** 2157–2164 (2014).
106. Parenti, I. *et al.* Expanding the clinical spectrum of the ‘ HDAC8-phenotype’ - implications for molecular diagnostics, counseling and risk prediction. *Clinical Genetics* **89,** 564–573 (2016).
107. Corsten-Janssen, N. *et al.* More Clinical Overlap between 22q11.2 Deletion Syndrome and CHARGE Syndrome than Often Anticipated. *Mol Syndromol* **4,** 235–245 (2013).
108. Randall, V. *et al.* Great vessel development requires biallelic expression of *Chd7* and *Tbx1* in pharyngeal ectoderm in mice . *J. Clin. Invest.* **119,** 3301–3310 (2009).
109. Fulcoli, F. G. *et al.* Rebalancing gene haploinsufficiency in vivo by targeting chromatin. *Nat Commun* **7,** 1–11 (2016).

110. Menegola, E. *et al.* Inhibition of histone deacetylase activity on specific embryonic tissues as a new mechanism for teratogenicity. *Birth Defects Research Part B: Developmental and Reproductive Toxicology* **74,** 392–398 (2005).
111. Peterson, G. M. & Naunton, M. Valproate: a simple chemical with so much to offer. *J Clin Pharm Ther* **30,** 417–421 (2005).
112. Jentink, J. *et al.* Valproic Acid Monotherapy in Pregnancy and Major Congenital Malformations. *N Engl J Med* **362,** 2185–2193 (2010).
113. Wu, G., Nan, C., Rollo, J. C., Huang, X. & Tian, J. Sodium valproate-induced congenital cardiac abnormalities in mice are associated with the inhibition of histone deacetylase. *J. Biomed. Sci.* **17,** 16 (2010).
114. Gurvich, N. *et al.* Association of valproate-induced teratogenesis with histone deacetylase inhibition in vivo. *FASEB J.* **19,** 1166–1168 (2005).
115. Deardorff, M. A. *et al.* HDAC8 mutations in Cornelia de Lange syndrome affect the cohesin acetylation cycle. *Nature* **489,** 313–317 (2013).
116. Boyle, M. I., Jespersgaard, C., Brøndum-Nielsen, K., Bisgaard, A. M. & Tümer, Z. Cornelia de Lange syndrome. *Clinical Genetics* **88,** 1–12 (2014).
117. Moser, M. A., Hagelkruys, A. & Seiser, C. Transcription and beyond: the role of mammalian class I lysine deacetylases. *Chromosoma* (2013). doi:10.1007/s00412-013-0441-x
118. Wang, Z. *et al.* Genome-wide mapping of HATs and HDACs reveals distinct functions in active and inactive genes. *Cell* **138,** 1019–1031 (2009).
119. Haberland, M., Montgomery, R. L. & Olson, E. N. The many roles of histone deacetylases in development and physiology: implications for disease and therapy. *Nat. Rev. Genet.* **10,** 32–42 (2009).
120. Kelly, R. D. W. & Cowley, S. M. The physiological roles of histone deacetylase (HDAC) 1 and 2: complex co-stars with multiple leading parts. *Biochem. Soc. Trans.* **41,** 741–749 (2013).
121. Lahm, A. *et al.* Unraveling the hidden catalytic activity of vertebrate class IIa histone deacetylases. *Proc. Natl. Acad. Sci. U.S.A.* **104,** 17335–17340 (2007).
122. Montgomery, R. L. *et al.* Histone deacetylases 1 and 2 redundantly regulate cardiac morphogenesis, growth, and contractility. *Genes Dev.* **21,** 1790–1802 (2007).
123. Trivedi, C. M. *et al.* Hdac2 regulates the cardiac hypertrophic response by modulating Gsk3 beta activity. *Nat. Med.* **13,** 324–331 (2007).
124. Montgomery, R. L. *et al.* Maintenance of cardiac energy metabolism by histone deacetylase 3 in mice. *J. Clin. Invest.* **118,** 3588–3597
125. Bhaskara, S. *et al.* Deletion of Histone Deacetylase 3 Reveals Critical

Roles in S Phase Progression and DNA Damage Control. *Mol. Cell* **30,** 61–72 (2008).
126. Knutson, S. K. *et al.* Liver-specific deletion of histone deacetylase 3 disrupts metabolic transcriptional networks. *EMBO J.* **27,** 1017–1028 (2008).
127. Hu, E. Cloning and Characterization of a Novel Human Class I Histone Deacetylase That Functions as a Transcription Repressor. *Journal of Biological Chemistry* **275,** 15254–15264 (2000).
128. Jurkin, J. *et al.* Distinct and redundant functions of histone deacetylases HDAC1 and HDAC2 in proliferation and tumorigenesis. *Cell Cycle* **10,** 406–412 (2011).
129. Montgomery, R. L. *et al.* Histone deacetylases 1 and 2 redundantly regulate cardiac morphogenesis, growth, and contractility. *Genes Dev.* **21,** 1790–1802 (2007).
130. Dovey, O. M. *et al.* Histone deacetylase 1 and 2 are essential for normal T-cell development and genomic stability in mice. *Blood* **121,** 1335–1344 (2013).
131. Jamaladdin, S. *et al.* Histone deacetylase (HDAC) 1 and 2 are essential for accurate cell division and the pluripotency of embryonic stem cells. *Proceedings of the National Academy of Sciences* **111,** 9840–9845 (2014).
132. Cowley, S. M. *et al.* The mSin3A Chromatin-Modifying Complex Is Essential for Embryogenesis and T-Cell Development. *Mol. Cell. Biol.* **25,** 6990–7004 (2005).
133. Hendrich, B., Guy, J., Ramsahoye, B., Wilson, V. A. & Bird, A. Closely related proteins MBD2 and MBD3 play distinctive but interacting roles in mouse development. *Genes Dev.* **15,** 710–723 (2001).
134. Wang, J. *et al.* Opposing LSD1 complexes function in developmental gene activation and repression programmes. *Nature* **446,** 882–887 (2007).
135. Yamaguchi, T. *et al.* Histone deacetylases 1 and 2 act in concert to promote the G1-to-S progression. *Genes Dev.* **24,** 455–469 (2010).
136. Lagger, G. *et al.* Essential function of histone deacetylase 1 in proliferation control and CDK inhibitor repression. *EMBO J.* **21,** 2672–2681 (2002).
137. Hoxha, E. *et al.* Histone Deacetylase 1 Deficiency Impairs Differentiation and Electrophysiological Properties of Cardiomyocytes Derived from Induced Pluripotent Cells. *Stem Cells* **30,** 2412–2422 (2012).
138. Dovey, O. M., Foster, C. T. & Cowley, S. M. Histone deacetylase 1 (HDAC1), but not HDAC2, controls embryonic stem cell differentiation. *Proc. Natl. Acad. Sci. U.S.A.* **107,** 8242–8247 (2010).
139. Liu, Z. *et al.* WNT signaling promotes Nkx2.5 expression and early cardiomyogenesis via downregulation of Hdac1. *Biochim. Biophys.*

Acta **1793,** 300–311 (2009).
140. Trivedi, C. M. *et al.* Hopx and Hdac2 interact to modulate Gata4 acetylation and embryonic cardiac myocyte proliferation. *Dev. Cell* **19,** 450–459 (2010).
141. Guenther, M. G., Barak, O. & Lazar, M. A. The SMRT and N-CoR corepressors are activating cofactors for histone deacetylase 3. *Mol. Cell. Biol.* **21,** 6091–6101 (2001).
142. Li, J. *et al.* Both corepressor proteins SMRT and N-CoR exist in large protein complexes containing HDAC3. *EMBO J.* **19,** 4342–4350 (2000).
143. Emiliani, S., Fischle, W., Van Lint, C., Al-Abed, Y. & Verdin, E. Characterization of a human RPD3 ortholog, HDAC3. *Proc. Natl. Acad. Sci. U.S.A.* **95,** 2795–2800 (1998).
144. Sun, Z. *et al.* Deacetylase-independent function of HDAC3 in transcription and metabolism requires nuclear receptor corepressor. *Mol. Cell* **52,** 769–782 (2013).
145. You, S.-H. *et al.* Nuclear receptor co-repressors are required for the histone-deacetylase activity of HDAC3 in vivo. *Nat. Struct. Mol. Biol.* **20,** 182–187 (2013).
146. Grégoire, S. *et al.* Histone deacetylase 3 interacts with and deacetylates myocyte enhancer factor 2. *Mol. Cell. Biol.* **27,** 1280–1295 (2007).
147. Singh, N. *et al.* Histone deacetylase 3 regulates smooth muscle differentiation in neural crest cells and development of the cardiac outflow tract. *Circ. Res.* **109,** 1240–1249 (2011).
148. Risebro, C. A. *et al.* Epistatic rescue of Nkx2.5 adult cardiac conduction disease phenotypes by prospero-related homeobox protein 1 and HDAC3. *Circ. Res.* **111,** e19–31 (2012).
149. Montgomery, R. L. *et al.* Maintenance of cardiac energy metabolism by histone deacetylase 3 in mice. *J. Clin. Invest.* **118,** 3588–3597 (2008).
150. Sun, Z. *et al.* Diet-induced lethality due to deletion of the Hdac3 gene in heart and skeletal muscle. *J. Biol. Chem.* **286,** 33301–33309 (2011).
151. Trivedi, C. M., Lu, M. M., Wang, Q. & Epstein, J. A. Transgenic overexpression of Hdac3 in the heart produces increased postnatal cardiac myocyte proliferation but does not induce hypertrophy. *J. Biol. Chem.* **283,** 26484–26489 (2008).
152. Martin, D. M., Mindell, M. H., Kwierant, C. A., Glover, T. W. & Gorski, J. L. Interrupted aortic arch in a child with trisomy 5q31.1q35.1 due to a maternal (20;5) balanced insertion. *Am. J. Med. Genet.* **116A,** 268–271 (2002).
153. Garcia-Martinez, V. & Schoenwolf, G. C. Primitive-streak origin of the cardiovascular system in avian embryos. *Dev. Biol.* **159,** 706–719

(1993).
154. Gourdie, R. G., Mima, T., Thompson, R. P. & Mikawa, T. Terminal diversification of the myocyte lineage generates Purkinje fibers of the cardiac conduction system. *Development* **121,** 1423–1431 (1995).
155. Kattman, S. J., Huber, T. L. & Keller, G. M. Multipotent Flk-1+ Cardiovascular Progenitor Cells Give Rise to the Cardiomyocyte, Endothelial, and Vascular Smooth Muscle Lineages. *Dev. Cell* **11,** 723–732 (2006).
156. Moretti, A. *et al.* Multipotent Embryonic Isl1+ Progenitor Cells Lead to Cardiac, Smooth Muscle, and Endothelial Cell Diversification. *Cell* **127,** 1151–1165 (2006).
157. Wu, S. M. *et al.* Developmental origin of a bipotential myocardial and smooth muscle cell precursor in the mammalian heart. *Cell* **127,** 1137–1150 (2006).
158. Chang, C.-P. & Bruneau, B. G. Epigenetics and cardiovascular development. *Annu. Rev. Physiol.* **74,** 41–68 (2012).
159. Suganuma, T. & Workman, J. L. Signals and Combinatorial Functions of Histone Modifications. *Annu. Rev. Biochem.* **80,** 473–499 (2011).
160. Yang, X.-J. & Seto, E. The Rpd3/Hda1 family of lysine deacetylases: from bacteria and yeast to mice and men. *Nature Reviews Molecular Cell Biology* **9,** 206–218 (2008).
161. Trivedi, C. M. *et al.* Hdac2 regulates the cardiac hypertrophic response by modulating Gsk3β activity. *Nat. Med.* **13,** 324–331 (2007).
162. McCulley, D. J. & Black, B. L. *Chapter 9 - Transcription Factor Pathways and Congenital Heart Disease*. *Heart Development* **100,** 253–277 (Elsevier Inc., 2012).
163. Takeuchi, J. K. & Bruneau, B. G. Directed transdifferentiation of mouse mesoderm to heart tissue by defined factors. *Nature* **459,** 708–711 (2009).
164. McFadden, D. G. *et al.* The Hand1 and Hand2 transcription factors regulate expansion of the embryonic cardiac ventricles in a gene dosage-dependent manner. *Development* **132,** 189–201 (2005).
165. Mullican, S. E. *et al.* Histone deacetylase 3 is an epigenomic brake in macrophage alternative activation. **25,** 2480–2488 (2011).
166. Yu, J., Li, Y., Ishizuka, T., Guenther, M. G. & Lazar, M. A. A SANT motif in the SMRT corepressor interprets the histone code and promotes histone deacetylation. *EMBO J.* **22,** 3403–3410 (2003).
167. Sancak, Y. *et al.* The Rag GTPases bind raptor and mediate amino acid signaling to mTORC1. *Science* **320,** 1496–1501 (2008).
168. Blelloch, R., Venere, M., Yen, J. & Ramalho-Santos, M. Generation of Induced Pluripotent Stem Cells in the Absence of Drug Selection. *Cell Stem Cell* **1,** 245–247 (2007).
169. Stewart, S. A. Lentivirus-delivered stable gene silencing by RNAi in

primary cells. *RNA* **9,** 493–501 (2003).
170. Kim, M.-S., Merlo, X., Wilson, C. & Lough, J. Co-activation of atrial natriuretic factor promoter by Tip60 and serum response factor. *J. Biol. Chem.* **281,** 15082–15089 (2006).
171. Yang, X.-J., Ogryzko, V. V., Nishikawa, J., Howard, B. H. & Nakatani, Y. A p300/CBP-associated factor that competes with the adenoviral oncoprotein E1A. *Nature* **382,** 319–324 (1996).
172. Xu, C.-R. *et al.* Chromatin 'prepattern' and histone modifiers in a fate choice for liver and pancreas. *Science* **332,** 963–966 (2011).
173. Adli, M. & Bernstein, B. E. Whole-genome chromatin profiling from limited numbers of cells using nano-ChIP-seq. *Nat Protoc* **6,** 1656–1668 (2011).
174. Dahl, J. A. & Collas, P. A rapid micro chromatin immunoprecipitation assay (ChIP). *Nat Protoc* **3,** 1032–1045 (2008).
175. Mukhopadhyay, A., Deplancke, B., Walhout, A. J. M. & Tissenbaum, H. A. Chromatin immunoprecipitation (ChIP) coupled to detection by quantitative real-time PCR to study transcription factor binding to DNA in Caenorhabditis elegans. *Nat Protoc* **3,** 698–709 (2008).
176. Feng, D. *et al.* A circadian rhythm orchestrated by histone deacetylase 3 controls hepatic lipid metabolism. *Science* **331,** 1315–1319 (2011).
177. Montgomery, R. L. *et al.* Maintenance of cardiac energy metabolism by histone deacetylase 3 in mice. *J. Clin. Invest.* **118,** 3588–3597 (2008).
178. Niu, Z. *et al.* Conditional mutagenesis of the murine serum response factor gene blocks cardiogenesis and the transcription of downstream gene targets. *J. Biol. Chem.* **280,** 32531–32538 (2005).
179. He, A., Kong, S. W., Ma, Q. & Pu, W. T. Co-occupancy by multiple cardiac transcription factors identifies transcriptional enhancers active in heart. *Proc. Natl. Acad. Sci. U.S.A.* **108,** 5632–5637 (2011).
180. Mori, A. D. & Bruneau, B. G. TBX5 mutations and congenital heart disease: Holt-Oram syndrome revealed. *Curr. Opin. Cardiol.* **19,** 211–215 (2004).
181. Kawamura, T. Acetylation of GATA-4 Is Involved in the Differentiation of Embryonic Stem Cells into Cardiac Myocytes. *Journal of Biological Chemistry* **280,** 19682–19688 (2005).
182. Barron, M. R. Serum Response Factor, an Enriched Cardiac Mesoderm Obligatory Factor, Is a Downstream Gene Target for Tbx Genes. *Journal of Biological Chemistry* **280,** 11816–11828 (2005).
183. Murakami, M., Nakagawa, M., Olson, E. N. & Nakagawa, O. A WW domain protein TAZ is a critical coactivator for TBX5, a transcription factor implicated in Holt-Oram syndrome. *Proceedings of the National Academy of Sciences* **102,** 18034–18039 (2005).
184. Wu, S. M., Chien, K. R. & Mummery, C. Origins and Fates of

Cardiovascular Progenitor Cells. *Cell* **132,** 537–543 (2008).
185. Greulich, F., Rudat, C. & Kispert, A. Mechanisms of T-box gene function in the developing heart. *Cardiovasc. Res.* **91,** 212–222 (2011).
186. Garg, V. *et al.* GATA4 mutations cause human congenital heart defects and reveal an interaction with TBX5. *Nature* **424,** 443–447 (2003).
187. You, S.-H. *et al.* Nuclear receptor co-repressors are required for the histone-deacetylase activity of HDAC3 in vivo. *Nat. Struct. Mol. Biol.* **20,** 182–187 (2013).
188. Parker, S. E. *et al.* Updated national birth prevalence estimates for selected birth defects in the United States, 2004-2006. *Birth Defects Res. Part A Clin. Mol. Teratol.* **88,** 1008–1016 (2010).
189. Buckingham, M., Meilhac, S. & Zaffran, S. Building the mammalian heart from two sources of myocardial cells. *Nat. Rev. Genet.* **6,** 826–835 (2005).
190. Verzi, M. P., McCulley, D. J., De Val, S., Dodou, E. & Black, B. L. The right ventricle, outflow tract, and ventricular septum comprise a restricted expression domain within the secondary/anterior heart field. *Dev. Biol.* **287,** 134–145 (2005).
191. Kelly, R. G., Brown, N. A. & Buckingham, M. E. The arterial pole of the mouse heart forms from Fgf10-expressing cells in pharyngeal mesoderm. *Dev. Cell* **1,** 435–440 (2001).
192. McCulley, D. J., Kang, J.-O., Martin, J. F. & Black, B. L. BMP4 is required in the anterior heart field and its derivatives for endocardial cushion remodeling, outflow tract septation, and semilunar valve development. *Dev. Dyn.* **237,** 3200–3209 (2008).
193. High, F. A. *et al.* Murine Jagged1/Notch signaling in the second heart field orchestrates Fgf8 expression and tissue-tissue interactions during outflow tract development. *J. Clin. Invest.* (2009). doi:10.1172/JCI38922DS1
194. Kelly, R. G. The second heart field. *Curr. Top. Dev. Biol.* **100,** 33–65 (2012).
195. Sanford, L. P. *et al.* TGFbeta2 knockout mice have multiple developmental defects that are non-overlapping with other TGFbeta knockout phenotypes. *Development* **124,** 2659–2670 (1997).
196. Bartram, U. *et al.* Double-Outlet Right Ventricle and Overriding Tricuspid Valve Reflect Disturbances of Looping, Myocardialization, Endocardial Cushion Differentiation, and Apoptosis in TGF- 2-Knockout Mice. *Circulation* **103,** 2745–2752 (2001).
197. Doetschman, T. *et al.* Transforming growth factor beta signaling in adult cardiovascular diseases and repair. *Cell Tissue Res* **347,** 203–223 (2011).
198. Lincoln, J. Y. & Yutzey, K. E. Molecular and developmental

mechanisms of congenital heart valve disease. *Birth Defects Res. Part A Clin. Mol. Teratol.* **91,** 526–534 (2011).
199. Waltenberger, J. *et al.* Involvement of transforming growth factor-beta in the formation of fibrotic lesions in carcinoid heart disease. *The American Journal of Pathology* **142,** 71–78 (1993).
200. Fielitz, J. *et al.* Activation of the Cardiac Renin-AngiotensinSystem and Increased Myocardial CollagenExpression in Human Aortic Valve Disease. *Journal of the American College of Cardiology* **37,** 1443–1449 (2001).
201. Walker, G. A. Valvular Myofibroblast Activation by Transforming Growth Factor- : Implications for Pathological Extracellular Matrix Remodeling in Heart Valve Disease. *Circ. Res.* **95,** 253–260 (2004).
202. Wang, H., Leinwand, L. A. & Anseth, K. S. Cardiac valve cells and their microenvironment—insights from in vitro studies. *Nat Rev Cardiol* **11,** 715–727 (2014).
203. Liu, A. C. & Gotlieb, A. I. Transforming Growth Factor. *The American Journal of Pathology* **173,** 1275–1285 (2010).
204. Leier, C. V., Call, T. D., Fulkerson, P. K. & Wooley, C. F. The Spectrum of Cardiac Defects in the Ehlers-Danlos Syndrome, Types I and III. *Annals of Internal Medicine* **92,** 171–178 (1980).
205. Buntinx, I. M. *et al.* Neonatal Marfan syndrome with congenital arachnodactyly, flexion contractures, and severe cardiac valve insufficiency. *Journal of Medical Genetics* **28,** 267–273 (1991).
206. Massagué, J. TGFβ signalling in context. *Nature Reviews Molecular Cell Biology* **13,** 616–630 (2012).
207. Yamaguchi, Y., Mann, D. M. & Ruoslahti, E. Negative regulation of transforming growth factor-beta by the proteoglycan decorin. *Nature* **346,** 281–284 (1990).
208. Corsi, A. *et al.* Phenotypic effects of biglycan deficiency are linked to collagen fibril abnormalities, are synergized by decorin deficiency, and mimic Ehlers-Danlos-like changes in bone and other connective tissues. *J. Bone Miner. Res.* **17,** 1180–1189 (2002).
209. Danielson, K. G. *et al.* Targeted disruption of decorin leads to abnormal collagen fibril morphology and skin fragility. *J. Cell Biol.* **136,** 729–743 (1997).
210. Jepsen, K. J. *et al.* A Syndrome of Joint Laxity and Impaired Tendon Integrity in Lumican- and Fibromodulin-deficient Mice. *Journal of Biological Chemistry* **277,** 35532–35540 (2002).
211. Pulkkinen, L. *et al.* Deficient expression of the gene coding for decorin in a lethal form of Marfan syndrome. *J. Biol. Chem.* **265,** 17780–17785 (1990).
212. Dupuis, L. E. & Kern, C. B. Small leucine-rich proteoglycans exhibit unique spatiotemporal expression profiles during cardiac valve development. *Dev. Dyn.* **243,** 601–611 (2014).

213. Vincent, T. *et al.* A SNAIL1–SMAD3/4 transcriptional repressor complex promotes TGF-. *Nat Cell Biol* **11,** 943–950 (2009).
214. Montgomery, R. L. *et al.* Histone deacetylases 1 and 2 redundantly regulate cardiac morphogenesis, growth, and contractility. *Genes Dev.* **21,** 1790–1802 (2007).
215. Haberland, M., Mokalled, M. H., Montgomery, R. L. & Olson, E. N. Epigenetic control of skull morphogenesis by histone deacetylase 8. *Genes Dev.* **23,** 1625–1630 (2009).
216. Lewandowski, S. L. *et al.* Histone deacetylase 3 modulates Tbx5 activity to regulate early cardiogenesis. *Hum. Mol. Genet.* **23,** 3801–3809 (2014).
217. Yang, L. *et al.* Isl1Cre reveals a common Bmp pathway in heart and limb development. *Development* **133,** 1575–1585 (2006).
218. Alva, J. A. *et al.* VE-Cadherin-Cre-recombinase transgenic mouse: A tool for lineage analysis and gene deletion in endothelial cells. *Dev. Dyn.* **235,** 759–767 (2006).
219. Carvalho, B. S. & Irizarry, R. A. A framework for oligonucleotide microarray preprocessing. *bioinformatics.oxfordjournals.org*
220. Gentleman, R. C. *et al.* Bioconductor: open software development for computational biology and bioinformatics. *Genome Biol.* **5,** R80 (2004).
221. R Development Core Team. R: A Language and Environment for Statistical Computing. (2011).
222. Kolde, R. pheatmap: Pretty heatmaps.
223. Lakkis, M. M. & Epstein, J. A. Neurofibromin modulation of ras activity is required for normal endocardial-mesenchymal transformation in the developing heart. *Development* **125,** 4359–4367 (1998).
224. Yamamura, H., Zhang, M., Markwald, R. R. & Mjaatvedt, C. H. A heart segmental defect in the anterior-posterior axis of a transgenic mutant mouse. *Dev. Biol.* **186,** 58–72 (1997).
225. Sun, Y. *et al.* Islet 1 is expressed in distinct cardiovascular lineages, including pacemaker and coronary vascular cells. *Dev. Biol.* **304,** 286–296 (2007).
226. Boucher, P., Gotthardt, M., Li, W.-P., Anderson, R. G. W. & Herz, J. LRP: role in vascular wall integrity and protection from atherosclerosis. *Science* **300,** 329–332 (2003).
227. Adrain, C. & Freeman, M. New lives for old: evolution ofpseudoenzyme function illustratedby iRhoms. *Nature Reviews Molecular Cell Biology* **13,** 489–498 (2012).
228. Neeb, Z., Lajiness, J. D., Bolanis, E. & Conway, S. J. Cardiac outflow tract anomalies. *WIREs Dev Biol* **2,** 499–530 (2013).
229. Bajolle, F. *et al.* Myocardium at the base of the aorta and pulmonary trunk is prefigured in the outflow tract of the heart and in subdomains of the second heart field. *Dev. Biol.* **313,** 25–34 (2008).

230. Tao, G., Kotick, J. D. & Lincoln, J. Heart valve development, maintenance, and disease: the role of endothelial cells. *Curr. Top. Dev. Biol.* **100,** 203–232 (2012).
231. Yasuda, H. *et al.* Failure to prevent progressive dilation of ascending aorta by aortic valve replacement in patients with bicuspid aortic valve: comparison with tricuspid aortic valve. *Circulation* **108 Suppl 1,** II291–4 (2003).
232. Gordon, K. J. & Blobe, G. C. Role of transforming growth factor-β superfamily signaling pathways in human disease. *Biochimica et Biophysica Acta (BBA) - Molecular Basis of Disease* **1782,** 197–228 (2008).
233. Piera-Velazquez, S., Li, Z. & Jimenez, S. A. Mini-Review. *The American Journal of Pathology* **179,** 1074–1080 (2011).
234. Margueron, R. & Reinberg, D. The Polycomb complex PRC2 and its mark in life. *Nature* **469,** 343–349 (2011).
235. Potthoff, M. J. MEF2 and HDAC proteins regulate striated muscle development and remodeling. PhD Thesis. (The University of Texas Southwestern Medical Center at Dallas).
236. Zaidi, S. *et al.* De novo mutations in histone-modifying genes in congenital heart disease. *Nature* **498,** 220–223 (2013).
237. Papaioannou, V. E. The T-box gene family: emerging roles in development, stem cells and cancer. *Development* **141,** 3819–3833 (2014).
238. Kruithof, B. P. T., Duim, S. N., Moerkamp, A. T. & Goumans, M.-J. TGFβ and BMP signaling in cardiac cushion formation: Lessons from mice and chicken. *Differentiation* **84,** 89–102 (2012).
239. Dijke, ten, P., Egorova, A. D., Goumans, M.-J. T. H., Poelmann, R. E. & Hierck, B. P. TGF-β Signaling in Endothelial-to-Mesenchymal Transition: The Role of Shear Stress and Primary Cilia. *Sci. Signal.* **5,** pt2–pt2 (2012).
240. Arthur, H. M. & Bamforth, S. D. TGFβ signaling and congenital heart disease: Insights from mouse studies. *Birth Defects Res. Part A Clin. Mol. Teratol.* **91,** 423–434 (2011).
241. Lockhart, M., Wirrig, E., Phelps, A. & Wessels, A. Extracellular matrix and heart development. *Birth Defects Res. Part A Clin. Mol. Teratol.* **91,** 535–550
242. Yetkin, E. & Waltenberger, J. Molecular and cellular mechanisms of aortic stenosis. *Int. J. Cardiol.* **135,** 4–13 (2009).
243. Akhurst, R. J. & Hata, A. Targeting the TGFβ signalling pathway in disease. *Nat Rev Drug Discov* **11,** 790–811 (2012).
244. Carvalho, A. C. *et al.* Absence of an aortic valve cusp, a cause of severe aortic regurgitation in infancy. *Pediatr Cardiol* **13,** 122–124 (1992).
245. Fernández, B. *et al.* Bicuspid aortic valves with different spatial

orientations of the leaflets are distinct etiological entities. *Journal of the American College of Cardiology* **54,** 2312–2318 (2009).
246. Waldron, L. *et al.* The Cardiac TBX5 Interactome Reveals a Chromatin Remodeling Network Essential for Cardiac Septation. *Dev. Cell* **36,** 262–275 (2016).
247. Zhang, X. *et al.* Histone deacetylase 3 (HDAC3) activity is regulated by interaction with protein serine/threonine phosphatase 4. *Genes Dev.* **19,** 827–839 (2005).
248. Ji, H. *et al.* EGF-induced ERK activation promotes CK2-mediated disassociation of α-Catenin from β-Catenin and transactivation of β-Catenin. *Mol. Cell* **36,** 547–559 (2009).